

Percolation thresholds of randomly rotating patchy particles on Archimedean lattices

Quancheng Wang,¹ Zhenfang He,¹ Junfeng Wang,² and Hao Hu^{1,*}

¹*School of Physics and Electronic Engineering, Anhui University, Hefei, Anhui 230601, China*

²*School of Physics, Hefei University of Technology, Hefei, Anhui 230009, China*

(Dated: December 22, 2021)

We study the percolation of randomly rotating patchy particles on 11 Archimedean lattices in two dimensions. Each vertex of the lattice is occupied by a particle, and in each model the patch size and number are monodisperse. When there are more than one patches on the surface of a particle, they are symmetrically decorated. As the proportion χ of the particle surface covered by the patches increases, the clusters connected by the patches grow and the system percolates at the threshold χ_c . We combine Monte Carlo simulations and the critical polynomial method to give precise estimates of χ_c for disks with one to six patches and spheres with one to two patches on the 11 lattices. For one-patch particles, we find that the order of χ_c values for particles on different lattices is the same as that of threshold values p_c for site percolation on same lattices, which implies that χ_c for one-patch particles mainly depends on the geometry of lattices. For particles with more patches, symmetry become very important in determining χ_c . With the estimates of χ_c for disks with one to six patches, by analyses related to symmetry, we are able to give precise values of χ_c for disks with an arbitrary number of patches on all 11 lattices. The following rules are found for patchy disks on each of these lattices: (i) as the number of patches n increases, values of χ_c repeat in a periodic way, with the period n_0 determined by the symmetry of the lattice; (ii) when $\text{mod}(n, n_0) = 0$, the minimum threshold value χ_{\min} appears, and the model is equivalent to site percolation with $\chi_{\min} = p_c$; (iii) disks with $\text{mod}(n, n_0) = m$ and $n_0 - m$ ($m < n_0/2$) share the same χ_c value.

I. INTRODUCTION

Patchy particles [1, 2] are created by modifying the surface of colloidal particles, where each modified area is regarded as a patch. One-patch particles with two distinct surface areas are usually called Janus particles, and two-patch particles are called triblock Janus particles. These particles can be designed in various shapes, e.g., spheres, dumbbells, disks, and rods. And the patches can be decorated with different properties, e.g., chemical, optical, electrical, and magnetic properties. As model systems with anisotropic interactions, patchy particles are used to study equilibrium gels and water [3, 4], and they can self-assemble into open lattices [5–7] such as the entropy stabilized kagome lattice [5, 6]. In two dimensions (2D), when patchy disks or spheres are compressed tightly, they form a triangular lattice. Putting Janus particles onto the densely packed triangular lattice, various continuous thermodynamic phase transitions and critical phenomena have recently been observed [8–10].

Percolation is extensively studied in stochastic processes, phase transitions and critical phenomena, and widely applied in various problems such as exploring gelation in polymers, transport behaviors in porous media, the spread of epidemics, the fractal structure of landscapes etc. [11, 12] There exist many studies on percolation of patchy particles in the continuum space, for which recent examples include different percolated states in mixtures of patchy colloids [13], reentrant percolation of inverse patchy colloids [14] and of patchy colloids on

patterned substrates [15], effects of surface heterogeneity on percolation thresholds of random patchy spheres [16], the design of patchy particle gels with tunable percolation thresholds [17]. However, except a study on directed percolation of patchy disks on the square lattice [18], we find that the percolation behavior of patchy particles on lattices remains largely unexplored, possibly due to that patchy particles are made in the continuum space [1, 2].

In this work, we study percolation of patchy particles on different lattices, in order to get more understanding of collective behaviors of the particles in 2D. As model systems, we assume that each vertex of the lattice is occupied by a patchy particle, and that particles rotate randomly. Two adjacent particles are considered as connected only when their patches are in contact with each other. As the proportion χ of the particle surface occupied by the patch(es) increases, the clusters formed by connected particles will gradually become larger. At a threshold value χ_c , a cluster that spans the entire lattice first forms, i.e. the percolation transition occurs. The threshold is an important parameter for percolation, and thus we focus on determining the χ_c values and exploring the dependence of these values on the symmetry and geometry of patchy particles and lattices.

For the purpose above, we first numerically study disks with one to six patches and spheres with one to two patches, on all 11 Archimedean lattices in 2D, which are shown in Fig. 1. When there are more than one patches on a particle, the patches locate symmetrically and share the same size, as shown for patchy disks in Fig. 2. Monte Carlo (MC) simulations are conducted to produce independent configurations, and the recently developed critical polynomial method [19–28] is combined with MC sampling to precisely estimate χ_c of these mod-

*Corresponding author: huhao@ahu.edu.cn

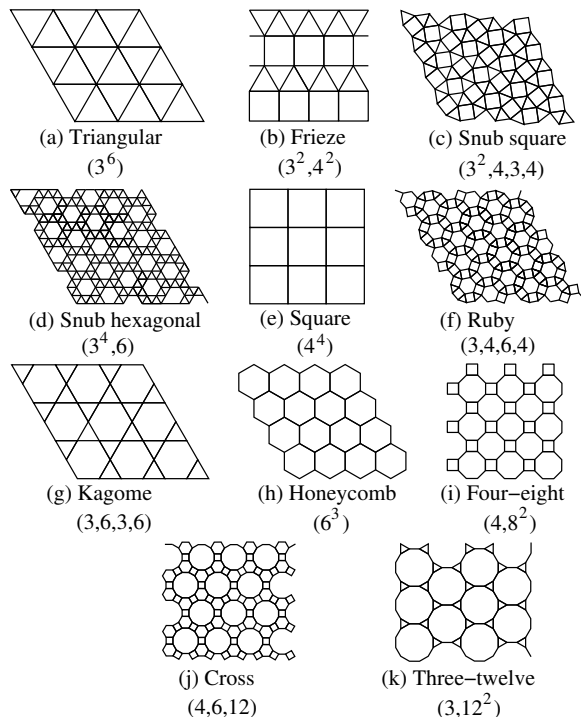


FIG. 1: The 11 Archimedean lattices in two dimensions. For each lattice, all vertices are equivalent if the lattice size is infinite or the boundary conditions are periodic. Lattice names are used as in Ref. [27], and under the names are symbols designated using the general notation proposed by Grünbaum and Shephard [29]. A brief introduction of the history and nomenclature of the lattices are available in Ref. [30].

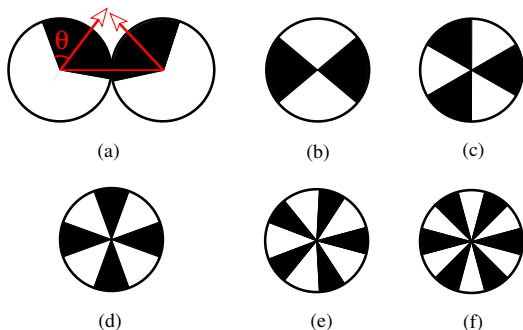


FIG. 2: Schematic drawings of patchy disks. On each disk the dark areas are patches, which share the same size and locate symmetrically when their number is more than one. The half-angle θ characterizes the size of a patch. (a)-(f) show particles containing one to six patches, respectively. (a) also exemplifies the connection of two particles, i.e. they are considered as connected if their patches touch each other. The red arrow indicates the direction of the particle, which is drawn by connecting the center of the particle and that of one patch.

els. For one-patch particles, it is found that the order of χ_c values on different Archimedean lattices is the same as that of threshold values p_c for site percolation on same lattices. This suggests that, for one-patch particles, the lattice geometry is the most important factor which affects χ_c values. For particles with more patches, their χ_c values on different lattices do not follow the same order as those for one-patch particles, which reflects that symmetry significantly influence percolation thresholds of particles with more than one patches.

The role of symmetry in determining the χ_c values is further exhibited in analytic calculations of the probabilities of different patch-covering structures of a particle near the above numerically estimated values of χ_c . These calculations lead to expressions of the probabilities as a function of χ , which allow us to prove the equality of χ_c values for various models or explain the difference between close χ_c values for distinct models. As results, we are able to give precise values of χ_c for disks with an arbitrary number of patches on all 11 Archimedean lattices in 2D. We find that χ_c values for patchy disks on each of the lattices are governed by the following rules: (i) χ_c values repeat in a periodic way as the number of patches n increases, with the period n_0 determined by the symmetry of the lattice; (ii) the minimum threshold value χ_{\min} appears when $\text{mod}(n, n_0) = 0$, for which the model of patchy disks is equivalent to site percolation with $\chi_{\min} = p_c$; (iii) disks with $\text{mod}(n, n_0) = m$ and $n_0 - m$ ($m < n_0/2$) share the same value of χ_c . These results could provide references for further studies, such as exploring at finite temperatures the connectivity and phase behaviors of patchy particles on lattices in 2D [8–10].

The remainder of this paper is organized as follows. Section II introduces the models and numerical methods. Section III presents main results. A brief conclusion and discussion is given in Section IV. More details can be found in the supplemental material (SM) [31].

II. MODELS AND NUMERICAL METHODS

A. Models

For the Archimedean lattices, all vertices are equivalent and the lengths of edges are equal, as shown in Fig. 1. For the model of a given type of patchy particles on one of the Archimedean lattices, each vertex of the lattice is occupied by a randomly rotating particle. The particle center locates right at the vertex and its diameter is set equal to the edge length of the lattice, thus two particles at the ends of an edge are in contact with each other. Two neighboring particles are connected if one patch on one particle touch another patch on the other particle (the two patches both cover the same edge). As shown in Fig. 2(a), the size of a patch is characterized by the half-angle θ . The one- and two-patch spheres can be drawn similar to Fig. 2(a-b), except that a patch is a

sphere cap with θ being the polar angle. For convenience of comparing thresholds of different types of particles, we also define the size of patches by the proportion χ of the particle surface covered by the patches, which is related to θ as

$$\chi = 2n\theta/2\pi = n\theta/\pi \quad (1)$$

for patchy disks, and as

$$\chi = \frac{n}{4\pi} \int_0^\theta \sin \theta d\theta \int_0^{2\pi} d\phi = n(1 - \cos \theta)/2 \quad (2)$$

for patchy spheres. Here n is the number of symmetrically distributed patches on a particle. In experiments, the patch size can be designed through surface modification or compartmentalization [1, 2].

B. The critical polynomial

The critical polynomial method is a powerful method proposed and developed in recent years to calculate percolation thresholds in two dimensions [19–28]. It originated from the fact that every exactly solved percolation threshold in 2D can be expressed as the unique root of a polynomial. For general (solved and unsolved) percolation models in 2D, the critical polynomial was first defined using a linearity hypothesis and symmetry analyses [19–21]. Then the recursive deletion-contraction algorithm [22] was proposed to find the polynomial. Latest developments of the method are the alternative probabilistic, geometrical interpretation of the critical polynomial [23] and transfer-matrix techniques for its calculation [24–27]. Unprecedented estimates for thresholds of unsolved planar-lattice models have been obtained, e.g., for bond percolation on the kagome lattice, the precision of the estimate is in the order of 10^{-17} [27]. The critical polynomial has also been combined with MC sampling to provide high-precision estimates of threshold values, e.g., for nonplanar and continuum percolation models [28], for which transfer-matrix calculations are difficult.

For a finite periodic lattice B in 2D, the probabilistic, geometrical definition of the critical polynomial [23] is

$$P_B \equiv R_2 - R_0. \quad (3)$$

Here R represents the wrapping (or crossing) probability [32, 33], where “wrapping” means that, when putting the periodic lattice in 2D onto a torus, there exist a percolation cluster which wraps around the torus. The quantity R_2 is the probability of wrapping in two directions, and R_0 is the probability of non-wrapping. If filling the infinite space in 2D using copies of B in some periodic way, wrapping in two directions means that there is a open cluster which connects every copy, and non-wrapping means that no infinite copies of B can be connected by open clusters [23].

Due to universality [23], the root $p(L)$ of $P_B(p, L) = 0$ gives an estimate of the percolation threshold that becomes more accurate as the linear size L of the lattice B is increased. Here p represents the control parameter for the percolation problem, e.g., the occupation probability ($p \in [0, 1]$) for bond or site percolation. From previous studies on the critical polynomial [19–27], it is known that $p(L) = p_c$ [$p_c \equiv p(L \rightarrow \infty)$] for exactly solved lattice models, even at the smallest L ; and that, for unsolved percolation problems, $p(L)$ very quickly approaches p_c as L increases. For example, on Archimedean lattices, the unsolved bond percolation thresholds behave as $[p(L) - p_c] \simeq \sum_{k=1}^{\infty} A_k L^{-\Delta_k}$, with $\Delta_1 = 4$ or 6 , and $\Delta_i > \Delta_j$ when $i > j$ [27]. The finite-size correction of P_B is much smaller than that for other quantities such as wrapping probabilities [28].

The critical polynomial P_B is a dimensionless quantity, since $P_B(p_c, L \rightarrow \infty) = 0$. Thus in the renormalization group formulation [34], P_B has the finite-size scaling formula [28]

$$P_B(t, u_1, u_2, L) = P_B(L^{y_t} t, L^{y_1} u_1, L^{y_2} u_2). \quad (4)$$

Here $t \propto p - p_c$ is the relevant thermal renormalization scaling field, and $y_t = 1/\nu = 3/4$ is the associated renormalization exponent. And u_1 and u_2 represent two leading irrelevant scaling fields with renormalization exponents $y_2 < y_1 < 0$. When assuming $y_2 > 2y_1$, by Taylor expansion to the first order, one gets

$$P_B(p, L) \simeq a_1(p - p_c)L^{y_t} + b_1 L^{y_1} + b_2 L^{y_2}, \quad (5)$$

where a_1 , b_1 and b_2 are non-universal amplitudes. The irrelevant exponents are related to Δ values as $y_1 = y_t - \Delta_1$ and $y_2 = y_t - \Delta_2$ [28]. Our MC data will be fitted by the above finite-size scaling formula, with p replaced by θ , though the irrelevant exponents may be different from those of bond percolation on Archimedean lattices [27].

C. Monte Carlo simulation

The MC method is used to sample independent configurations for 88 models, including six types of patchy disks and two types of patchy spheres, on all 11 Archimedean lattices in 2D. For a single configuration, a random direction is generated for each particle to simulate the random rotation. In simulations, each lattice is encoded with the aid of a square or triangular array, whose correspondence with the actual lattice is shown in Figs.S1-S11 of the SM [31], and periodic boundary conditions are employed for the lattices. The number of vertices (equivalent to the number of particles) on each lattice can be calculated from L , as shown in Table S1 of the SM [31]. Hereafter L is the linear size of the square or triangular array for encoding the lattices, which is in proportion to the actual linear size. We conduct simulations at different patch sizes and systems sizes, and use sampled values of P_B to determine the percolation threshold θ_c (χ_c).

In our MC simulations, we simulated systems with up to $O(10^5)$ particles. At least 10^8 independent configurations were generated for each set of (θ, L) values, for all 88 models (up to 10^{10} independent configurations for one-patch disks when $L < 16$, as shown in Table S2 of the SM [31]). The total simulation time was about 14.6 months if using a computer workstation with 2 Intel Xeon Scalable Gold 6130 CPU and 8×16 GB DDR4 ECC Registered Shared Memory (time for each model is shown in Table S3 of the SM [31]).

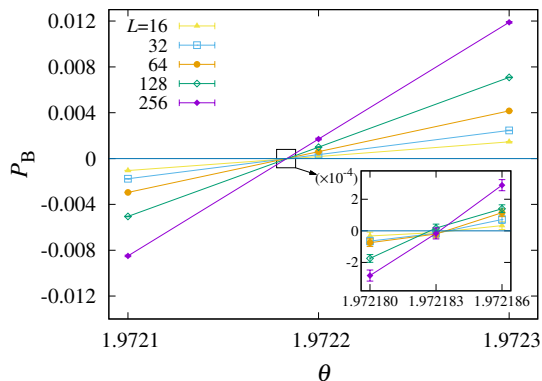


FIG. 3: Plot of P_B versus θ for one-patch disks on triangular lattices for different linear sizes L . The lines are added to guide the eyes.

III. RESULTS

We first present numerical results for one-patch particles, then for particles with two to six patches. Precise estimates of χ_c for these particles on 11 Archimedean lattices are obtained by combining MC simulations and the critical polynomial method. It is found that the lattice geometry mainly determines χ_c for one-patch particles, and that the symmetry of patches and lattices significantly affects χ_c for particles with more patches. Furthermore, with the above numerical estimates of χ_c , by analyses related to symmetry, we give values of χ_c for disks with an arbitrary number of patches on all 11 Archimedean lattices. We also present the rules governing χ_c values of patchy disks on these lattices.

A. Numerical results for one-patch particles

1. One-patch disks

For one-patch disks on the triangular lattice, the plot of P_B versus θ is shown in Fig. 3. It can be seen that curves for different sizes approximately cross near $\theta_c \simeq 1.972183$. To more precisely estimate the percolation threshold θ_c , we use Eq. (5), with p replaced by θ , to

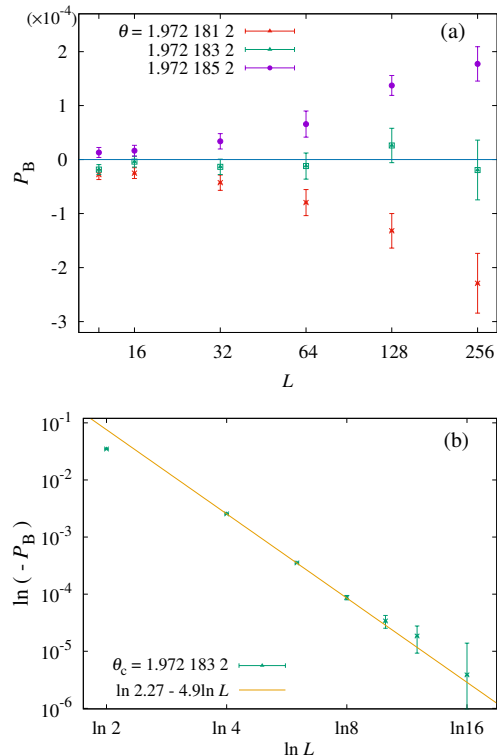


FIG. 4: Plots for one-patch disks on the triangular lattice: (a) P_B versus L at $\theta_c = 1.9721832$ and two nearby values of θ . As θ deviates from θ_c , the curves bend upwards ($\theta > \theta_c$) or downwards ($\theta < \theta_c$). (b) $\ln(-P_B)$ versus $\ln L$ at θ_c for small sizes L . The slope of the straight line is given by the correction exponent $y_1 \simeq -4.9$.

fit the data of P_B according to the least-square criterion. When performing the fits, we gradually increase L_{\min} and exclude data points for $L < L_{\min}$. In general, the fit results are acceptable, only when χ^2 is less than or close to the degree of freedom (DOF), and the decrease of χ^2 per DOF does not exceed one when increasing L_{\min} . Fits are made with fixed $y_t = 3/4$ and the results are shown in Table I. When setting $b_2 = 0$, the fit results show that the leading irrelevant exponent is $y_1 \simeq -4.9$. When y_2 is fixed at -6 , -7 or -8 , the fit results are also consistent with $y_1 \simeq -4.9$. Thus we put our final estimate as $y_1 = -4.9(3)$. And from Table I, the percolation threshold of one-patch disks on the triangular lattice is estimated to be $\theta_c = 1.97218320(8)$, i.e., $\chi_c = 0.62776541(3)$. All error bars of quantities in this work can be regarded as one-sigma.

To demonstrate the above estimates of θ_c , we plot in Fig. 4(a) P_B versus L at θ_c and two nearby values. It can be seen that when θ deviates from θ_c , the curves bend upwards ($\theta > \theta_c$) or downwards ($\theta < \theta_c$) as the size L increases. Since $P_B \simeq b_1 L^{y_1}$ at θ_c , the estimate of $y_1 \simeq -4.9$ is illustrated in Fig. 4(b) as the slope of the straight line.

For one-patch disks on other 10 Archimedean lattices,

TABLE I: Fit results of the critical polynomial P_B for one-patch disks on the triangular lattice.

L_{\min}	χ^2/DOF	θ_c	a_1	b_1	y_1	b_2	y_2
6	63.6/79	1.972 183 20(7)	-1.65(4)	-2.1(6)	-4.9(2)		
8	62.6/76	1.972 183 20(7)	-1.65(4)	-2.2(30)	-4.9(6)		
4	83.8/88	1.972 183 20(7)	-1.65(4)	-2.2(25)	-4.9(4)	0.3(53)	-6
2	84.8/91	1.972 183 21(7)	-1.65(4)	-3.7(2)	-5.11(4)	9.2(5)	-7
4	83.8/88	1.972 183 20(7)	-1.65(4)	-2.2(13)	-4.9(3)	0.5(85)	-7
2	84.3/91	1.972 183 21(7)	-1.65(4)	-2.7(1)	-4.97(3)	13.0(6)	-8

we also conduct similar analyses for the simulation data. Plots of P_B versus θ are shown in Fig. S12 of the SM [31]. Fits of the data also yield precise values of the percolation threshold χ_c for these lattices, as summarized in Table II. By observing the above χ_c values for one-patch disks on all 11 Archimedean lattices and p_c values for site percolation on same lattices, we find that the two sets of values follow the same order, as plotted in Fig. 5. The order can be regarded as from lattices with large coordination numbers to those with small coordination numbers, and when the coordination numbers are the same, it is from lattices with small variances of angles (around a vertex) to those with large variances. Thus, similar to p_c for site percolation, χ_c for one-patch disks on Archimedean lattices are mainly influenced by the lattice geometry.

The threshold values of one-patch disks on the frieze and snub square lattices are very close since the two lattices share the same coordination number and variance of angles. We find that their order can also be understood from geometry as follows. The patch of a disk can cover several neighboring edges connecting to the disk center, and various patch-covering structures occur with different probabilities, which can be obtained by analyzing the configurations as exemplified by the calculations for the frieze lattice in the SM [31]. In Table III, we show these probabilities for patch sizes χ near χ_c of the two lattices. From the table, it is observed that 3-edge patch-covering occurs with same probabilities on the two lattices, as well as 4-edge patch-covering. However, for 3-edge patch-covering, the frieze lattice has a structure with two adjacent $\pi/2$ -angles; and for 4-edge covering, the frieze lattice has two structures (both occurring with probability $\chi - 2/3$) with two adjacent $\pi/2$ -angles, while the snub square lattice only has one structure (occurring with probability $\chi - 2/3$) with two $\pi/2$ -angles. Since structures with two adjacent $\pi/2$ -angles are more open than other structures, the frieze lattice has a slightly lower percolation threshold than the snub square lattice, which is confirmed by our numerical estimates in Table II.

Besides χ_c , we also get estimates of the leading irrelevant exponent y_1 for one-patch disks on other Archimedean lattices. The results of y_1 are summarized in Table IV. For lattices whose values of y_1 are absent in the table, the finite corrections are also small, but the current data are not sufficient for determining y_1 . The

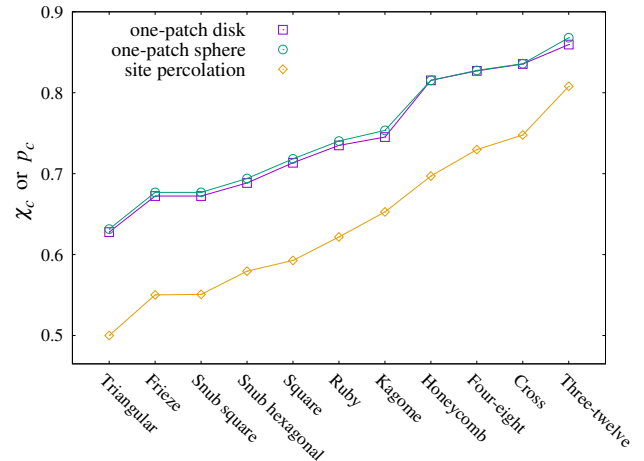


FIG. 5: Plots of percolation thresholds χ_c for one-patch disks and spheres, and p_c for site percolation. The values of the thresholds are summarized in Table II, where p_c values come from the cited references. The lines are added to guide the eyes.

presented estimates of y_1 are close to $y_1 = y_t - \Delta_1 = -3.25$ or -5.25 for unsolved bond percolation models on Archimedean lattices [27]. Besides the triangular lattice, we also make plots of P_B versus L at the estimated thresholds for one-patch disks on other lattices, as shown in Fig. S20 of the SM [31], which demonstrate the scaling $P_B(\theta_c, L) \simeq b_1 L^{y_1}$ with the estimated values of y_1 .

2. One-patch spheres

To observe the effect of particle shape on the percolation threshold, we also conduct simulations for one-patch spheres on Archimedean lattices. Similar analyses are performed for the simulation data. The resulting threshold values χ_c are also summarized in Table II and plotted in Fig. 5. It can be seen that, except on the honeycomb lattice, χ_c values for one-patch spheres are slightly larger than those for one-patch disks, and the calculated differences $[(\chi_c^{\text{sphere}} - \chi_c^{\text{disk}})/\chi_c^{\text{disk}}]$ are at most 1.1%. On the honeycomb lattice, within error bars, one-patch disks

TABLE II: Percolation thresholds χ_c of patchy particles on Archimedean lattices. The site-percolation thresholds p_c for these lattices are also included for comparison.

	Lattice	Triangular	Frieze	Snub square	Snub hexagonal
Disk	One-patch	0.627 765 41(3)	0.672 338 8(1)	0.672 346 35(4)	0.688 526 01(4)
	Two-patch	0.554 469 9(4)	0.624 383 7(6)	0.622 832 9(4)	0.625 385 2(6)
	Three-patch	0.558 806 6(7)	0.623 505 (1)	0.620 411 9(5)	0.617 753 2(7)
	Four-patch	0.554 469 2(4)	0.645 671 6(5)	0.670 484 3(5)	0.625 384 5(6)
	Five-patch	0.627 765 6(4)	0.658 762 8(6)	0.627 557 4(8)	0.688 525 6(5)
	Six-patch	0.500 000 1(5)	0.692 899 0(9)	0.756 361 (1)	0.579 497 9(9)
Sphere	One-patch	0.631 475 6(3)	0.676 869 4(4)	0.676 877 1(3)	0.694 042 7(3)
	Two-patch	0.532 379 5(7)	0.606 503 6(4)	0.605 554 2(5)	0.611 814 2(6)
p_c		1/2	0.550 213 (3) [30]	0.550 806 (3) [30]	0.579 498 (3) [30]
	Lattice	Square	Ruby	Kagome	Honeycomb
Disk	One-patch	0.713 444 50(3)	0.734 894 0(1)	0.745 229 66(5)	0.815 301 86(3)
	Two-patch	0.676 345 5(3)	0.717 490 7(3)	0.687 495 0(2)	0.815 301 6(3)
	Three-patch	0.713 444 6(3)	0.712 619 8(6)	0.725 743 3(6)	0.697 040 4(9)
	Four-patch	0.592 746 5(4)	0.775 605 0(8)	0.687 494 9(4)	0.815 301 9(3)
	Five-patch	0.713 444 4(8)	0.726 257 4(7)	0.745 229 4(8)	0.815 301 8(5)
	Six-patch	0.676 345 4(3)	0.764 013 5(7)	0.652 701 (2)	0.697 040 3(8)
Sphere	One-patch	0.718 297 8(6)	0.740 310 8(3)	0.753 481 7(3)	0.815 301 9(3)
	Two-patch	0.657 338 0(3)	0.706 489 1(8)	0.670 797 2(7)	0.806 134 8(4)
p_c		0.592 746 050 792 10(2) [25]	0.621 812 07(7) [24]	$1 - 2 \sin(\pi/18)$ $= 0.652 703 644\dots$ [35]	0.697 040 230(5) [24]
	Lattice	Four-eight	Cross	Three-twelve	
Disk	One-patch	0.827 011 22(3)	0.835 468 95(7)	0.859 494 83(5)	
	Two-patch	0.827 010 8(2)	0.835 469 0(4)	0.859 495 2(4)	
	Three-patch	0.815 649 0(4)	0.839 888 2(5)	0.859 495 3(5)	
	Four-patch	0.856 560 1(4)	0.865 225 2(7)	0.859 494 7(5)	
	Five-patch	0.815 649 6(4)	0.821 517 4(7)	0.843 143 7(8)	
	Six-patch	0.827 011 3(3)	0.839 888 4(5)	0.903 950 3(5)	
Sphere	One-patch	0.827 533 2(2)	0.835 822 4(4)	0.867 995 5(3)	
	Two-patch	0.818 019 5(4)	0.826 182 5(5)	0.852 055 5(5)	
p_c		0.729 723 2(5) [24]	0.747 800 2(2) [24]	$[1 - 2 \sin(\pi/18)]^{1/2}$ $= 0.807 900 764\dots$ [30]	

and spheres are found to share the same threshold. The thresholds χ_c for one-patch spheres on different lattices also follow the same order as that for one-patch disks, implying that for one-patch spheres χ_c are also mainly influenced by the lattice geometry.

We also get the estimates of y_1 for one-patch spheres on the lattices, as summarized in Table IV. The values of y_1 for one-patch spheres and disks are very close for most lattices. Plots of P_B versus θ or L for one-patch spheres are presented in Fig.S13 and S21 of the SM [31], which demonstrate our estimates of χ_c and y_1 .

B. Numerical results for particles with two to six patches

We also conduct MC simulations for disks with two to six patches and spheres with two patches, on all 11 Archimedean lattices. Plots of P_B versus θ are shown in Fig. S14 to S19 of the SM [31], in which approximate intersections of lines for different sizes can be observed. By fitting the data of P_B near the intersection points, we also obtain precise percolation thresholds for these models, as summarized in Table II. These threshold values are plotted together with those for site percolation, as in Fig. 6.

TABLE III: Probabilities of different patch-covering structures of a particle, for one-patch disks on the frieze and snub square lattices, as a function of χ near estimated χ_c of the two lattices. Bold lines indicate that corresponding edges are covered by the patch of a disk placed on the central vertex. Some details for calculating these probabilities are given in the SM [31].

Lattice	Type	Structure	Probability	Probability Sum
Frieze	3-edge		$2(3/4 - \chi)$	$4 - 5\chi$
			$3(5/6 - \chi)$	
	4-edge		$2(\chi - 7/12)$	$5\chi - 3$
			$\chi - 1/2$	
			$2(\chi - 2/3)$	
	Snub square	3-edge		$2(3/4 - \chi)$
			$3(5/6 - \chi)$	
4-edge			$2(\chi - 7/12)$	$5\chi - 3$
			$2(\chi - 7/12)$	
			$\chi - 2/3$	

TABLE IV: Results of y_1 from fitting the data of the critical polynomial P_B , for one-patch disks or spheres on different Archimedean lattices. Dashed entries indicate that the values cannot be determined with the current data.

Lattice	y_1 (disk)	y_1 (sphere)
Triangular	-4.9(3)	-3.1(1)
Frieze	-3.3(1)	-3.3(1)
Snub square	-3.7(1)	-3.9(1)
Snub hexagonal	—	—
Square	-3.3(4)	-3.5(2)
Ruby	—	—
Kagome	-5.2(4)	-5.4(1)
Honeycomb	-3.7(1)	-4.2(1)
Four-eight	-4.7(4)	-3.9(1)
Cross	—	—
Three-twelve	-3.1(2)	—

1. Two-patch particles

From plots for two-patches particles (disks or spheres) in Fig. 6, comparing with plots for one-patches parti-

cles in Fig. 5, an obvious feature is that the curves become non-monotonic. The local minimum appears at the kagome lattice, for which the symmetry of the two triangles connected to a vertex matches the symmetry of the two patches on a particle. Thus symmetry become very important in determining χ_c values of two-patches particles.

From Table II, if one compares the χ_c values for two-patch particles with those for one-patch particles in more detail, it can be found that, while models of one-patch particles have slightly lower χ_c values on the frieze lattice than on the snub square lattice, models of two-patches particle have slightly higher χ_c values on the frieze lattice than on the snub square lattice. This can also be understood by calculating probabilities of different patch-covering structures of a particle, similar to calculations leading to Table III. For two-patch particles on the snub square lattice, the symmetry of two patches on the particle approximately matches the symmetry of two squares (or two triangles) connected to a vertex, which causes the χ_c value on the snub square lattice to be slightly lower than that on the frieze lattice.

In Sec. III A, for one-patch particles, it is found that differences of χ_c between disks and spheres are very small. However, for two-patch particles, in Fig. 6, it is

seen that on most Archimedean lattices the differences of χ_c between disks and spheres are significantly larger than those for one-patch particles. And on a given lattice, while one-patch spheres has slightly higher χ_c than one-patch disks (except that on the honeycomb lattice one-patch disks and spheres share the same χ_c), two-patch spheres have lower χ_c than two-patch disks. Therefore, though not affecting the order of χ_c values for different lattices, the particle shape is still important in determining the values of χ_c .

To understand the change of χ_c values between one-patch and two-patch particles, for three regular lattices (triangular, square and honeycomb), we plot the probabilities of different patch-covering structures of a particle for χ near χ_c , as in Fig. 7. From Fig. 7(a) and (c), it can be seen that, for one-patch particles, the lower value of χ_c for disks (comparing with that for spheres) is correlated with higher probabilities of large-edge patch-covering structures, e.g., 4-edge and 3-edge for the triangular and square lattices, respectively. From Fig. 7(b),

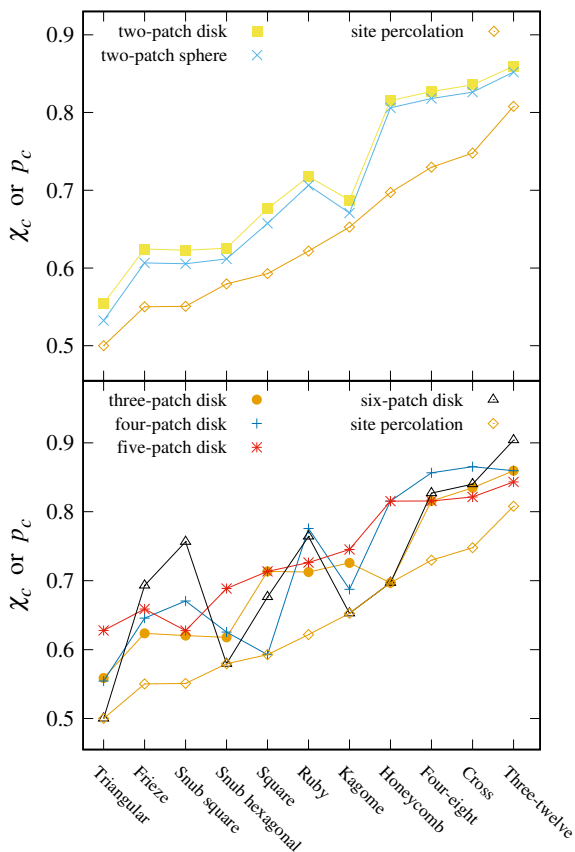


FIG. 6: Plots of percolation thresholds χ_c for particles with two to six patches, and p_c for site percolation, on 11 Archimedean lattices. The values of the thresholds are summarized in Table II, where p_c values come from the cited references. The lines are added to guide the eyes.

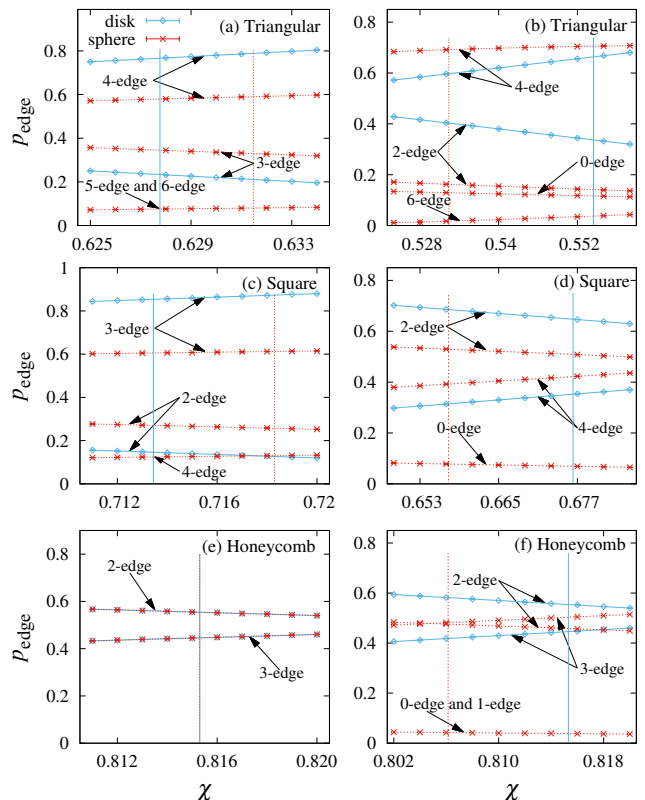


FIG. 7: Probabilities of different patch-covering structures of a particle for χ near χ_c , on the triangular, square and honeycomb lattices. Plots (a), (c) and (e) are for one-patch particles, and plots (b), (d) and (f) are for two-patch particles. Vertical solid and dashed lines indicate values of χ_c for the disks and spheres, respectively. For one-patch disks and spheres on the honeycomb lattice, the probabilities are the same, which leads to the equality of χ_c for spheres and disks.

(d) and (f), one also see that, for two-patch particles, the lower value of χ_c for spheres (comparing with that for disks) is also correlated with higher probabilities of large-edge patch-covering structures, e.g., 4 and 6-edge for the triangular lattice, 4-edge for the square lattice, and 3-edge for the honeycomb lattice.

2. Three- to six-patch disks

For disks with three to six patches, the role of symmetry is more explicitly exhibited. From Fig. 6, it can be seen that curves for these patchy particles are all non-monotonic. Similar to that for two-patch particles at the kagome lattice, the local minimum of χ_c for four-patch disks at the kagome lattice and for five-patch disks at the snub square lattice can also be understood by the approximate matching of the symmetry of patches on a particle and the symmetry of the lattice. From Fig. 6 and Table II, it is interesting to find that χ_c values of

some models are numerically equal to p_c values of site percolation on same lattices, such as three-patch disks on the honeycomb lattice, four-patch disks on the square lattice, six-patch disks on the triangular, snub hexagonal, kagome, and honeycomb lattices. For each of these models, the symmetry of the patches on a particle perfectly matches the symmetry of the lattice, which leads to the fact that patches of a particle either cover all edges connected to the particle center with probability χ or cover no edge with probability $1 - \chi$. Thus the models are exactly equivalent to the corresponding site percolation models with $\chi_c = p_c$. For other models considered, at $\chi = p_c$, the probability of all-edge patch-covering structure is smaller than p_c and other patch-covering structures lead to lower connection. Therefore, their χ_c values should be larger than p_c for site percolation on same lattices, which is supported by results in Table II and can be easily seen in Figs. 5 and 6.

From Table II, it is also interesting to see that, within error bars, χ_c of some different patchy particles on a given lattice share the same value. These include:

- on the triangular (or snub hexagonal, or kagome) lattice, χ_c of one- and five-patch disks, χ_c of two- and four-patch disks;
- on the square lattice, χ_c of one-, three- and five-patch disks, and χ_c of two- and six-patch disks;
- on the honeycomb lattice, χ_c of one-, two-, four-, five-patch disks, and of one-patch spheres, and χ_c of three- and six-patch disks;
- on the four-eight lattice, χ_c of one-, two- and six-patch disks, and χ_c of three- and five-patch disks;
- on the cross lattice, χ_c of one- and two-patch disks, and χ_c of three- and six-patch disks;
- on the three-twelve lattice, χ_c of one- to four-patch disks.

The above equalities of χ_c values can be understood by calculating probabilities of different patch-covering structures of a particle for χ near χ_c . For example, on the honeycomb lattice, for one-patch spheres, it can be verified numerically that, the patch-covering probabilities are equal to those for one-patch disks [e.g., see Fig. 7(e)]. For patchy disks, similar to results in Table III, by analytical calculations we can obtain the probabilities of different patch-covering structures of a particle as a function of χ near χ_c , as presented in the following section. Since percolation of patchy particles can be understood as connection of patch-covering structures of particles at the vertices, and there is only a single percolation threshold for a given model, same expressions (as functions of χ) for these probabilities near χ_c can prove that these equalities of χ_c values hold exactly.

C. Results for disks with an arbitrary number of patches

In the previous subsection, it is found that several models of patchy disks are equivalent with site percolation on same lattices. This result can be generalized to disks with more patches: n -patch ($n > 0$) disks with $\text{mod}(n, 3) = 0$ on the honeycomb lattice, with $\text{mod}(n, 4) = 0$ on the square lattice, with $\text{mod}(n, 6) = 0$ on the triangular, snub hexagonal and kagome lattices, with $\text{mod}(n, 8) = 0$ on the four-eight lattice, with $\text{mod}(n, 12) = 0$ on the frieze, snub square, ruby, cross and three-twelve lattices. These models are equivalent to site percolation since the patches on a disk either cover all edges connecting to the disk center with probability χ or cover no edge with probability $1 - \chi$.

It is also found in previous subsections that several models of patchy disks can share the same χ_c value. Considering the above equivalences with site percolation, and observing these equalities of χ_c values [e.g. on the square lattice the equality of χ_c for disks with one (two) and five (six) patches], we wonder if χ_c values on a given lattice appear in a periodic way as the number of patches n increases, and if there is any other rule governing the χ_c values.

To explore possible periodic behaviors, we first try to calculate probabilities of different patch-covering structures of a disk as a function of χ for three regular lattices (honeycomb, square and triangular), near previously estimated values of χ_c in Table II. Exemplary calculations for the triangular lattice and some calculation details for other two lattices are included in the SM [31]. It is found that indeed there are periodic behaviors for these probabilities of different patch-covering structures, as summarized in Table V. As mentioned in the previous subsection, same expressions as functions of χ for these probabilities near estimated χ_c prove that the equality of χ_c values hold exactly. Thus, from results in Table II, as the number of patches on a disk n increases, χ_c values appear with a period $n_0 = 3, 4$ and 6 for the honeycomb, square and triangular lattices, respectively. Since the snub hexagonal and kagome lattices can be regarded as sub lattices of the triangular lattice, we then calculate probabilities of different patch-covering structures of a disk on these two lattices by making use of the triangular lattice, as shown in Table S5 and S6 of the SM [31]. The results for the snub hexagonal and kagome are also summarized in Table V, which confirm that on these two lattices χ_c values appear with a period $n_0 = 6$.

For calculating probabilities of different patch-covering structures of a patchy disk at a vertex of the four-eight lattice, we can first place the disk at the center of a regular octagon and consider the patch-covering of edges connecting the center and the vertices of the octagon, then use these intermediate results to get the final results. Some details are shown in Tables S7 and S8 of the SM [31], and the final results are also summarized in Table V, which shows that on the four-eight lattice χ_c

TABLE V: Probabilities of different patch-covering structures as a function of χ near χ_c , for n -patch disks on the honeycomb, square, triangular, snub hexagonal, kagome and four-eight lattices. For each lattice, the last row shows estimates of percolation thresholds χ_c by combining numerical estimates in Table II. *Regarding 2-edge structures on the kagome lattice, for n -patch disks with $\text{mod}(n, 6) = 3$, the two edges have a $2\pi/3$ angle, while for disks with $\text{mod}(n, 6) = 2$ or 4 , the two edges are on the same straight line.

		$\text{mod}(n, 3)$				
	Type	1	2			
Honeycomb	0-edge					
	2-edge	$3 - 3\chi$	$3 - 3\chi$			
	3-edge	$3\chi - 2$	$3\chi - 2$			
	χ_c	0.815 301 8(3)	0.815 301 8(3)			
		$\text{mod}(n, 4)$				
	Type	1	2	3		
Square	0-edge					
	2-edge	$3 - 4\chi$	$2 - 2\chi$	$3 - 4\chi$		
	3-edge	$4\chi - 2$		$4\chi - 2$		
	4-edge		$2\chi - 1$			
	χ_c	0.713 444 5(4)	0.676 345 5(4)	0.713 444 5(4)		
		$\text{mod}(n, 6)$				
	Type	1	2	3	4	5
Triangular	2-edge		$2 - 3\chi$		$2 - 3\chi$	
	3-edge	$4 - 6\chi$		$2 - 2\chi$		$4 - 6\chi$
	4-edge	$6\chi - 3$	$3\chi - 1$		$3\chi - 1$	$6\chi - 3$
	6-edge			$2\chi - 1$		
	χ_c	0.627 765 5(2)	0.554 469 6(4)	0.558 806 6(7)	0.554 469 6(4)	0.627 765 5(2)
		$\text{mod}(n, 6)$				
	Type	1	2	3	4	5
Snub hexagonal	1-edge		$2/3 - \chi$		$2/3 - \chi$	
	2-edge		$4/3 - 2\chi$	$1 - \chi$	$4/3 - 2\chi$	
	3-edge	$10/3 - 4\chi$	$2\chi - 2/3$	$1 - \chi$	$2\chi - 2/3$	$10/3 - 4\chi$
	4-edge	$3\chi - 5/3$	$\chi - 1/3$		$\chi - 1/3$	$3\chi - 5/3$
	5-edge	$\chi - 2/3$		$2\chi - 1$		$\chi - 2/3$
	χ_c	0.688 525 8(3)	0.625 384 9(7)	0.617 753 2(7)	0.625 384 9(7)	0.688 525 8(3)
		$\text{mod}(n, 6)$				
	Type	1	2	3	4	5
Kagome	2-edge	$5/3 - 2\chi$	$2 - 2\chi$	$(2 - 2\chi)^*$	$2 - 2\chi$	$5/3 - 2\chi$
	3-edge	$2/3$				$2/3$
	4-edge	$2\chi - 4/3$	$2\chi - 1$	$2\chi - 1$	$2\chi - 1$	$2\chi - 4/3$
	χ_c	0.745 229 5(5)	0.687 494 9(4)	0.725 743 3(6)	0.687 494 9(4)	0.745 229 5(5)
		$\text{mod}(n, 8)$				
	Type	1 or 7	2 or 6	3 or 5	4	
Four-eight	1-edge			$7/4 - 2\chi$	$1 - \chi$	
	2-edge	$3 - 3\chi$	$3 - 3\chi$	$\chi - 1/2$	$1 - \chi$	
	3-edge	$3\chi - 2$	$3\chi - 2$	$\chi - 1/4$	$2\chi - 1$	
	χ_c	0.827 011 0(1)	0.827 011 0(1)	0.815 649 3(4)	0.856 560 1(4)	

TABLE VI: Probabilities of different patch-covering structures as a function of χ near χ_c , for n -patch disks on the frieze, snub square, ruby, cross and three-twelve lattices. For each lattice, the last row shows estimates of percolation thresholds χ_c by combining numerical estimates in Table II. *On the cross lattice, the 1 and 2-edge structures for n -patch disks with $\text{mod}(n, 12) = 4$ are different from those for disks with $\text{mod}(n, 12) = 3$ or 6.

	Type	$\text{mod}(n, 12)$						
		1 or 11	2 or 10	3 or 9	4 or 8	5 or 7	6	
Frieze	1-edge				$4/3 - 2\chi$	$4/3 - 2\chi$	$1 - \chi$	
	2-edge		$2 - 3\chi$	$3/2 - 2\chi$	$\chi - 1/3$	$\chi - 1/3$		
	3-edge	$4 - 5\chi$	χ	$1/2$	$2/3 - \chi$	$1/6$		
	4-edge	$5\chi - 3$	$2\chi - 1$	$\chi - 1/2$	$2\chi - 2/3$	$1/3$	$1 - \chi$	
	5-edge			$\chi - 1/2$		$\chi - 1/2$	$2\chi - 1$	
	χ_c	0.6723388(1)	0.6243837(6)	0.623505(1)	0.6456716(5)	0.6587628(6)	0.6928990(9)	
Snub square	0-edge					$2/3 - \chi$		
	1-edge					$1/6$		
	2-edge		$2 - 3\chi$	$3/2 - 2\chi$		$1/6$	$1 - \chi$	
	3-edge	$4 - 5\chi$	χ	$1 - \chi$	$2 - 2\chi$	$1/6$	$1 - \chi$	
	4-edge	$5\chi - 3$	$2\chi - 1$	$3\chi - 3/2$	$1/3$	$1/6$		
	5-edge				$2\chi - 4/3$	$\chi - 1/3$	$2\chi - 1$	
χ_c	0.67234635(4)	0.6228329(4)	0.6204119(5)	0.6704843(5)	0.6275574(8)	0.756361(1)		
Ruby	1-edge			$3/2 - 2\chi$		$3/2 - 2\chi$		
	2-edge	$7/3 - 3\chi$	$5/3 - 2\chi$	$\chi - 1/2$	$2 - 2\chi$	$\chi - 1/3$	$2 - 2\chi$	
	3-edge	$2\chi - 2/3$	$2/3$	$1/2$		$1/6$		
	4-edge	$\chi - 2/3$	$2\chi - 4/3$	$\chi - 1/2$	$2\chi - 1$	$\chi - 1/3$	$2\chi - 1$	
	χ_c	0.7348940(1)	0.7174907(3)	0.7126198(6)	0.7756050(8)	0.7262574(7)	0.7640135(7)	
	Cross	1-edge			$1 - \chi$	$(1 - \chi)^*$	$11/12 - \chi$	$1 - \chi$
2-edge		$3 - 3\chi$	$3 - 3\chi$	$1 - \chi$	$(1 - \chi)^*$	$7/6 - \chi$	$1 - \chi$	
3-edge		$3\chi - 2$	$3\chi - 2$	$2\chi - 1$	$2\chi - 1$	$2\chi - 13/12$	$2\chi - 1$	
χ_c		0.8354690(2)	0.8354690(2)	0.8398883(5)	0.8652252(7)	0.8215174(7)	0.8398883(5)	
Three-twelve		1-edge					$11/6 - 2\chi$	$1 - \chi$
		2-edge	$3 - 3\chi$	$3 - 3\chi$	$3 - 3\chi$	$3 - 3\chi$	$1/6$	$1 - \chi$
	3-edge	$3\chi - 2$	$3\chi - 2$	$3\chi - 2$	$3\chi - 2$	$2\chi - 1$	$2\chi - 1$	
	χ_c	0.8594950(4)	0.8594950(4)	0.8594950(4)	0.8594950(4)	0.8431437(8)	0.9039503(5)	

values appear with a period $n_0 = 8$. Similarly, we can make use of the regular dodecagon to get probabilities of different patch-covering structures of a patchy disk at a vertex of other five Archimedean lattice in 2D. Some details for these calculations are included in Tables S9 to S23 of the SM [31]. Final results for these five lattices are summarized in Table VI, which prove that χ_c values on these lattices appear with a period $n_0 = 12$.

It should be noted that, for the lattices with periods $n_0 = 12$ and 8, when performing the calculations for probabilities of different patch-covering structures of a disk, we have made use of an assumed symmetry from observing expressions of other lattices. Namely, for the honeycomb, square, triangular, snub hexagonal and kagome lattices, it is found that there is a symmetry between models with $\text{mod}(n, n_0) = m$ ($0 < m < n_0/2$) and $\text{mod}(n, n_0) = n_0 - m$. Our results confirm that indeed this symmetry also holds for the lattices with $n_0 = 8$ and 12. This symmetry allows us to give the χ_c values of patchy disks with $\text{mod}(n, n_0) > 6$, without performing additional numerical simulations. We have tried to understand this symmetry by observing the patch-covering structures, and found that this symmetry is associated with some symmetries of the structures, as shown in Fig. S25 of the SM [31], but we have not got a simple reasoning why this symmetry exists.

We also note that, for a fixed value of j , when probabilities of j -edge patch-covering are the same for different models, the detailed structures with j -edge patch-covering still can be different. This can be clearly seen from Table III. Here, for Table V, on the kagome lattice, though probabilities of j -edge patch-covering are the same for n -patch disks with $\text{mod}(n, 6) = 2, 3$ and 4, the detailed structures of 2-edge patch-covering for disks with $\text{mod}(n, 6) = 3$ are different from those with $\text{mod}(n, 6) = 2$ and 4. Since 2-edge structures for disks with $\text{mod}(n, 6) = 2$ and 4 are more open than those for disks with $\text{mod}(n, 6) = 3$, the χ_c value of the latter is larger than that of the other two. Similarly, on the cross lattice, since the 2-edge structures for disks with $\text{mod}(n, 12) = 3$ and 6 are more open than that for disks with $\text{mod}(n, 12) = 4$, the χ_c value of the latter is larger than that of the former two.

IV. CONCLUSION AND DISCUSSION

To summarize, we study in this work the percolation of patchy particles which are randomly rotating on 11 Archimedean lattices in 2D. We combine MC simulations with the recently developed critical polynomial method to give precise estimates of the threshold values χ_c for 88 models, including disks with one to six patches and spheres with one to two patches, on the 11 lattices. These estimates are summarized in Table II. For one-patch particles, it is found that χ_c values on different lattices follow the same order as p_c values for site percolation on same lattices, which implies that in this case χ_c is mainly in-

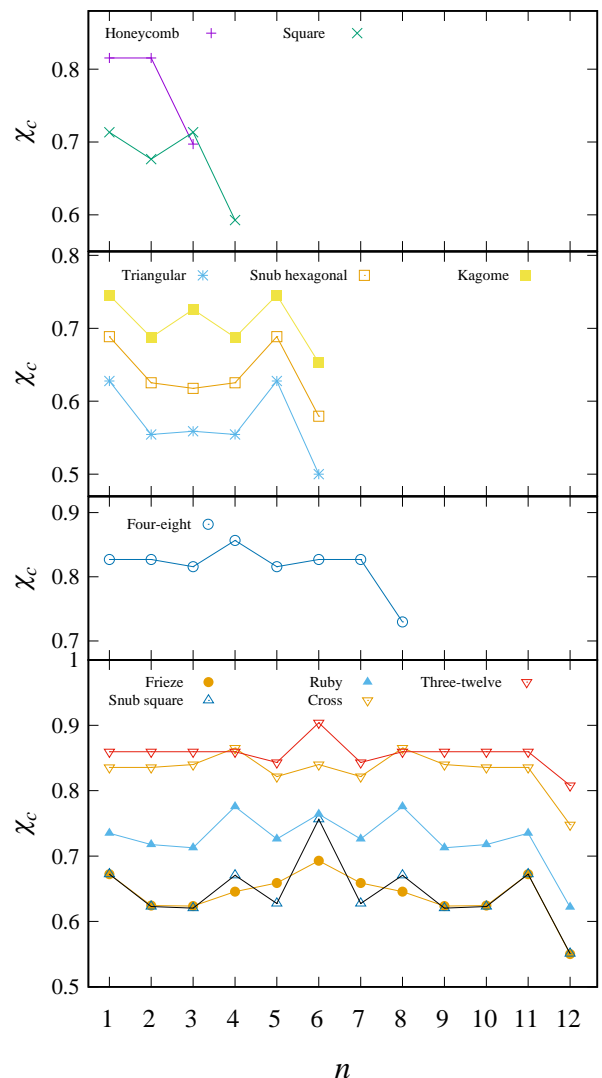


FIG. 8: The percolation threshold χ_c versus the number of patches on a disk n . As n increases, χ_c values appear in periodic ways, with the period being $n_0 = 3$ for the honeycomb lattice, $n_0 = 4$ for the square lattice, $n_0 = 6$ for the triangular, snub hexagonal and kagome lattices, $n_0 = 8$ for the four-eight lattice, and $n_0 = 12$ for the remaining five lattices. For each lattice, the minimum threshold value χ_{\min} appears when $\text{mod}(n, n_0) = 0$, and χ_{\min} is equal to the threshold p_c of site percolation on the same lattice. Moreover, χ_c for $\text{mod}(n, n_0) = m$ ($0 < m < n_0/2$) is the same as χ_c for $\text{mod}(n, n_0) = n_0 - m$. Detailed values of χ_c (or p_c) can be read from Table II for $\text{mod}(n, n_0) = 0$, and from Tables V and VI for $\text{mod}(n, n_0) \neq 0$.

fluenced by the geometry of the lattices. When there are more symmetrically distributed patches on a particle, the symmetry of the patches play an important role, in addition to the geometry of the lattices. The χ_c values on different lattices do not follow the same order as those for one-patch particles.

Furthermore, to explore the role of symmetry, we con-

sider χ_c of disks with an arbitrary number ($n > 0$) of symmetrically distributed patches. By analyzing probabilities of different patch-covering structures of a patchy disk at a vertex as functions of χ near the above estimates of χ_c , we give χ_c values for these n -patch disks on all 11 Archimedean lattices in 2D. The χ_c values are plotted in Fig. 8, in which the following rules are summarized: (i) for a given lattice, χ_c values appear in a periodic way, with the period n_0 determined by the symmetry of the lattice. We find that $n_0 = 3$ for the honeycomb lattice, $n_0 = 4$ for the square lattice, $n_0 = 6$ for the triangular, snub hexagonal and kagome lattices, $n_0 = 8$ for the four-eight lattice, and $n_0 = 12$ for the remaining five lattices. (ii) the minimum threshold value χ_{\min} of a lattice presents when $\text{mod}(n, n_0) = 0$. Actually, at this condition, the model is equivalent to site percolation on the same lattice, with χ_{\min} being equal to the site-percolation threshold p_c , whose value is given in Table II. (iii) for each lattice, χ_c for $\text{mod}(n, n_0) = m$ ($0 < m < n_0/2$) is the same as that for $\text{mod}(n, n_0) = n_0 - m$. In addition, we find that there exist other equalities between χ_c values, such as χ_c values of disks with $\text{mod}(n, 8) = 1$ and 2 on the four-eight lattice, those of disks with $\text{mod}(n, 12) = 1$ and 2, and of disks with $\text{mod}(n, 12) = 3$ and 6, both on the cross lattice, and those of disks with $\text{mod}(n, 12) = 1, 2, 3$ and 4 on the three-twelve lattice. The precise values of χ_c for n -patch disks with $\text{mod}(n, n_0) \neq 0$ are summarized in Tables V and VI.

Precise values of χ_c for one- and two-patch spheres are also available in Table II. Comparing with one- and two-patch disks, our numerical results for the spheres suggest that changing the shape from disk to sphere does not affect the order of χ_c values for different lattices, but does affect the values of χ_c . It may be interesting to investigate χ_c of spheres with more patches, since more symmetries of patches are available on the sphere surface. Besides, the current work can also be extended to other lattices. One example is the Lieb lattice in 2D. Percolation of four-patch disks on this lattice is equivalent to site percolation on the same lattice. Similar to the results in Sec. III B, this can be proved as the patches on a disk either cover all neighboring edges with probability χ or cover no edge with probability $1 - \chi$. By MC simulations of site percolation and the critical polynomial method, we determine the threshold value as $\chi_c = p_c = 0.739\,706\,0(6)$ [31], which is much more precise than a recent estimate $0.739\,6(5)$ [36]. It should be noted

that site percolation on the Lieb lattice in 2D is equivalent to site-bond percolation on the square lattice with same site and bond occupation probabilities, for which empirical formulas combined with latest threshold values of both pure bond and pure site percolation lead to $p_c \simeq 0.742\,2$ [37] or $p_c \simeq 0.737\,6$ [38]. These values are quite close to our estimate above.

In the above models, we assume that each particle is randomly rotating with its center being fixed at a vertex of the lattice. For a system in which there are interactions between patchy particles, this corresponds to the high-temperature limit of the system at full occupancy of the lattice. Since there is no correlation between different particles, the universality class of the percolation transitions is the same as ordinary percolation in 2D. It will be interesting to investigate the interplay of percolation and different thermodynamic phases for patchy particles at finite temperatures on lattices in 2D [8–10], where universal properties might be different. Percolation and phase transitions of patchy particles in continuum space in 2D also demand more investigations [39, 40].

Finally, we note that our calculation of the probabilities of different patch-covering structures of a particle implies a new way to define the models: the “patch-covering” structures of a particle can be regarded as discrete states of a vertex, and various states of a vertex occur with different probabilities. This transforms the continuously rotating particle model to a discrete “spin” model on the lattices, for which more efficient numerical simulations may be performed. New models are obtained if one allows the states to be different from those of the patchy particles.

Acknowledgments

J. Wang and H. Hu thank W. Xu and Y. Deng for a previous collaboration on combining MC simulations and the critical polynomial method to study nonplanar and continuum percolation models [28]. This work was supported by the National Natural Science Foundation of China under Grant No. 11905001, and by the Anhui Provincial Natural Science Foundation under Grant No. 1908085QA23. We also acknowledge the High-Performance Computing Platform of Anhui University for providing computing resources.

-
- [1] A. Walther and A. H. E. Mueller, Janus particles: synthesis, self-assembly, physical properties, and applications, *Chem. Rev.* **113**, 5194 (2013).
 [2] J. Zhang, B. A. Grzybowski and S. Granick, Janus particle synthesis, assembly, and application, *Langmuir* **28**, 6964 (2017).
 [3] F. Sciortino and E. Zaccarelli, Equilibrium gels of limited

- valence colloids, *Cur. Opin. Colloid Interface Sci.* **30**, 90 (2017).
 [4] F. Smalenburg, L. Filion and F. Sciortino, Erasing nonman’s land by thermodynamically stabilizing the liquid-liquid transition in tetrahedral particles, *Nat. Phys.* **10**, 653 (2014).
 [5] Q. Chen, S. C. Bae and S. Granick, Directed self-

- assembly of a colloidal kagome lattice, *Nature* **469**, 381 (2011).
- [6] X. M. Mao, Q. Chen and S. Granick, Entropy favours open colloidal lattices, *Nat. Mater.* **12**, 217 (2013).
- [7] Z. W. Li, Y. W. Sun, Y. H. Wang, Y. L. Zhu, Z. Y. Lu and Z. Y. Sun, Kinetics-controlled design principles for two-dimensional open lattices using atom-mimicking patchy particles, *Nanoscale* **12**, 4544 (2020).
- [8] K. Mitsumoto and H. Yoshino, Orientational ordering of closely packed Janus particles, *Soft Matter* **14**, 3919 (2018).
- [9] A. Patrykiewicz and W. Rzyśko, Order-disorder transitions in systems of Janus-like particles on a triangular lattice, *Physica A* **548**, 123883 (2020).
- [10] A. Patrykiewicz and W. Rzyśko, Two-dimensional Janus-like particles on a triangular lattice, *Soft Matter* **16**, 6633-6642 (2020).
- [11] D. Stauffer and A. Aharony, *Introduction to Percolation Theory*, 2nd ed. (Taylor & Francis, London, 1994).
- [12] A. A. Saberi, Recent advances in percolation theory and its applications, *Phys. Rep.* **578**, 1 (2015).
- [13] F. Seiferling, D. de las Heras and M. M. T. da Gama, Percolation in binary and ternary mixtures of patchy colloids, *J. Chem. Phys.* **145**, 074903 (2016).
- [14] J. L. B. de Araújo, F. F. Munarin, G. A. Farias, F. M. Peeters and W. P. Ferreira, Structure and reentrant percolation in an inverse patchy colloidal system, *Phys. Rev. E* **95**, 062606 (2017).
- [15] L. L. Treffenstädt, N. A. M. Araújo and D. de las Heras, Percolation of functionalized colloids on patterned substrates, *Soft Matter* **14**, 3572 (2018).
- [16] G. Wang and J. W. Swan, Surface heterogeneity affects percolation and gelation of colloids: dynamic simulations with random patchy spheres, *Soft Matter* **15**, 5094 (2019).
- [17] J. Song, M. H. Rizvi, B. B. Lynch, J. Ilavsky, D. Mankus, J. B. Tracy, G. H. McKinley and N. Holtan-Andersen, Programmable anisotropy and percolation in supramolecular patchy particle gels, *ACS Nano* **14**, 17018-17027 (2021).
- [18] M. J. Kartha and A. G. Banpurkar, Why patchy diffusion-limited aggregation belongs to the directed-percolation universality class, *Phys. Rev. E* **94**, 062108 (2016).
- [19] C. R. Scullard and R. M. Ziff, Critical surfaces for general bond percolation problems, *Phys. Rev. Lett.* **100**, 185701 (2008).
- [20] C. R. Scullard and R. M. Ziff, Critical surfaces for general inhomogeneous bond percolation problems, *J. Stat. Mech.* **P03021** (2010).
- [21] C. R. Scullard, Polynomial sequences for bond percolation critical thresholds, *J. Stat. Mech.* **P09022** (2011).
- [22] C. R. Scullard, Percolation critical polynomials as a graph invariant, *Phys. Rev. E* **86**, 041131 (2012).
- [23] C. R. Scullard and J. L. Jacobsen, Transfer matrix computation of generalized critical polynomials in percolation, *J. Phys. A: Math. Theor.* **45**, 494004 (2012).
- [24] J. L. Jacobsen, High-precision percolation thresholds and Potts-model critical manifolds from graph polynomials, *J. Phys. A: Math. Theor.* **47**, 135001 (2014).
- [25] J. L. Jacobsen, Critical points of Potts and $O(N)$ models from eigenvalue identities in periodic Temperley-Lieb algebras, *J. Phys. A: Math. Theor.* **48**, 454003 (2015).
- [26] C. R. Scullard and J. L. Jacobsen, Potts - model critical manifolds revisited, *J. Phys. A: Math. Theor.* **49**, 125003 (2016).
- [27] C. R. Scullard and J. L. Jacobsen, Bond percolation thresholds on Archimedean lattices from critical polynomial roots, *Phys. Rev. Res.* **2**, 012050(R) (2020).
- [28] W. H. Xu, J. F. Wang, H. Hu and Y. J. Deng, Critical polynomials in the nonplanar and continuum percolation models, *Phys. Rev. E* **103**, 022127 (2021).
- [29] B. Grünbaum and G. C. Shephard, *Tillings and Patterns* (Freeman, New York, 1987).
- [30] P. N. Suding and R. M. Ziff, Site percolation thresholds for Archimedean lattices, *Phys. Rev. E* **60**, 275 (1999).
- [31] The Supplemental Material is available at: <http://xxx>.
- [32] R. P. Langlands, C. Pichet, Ph. Pouliot and Y. Saint-Aubin, On the universality of crossing probabilities in two-dimensional percolation, *J. Stat. Phys.* **67**, 553 (1992).
- [33] H. T. Pinson, Critical percolation on the torus, *J. Stat. Phys.* **75**, 1167 (1994).
- [34] M. P. Nightingale in *Finite-size Scaling and Numerical Simulation of Statistical Systems*, edited by V. Privman (World Scientific, Singapore, 1990).
- [35] M. F. Sykes and J. W. Essam, Exact critical percolation probabilities for site and bond problems in two dimensions, *J. Math. Phys.* **5**, 1117 (1964).
- [36] W. S. Oliveira, J. P. de Lima, N. C. Costa and R. R. dos Santos, Percolation on Lieb lattices, *Phys. Rev. E* **104**, 064122 (2021).
- [37] M. Yanuka and R. Engelman, Bond-site percolation: empirical representation of critical probabilities, *J. Phys. A: Math. Gen.* **23**, L339 (1990).
- [38] Y. Y. Tarasevich, S. van der Marck, An investigation of site-bond percolation on many lattices, *Int. J. Mod. Phys. C* **10**(7), 1193 (1999).
- [39] T. Huang, Y. Han and Y. Chen, Melting and solid-solid transitions of two-dimensional crystals composed of Janus spheres, *Soft Matter* **16**, 3015 (2020).
- [40] Y. H. Liang, B. Ma and M. O. de la Cruz, Reverse order-disorder transition of Janus particles confined in two dimensions, *Phys. Rev. E* **103**, 062607 (2021).

Supplemental material for: “Percolation thresholds of randomly rotating patchy particles on Archimedean lattices”

Quancheng Wang,¹ Zhenfang He,¹ Junfeng Wang,² and Hao Hu^{1,*}

¹*School of Physics and Electronic Engineering, Anhui University, Hefei, Anhui 230601, China*

²*School of Physics, Hefei University of Technology, Hefei, Anhui 230009, China*

Further simulation details. In our simulations, the vertices and edges of lattices are encoded with the aid of square or triangular arrays, whose correspondences with the actual lattices are shown below in Figs. S1 to S11. For each figure (except the figure for the square or triangular lattice), the plot on the left side shows the array for encoding, and the one on the right side shows the actual lattice. On the square or triangular array, a region of size $L_x \times L_y$ is shown, whose correspondence in the actual lattice is also drawn, with the length of each edge being one. The linear size in the main text is defined as $L \equiv L_x$. The number of vertices in each lattice can be calculated from L as shown in Table S1. The number of independent samples taken for one-patch disks on the lattices are summarized in Table S2. The simulation time consumed for each model is presented in Table S3.

More plots for estimating the thresholds values. In the main text we only show plots for estimating the threshold value of one-patch disks on the triangular lattice. Below Figs. S12 to S19 show the intersection of P_B near the percolation thresholds for other 87 patchy particle models. For one-patch particles, to demonstrate our estimates of the correction exponent y_1 , we also make plots of P_B for small sizes L at the percolation thresholds, as in Figs. S20 and S21. For site percolation on the Lieb lattice in 2D, Fig. S22 demonstrates our estimates of $p_c = 0.739\,706\,0(6)$ and $y_1 \simeq -3.6$.

Calculations for one-patch disks on the frieze lattice. Here we present details for calculating probabilities of different patch-covering structures, for one-patch disks on the frieze lattice. The final results have already been given in Table III of the main text. Calculations for other patchy particles on the frieze or other lattices can be performed in a similar way.

When a one-patch disk rotates randomly at a vertex of the frieze lattice, for patch sizes χ near $\chi_c = 0.672\,338\,8(1)$, there exist only 3-edge and 4-edge patch-covering structures. There are two types of 3-edge patch-covering structures: one type has the blank sector covering two edges at an angle of $\pi/2$, as shown in Fig. S23 (a) and (b); and the other type has the blank sector covering two edges at an angle of $\pi/6$, as shown in Fig. S23 (c), (d) and (e). For the first type, if not changing the patch-covering states of edges, the disk can rotate within an angle $\chi_{3,1}$ (values of χ , χ_i or $\chi_{i,j}$ are angles in units of 2π), whose value can be calculated as

$$\chi_{3,1} = 1 - \chi - \frac{1}{4} = \frac{3}{4} - \chi. \quad (\text{S1})$$

For the other type, if not changing the patch-covering states, the disk can rotate within another angle $\chi_{3,2}$ as

$$\chi_{3,2} = 1 - \chi - \frac{1}{6} = \frac{5}{6} - \chi. \quad (\text{S2})$$

Thus the probability of 3-edge patch-covering structures is the summation of $\chi_{i,j}$ corresponding to Fig. S23 (a-e)

$$\chi_3 = 2\chi_{3,1} + 3\chi_{3,2} = 4 - 5\chi. \quad (\text{S3})$$

There are three types of 4-edge patch-covering structures: the first type has the blank sector covering edge 3 or 1, as shown in Fig. S23 (f) and (g), respectively; the second type has the blank sector covering edge 2, as shown in Fig. S23 (h); and the last type has the blank sector covering edge 5 or 4, as shown in Fig. S23 (i) and (j), respectively. The angles the disk can rotate without changing the patch-covering states of edges are correspondingly given for the three types as

$$\chi_{4,1} = \frac{1}{4} + \frac{1}{6} - (1 - \chi) = \chi - \frac{7}{12}, \quad (\text{S4})$$

$$\chi_{4,2} = \frac{1}{4} \times 2 - (1 - \chi) = \chi - \frac{1}{2}, \quad (\text{S5})$$

*Corresponding author: huhao@ahu.edu.cn

$$\chi_{4,3} = \frac{1}{6} \times 2 - (1 - \chi) = \chi - \frac{2}{3} . \quad (\text{S6})$$

Thus the total probability of 4-edge structures is

$$\chi_4 = 2\chi_{4,1} + \chi_{4,2} + 2\chi_{4,3} = 5\chi - 3 . \quad (\text{S7})$$

Calculations for disks with an arbitrary number of patches. Here we present details for obtaining probabilities of different patch-covering structures in Tables V and VI of the main text. We take the model of n -patch (n being positive integers) disks on the triangular lattice as an example to illustrate the calculations, and perform calculations on other lattices in a similar way.

For n -patch disks on the triangular lattice, we classify the particles by their values of $\chi \pmod{(n,6)}$ and conduct calculation for each value of $\chi \pmod{(n,6)}$. For the case of $\chi \pmod{(n,6)} = 1$ ($n = 6m + 1$, with m being non-negative integers), the assumed value of χ_c is 0.627 765 5(2), as taken from the main text. For χ near χ_c , there are two types of patch-covering structures, i.e. 3-edge and 4-edge structures, and it can be proved that (the 3 or 4) edges are covered by the patches consecutively. For convenience, we label patches and edges in a counterclockwise way, as exemplified for seven-patch disks in Fig. S24. Initially we set the right (assuming the observer stands at the disk center and faces outwards) boundary of patch 1 at edge 1 of the lattice. When the disk rotates counterclockwise within an angle χ_1 , the structure always belongs to the 3-edge type; and when the disk rotates clockwise within an angle χ_2 , the structure always belongs to the 4-edge type. The values of χ_1 and χ_2 are determined as follows.

When the disk rotates counterclockwise by a small angle, for calculating χ_1 , since initially edges 2, 3 and 4 are being covered by the patches, the structure only changes its type if these three edges keep being covered and a new edge (5 or 6) becomes covered. The angle between edge 5 and the nearest patch to its right side is

$$\chi_{5,\text{right}} = 2m \cdot \frac{1}{n} + \frac{1 - \chi}{n} - \frac{1}{3} . \quad (\text{S8})$$

Here $1/3$ is the fraction of the disk between edge 5 and edge 1; $1/n$ is the fraction the disk occupied by a patch and a neighboring blank sector, and there are $2m + 1/3$ such units between edge 5 and edge 1; and $(1 - \chi)/n$ is the fraction of the disk occupied by a blank sector. We also derive the angle between edge 6 and the nearest patch to its right side as

$$\chi_{6,\text{right}} = m \cdot \frac{1}{n} + \frac{1 - \chi}{n} - \frac{1}{6} . \quad (\text{S9})$$

Since $\chi_{6,\text{right}} - \chi_{5,\text{right}} = 1/[6(6m + 1)] > 0$, when the disk rotates counterclockwise, the patches cover edge 5 earlier than edge 6. If representing $\chi_{k,\text{right}}$ as the angle between edge k ($k = 2, 3, 4$) and the right boundary of the patch covering the edge, in a similar way, we get $\chi_{5,\text{right}} < \chi_{k,\text{right}}$, which means that, when the disk rotates counterclockwise, the patches encounter edge 5 before leaving edge k . Thus we have $\chi_1 = \chi_{5,\text{right}}$, and by substituting $n = 6m + 1$ to Eq. (S8) we get

$$\chi_1 = \frac{1 - \chi}{n} + \frac{n - 1}{3} \cdot \frac{1}{n} - \frac{1}{3} . \quad (\text{S10})$$

When the disk rotates clockwise by a small angle, for calculating χ_2 , we need consider when one of edges (2, 3, 4) becomes not covered, and ensures that this happens before any patch covers edge 5 or 6. Using calculations similar to the above, we find that edge 4 is the first one to become uncovered, without covering of edge 5 or 6, and the value of χ_2 is given by

$$\chi_2 = \frac{\chi}{n} + \frac{n - 1}{2} \cdot \frac{1}{n} - \frac{1}{2} . \quad (\text{S11})$$

Starting from the initial condition above, if the disk rotates persistently in counterclockwise direction, one shall observe changes of patch-covering structures in a periodic way: within an angle χ_1 it belongs to the 3-edge type, within another angle χ_2 it belongs to the 4-edge type, and this repeats six times within a total interval of $1/n$, where $1/n$ is the angle of a patch and a blank sector. Each time the patch-covering structure changes its type, the boundary of one patch is at an edge, and the patch is to the left or right side of the edge. These are exemplified using the seven-patch disk in Fig. S24. After a rotation of total angle $1/n$, the condition is the same as the initial condition, except that the label of the patch is different. Thus we get the probability of 3-edge structure as

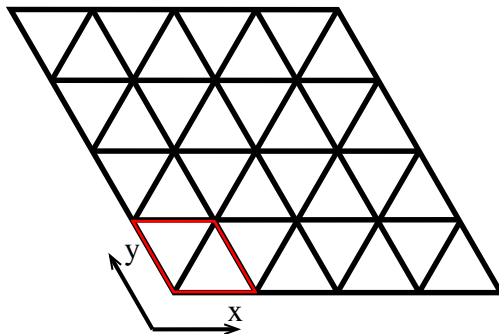
$$\chi_1 \cdot 6 \cdot n = \left(\frac{1 - \chi}{n} + \frac{n - 1}{3} \cdot \frac{1}{n} - \frac{1}{3} \right) \cdot 6 \cdot n = 4 - 6\chi , \quad (\text{S12})$$

and the probability of 4-edge structure as

$$\chi_2 \cdot 6 \cdot n = \left(\frac{\chi}{n} + \frac{n-1}{2} \cdot \frac{1}{n} - \frac{1}{2} \right) \cdot 6 \cdot n = 6\chi - 3 . \quad (\text{S13})$$

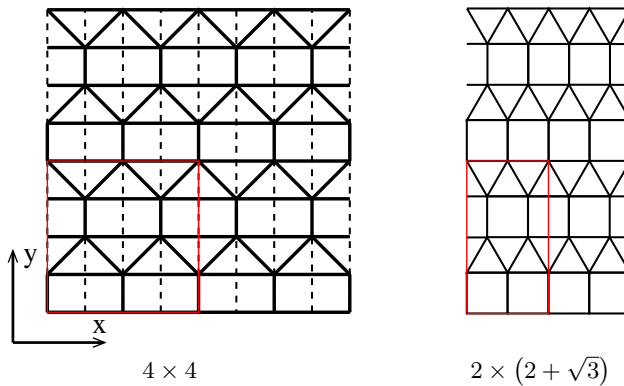
The calculations for other models are performed in a similar way. For cases of $\text{other} \pmod{(n, 6)}$ on the triangular lattice, of $\text{other} \pmod{(n, 4)}$ on the square lattice, and of $\text{other} \pmod{(n, 3)}$ on the honeycomb lattice, the results are summarized in Table S4. For the snub hexagonal and kagome lattices, the results are obtained by using intermediate results on the triangular lattice, as shown in Tables S5 and S6, respectively. For the four-eight lattice, the results are derived by considering patch-covering of a disk at the center of a regular octagon, as shown in Tables S7 and S8. For the remaining five lattices, results are derived by considering patch-covering of a disk at the center of a regular dodecagon, as shown in Tables S9 to S23.

Demonstration for symmetries between n -patch disks with $\text{other} \pmod{(n, n_0)} = m$ and $n_0 - m$. Through the calculations of probabilities of patch-covering structures, we have proved the equality of χ_c values between n -patch disks with $\text{other} \pmod{(n, n_0)} = m$ ($0 < m < n_0/2$) and $n_0 - m$ on a given lattice. To understand this equality, we find that there exist some symmetries between the patch-covering structures, as demonstrated for three regular lattices (honeycomb, square and triangular) in Fig. S25.



1×1

FIG. S1: Triangular lattice.



4×4

$2 \times (2 + \sqrt{3})$

FIG. S2: Frieze lattice.

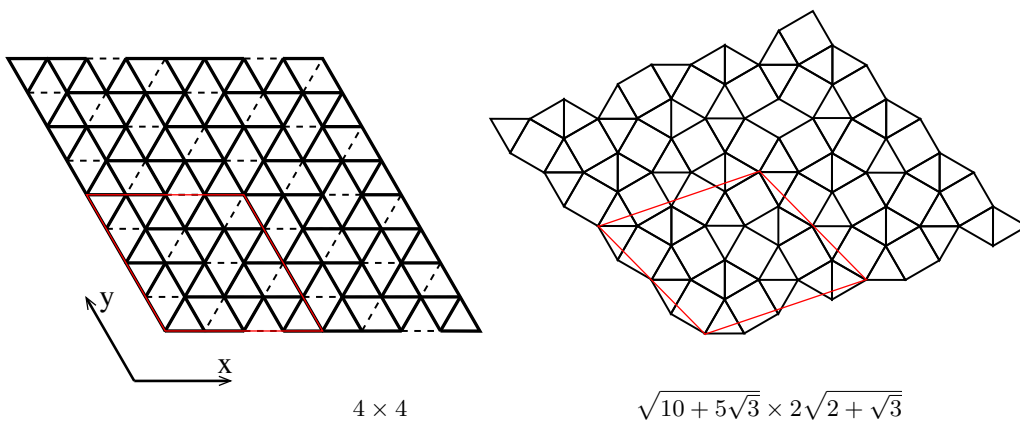


FIG. S3: Snub square lattice.

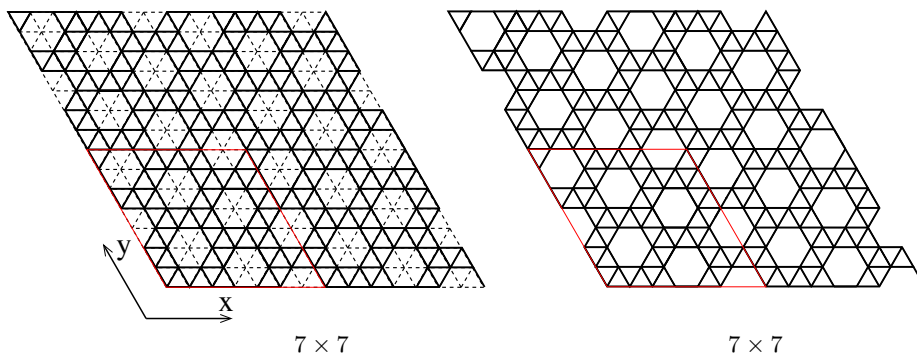


FIG. S4: Snub hexagonal lattice.

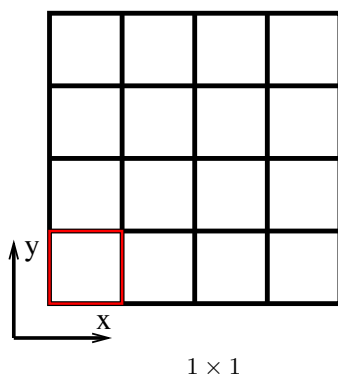


FIG. S5: Square lattice.

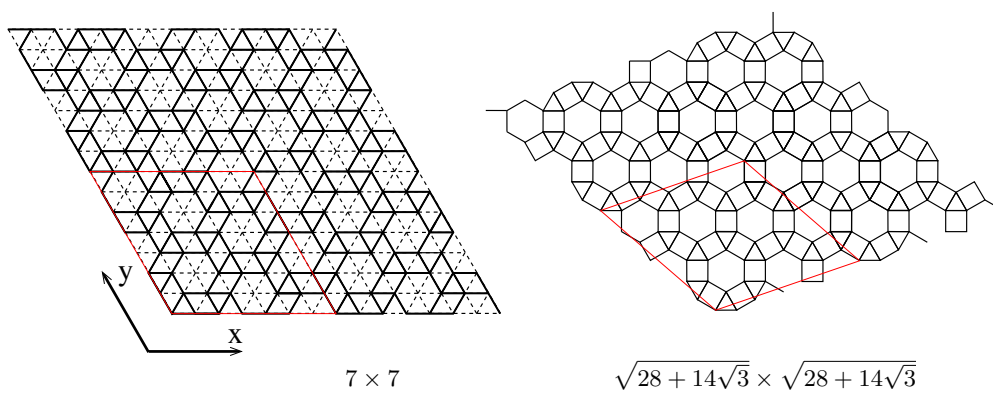


FIG. S6: Ruby lattice.

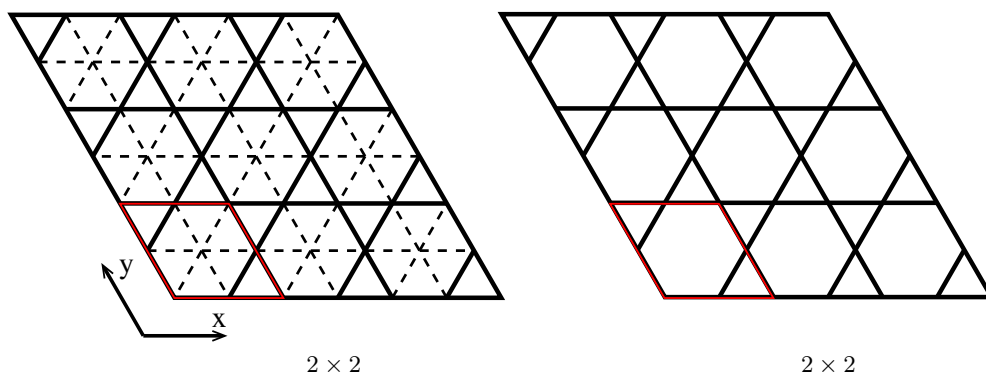


FIG. S7: Kagome lattice.

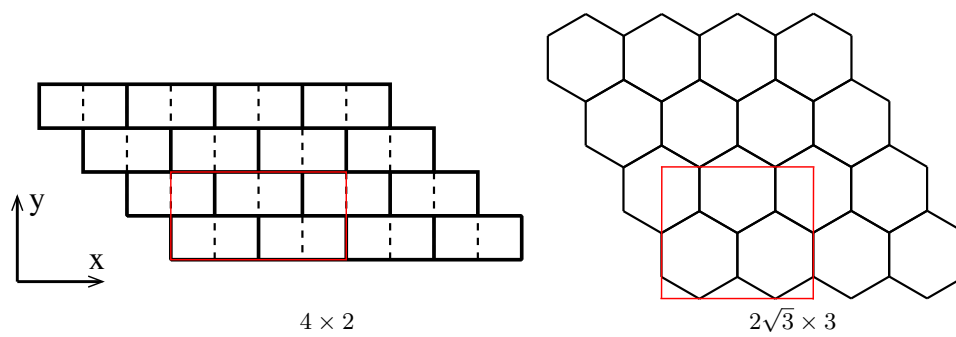


FIG. S8: Honeycomb lattice.

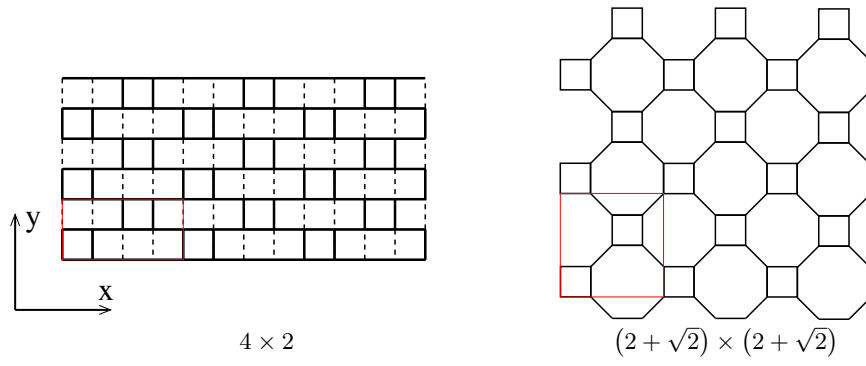


FIG. S9: Four-eight lattice.

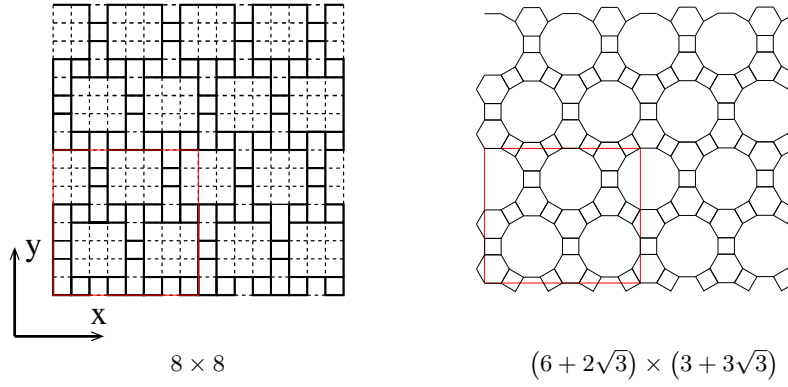


FIG. S10: Cross lattice.

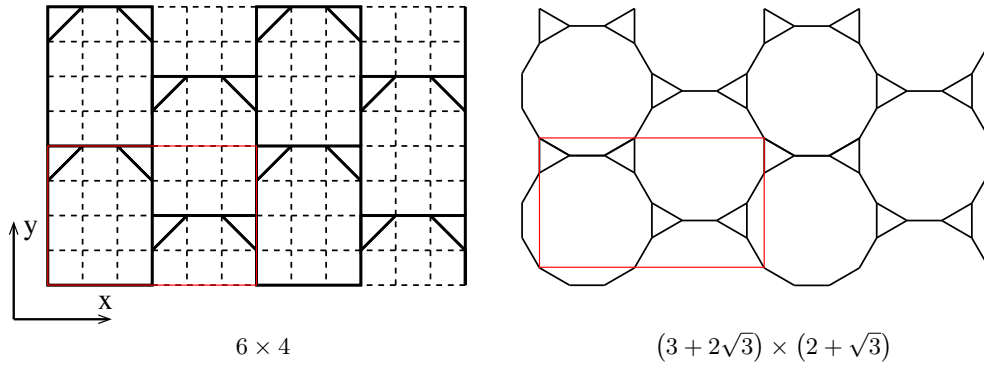


FIG. S11: Three-twelve lattice.

TABLE S1: The number of vertices of Archimedean lattices with the linear size L .

Triangular	Frieze	Snub square	Snub hexagonal	Square	Ruby
L^2	$L^2/2$	L^2	$6L^2/7$	L^2	$6L^2/7$
Kagome	Honeycomb	Four-eight	Cross	Three-twelve	
$3L^2/4$	$L^2/2$	$L^2/2$	$3L^2/4$	$L^2/3$	

TABLE S2: The number of independent samples taken at each patch size θ for one-patch disks on Archimedean lattices. For other models, the sample sizes are smaller but still being larger than or equal to 10^8 .

Triangular	L	2 – 16	32 – 128	256
	Sample size	10^{10}	10^9	10^8
Frieze	L	4 – 16	32 – 128	256
	Sample size	10^{10}	10^9	10^8
Snub square	L	4 – 16	32 – 64	128 – 256
	Sample size	10^{10}	10^9	10^8
Snub hexagonal	L	7 – 35	70 – 140	280
	Sample size	10^{10}	10^9	10^8
Square	L	2 – 16	32 – 128	256
	Sample size	10^{10}	10^9	10^8
Ruby	L	7 – 14	35 – 140	280
	Sample size	10^{10}	10^9	10^8
Kagome	L	2 – 16	32 – 128	256
	Sample size	10^{10}	10^9	10^8
Honeycomb	L	4 – 32	64 – 256	512
	Sample size	10^{10}	10^9	10^8
Four-eight	L	4 – 32	64 – 256	512
	Sample size	10^{10}	10^9	10^8
Cross	L	8 – 16	32 – 128	256
	Sample size	10^{10}	10^9	10^8
Three-twelve	L	6 – 24	48 – 192	384
	Sample size	10^{10}	10^9	10^8

TABLE S3: Simulation time for patchy particles on Archimedean lattices. The unit of time is one hour, using one processor of an Intel Xeon Scalable Gold 6130 CPU under the hyper-threading mode.

Lattice	Disk						Sphere	
	One-patch	Two-patch	Three-patch	Four-patch	Five-patch	Six-patch	One-patch	Two-patch
Triangular	28276	7213	333	5906	856	2594	7308	1279
Frieze	45676	3221	2358	2179	1380	2768	1401	1149
Snub square	26817	2158	1042	459	1235	771	4086	579
Snub hexagonal	44204	2869	2375	2912	1346	1021	6741	466
Square	38914	3982	818	2012	1025	2491	3186	1518
Ruby	48448	7251	1392	4147	1184	1311	12140	611
Kagome	29382	4825	1171	1785	648	1254	5453	345
Honeycomb	60222	1886	3429	14547	1149	1386	7381	345
Four-eight	52055	3506	531	1068	2056	1451	8403	676
Cross	16923	11950	1738	442	1136	1184	5542	278
Three-twelve	63629	1567	702	644	904	1639	17737	627

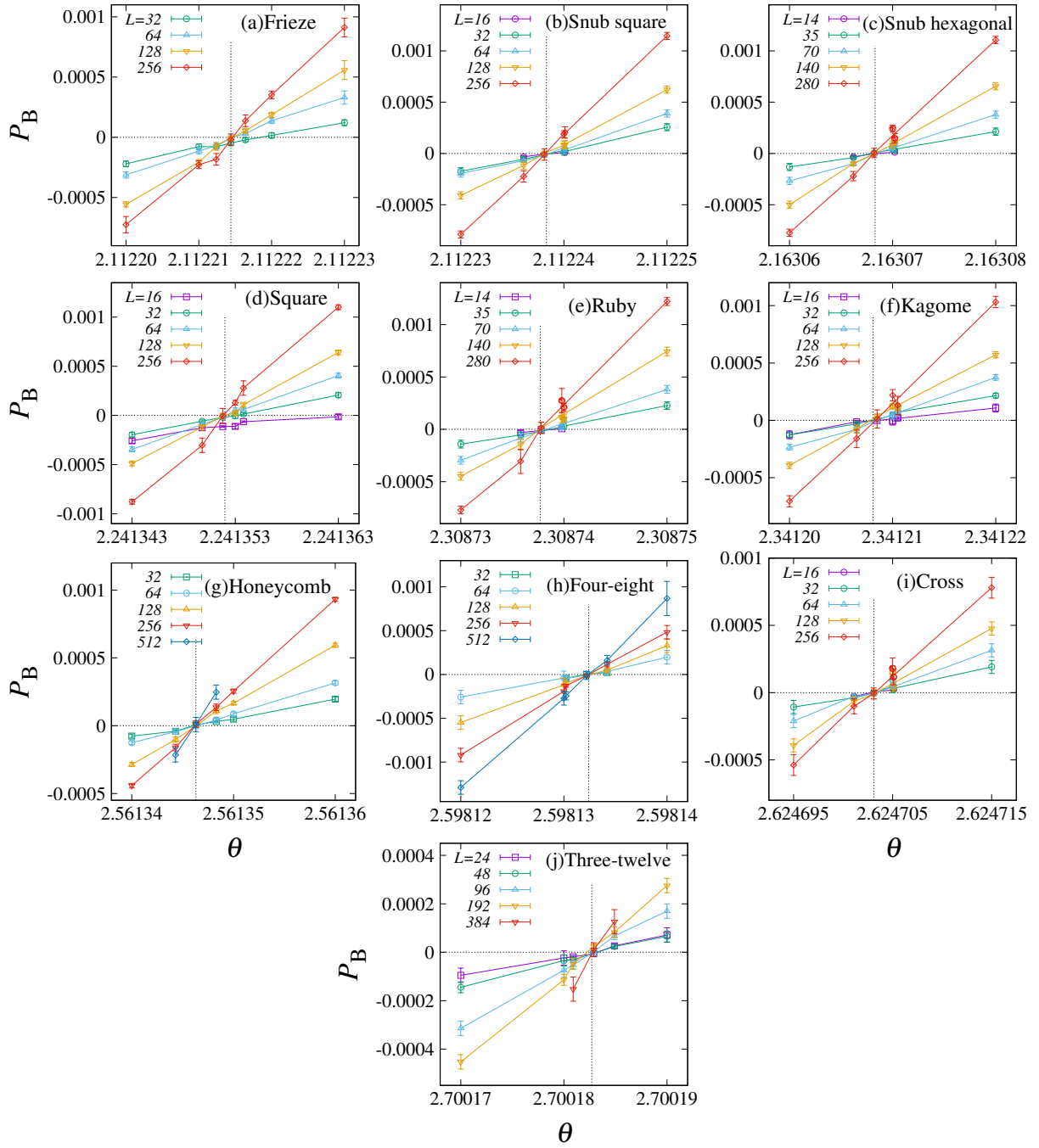


FIG. S12: Intersection plots for one-patch disks on different lattices. The vertical dashed lines show the estimated threshold values θ_c .

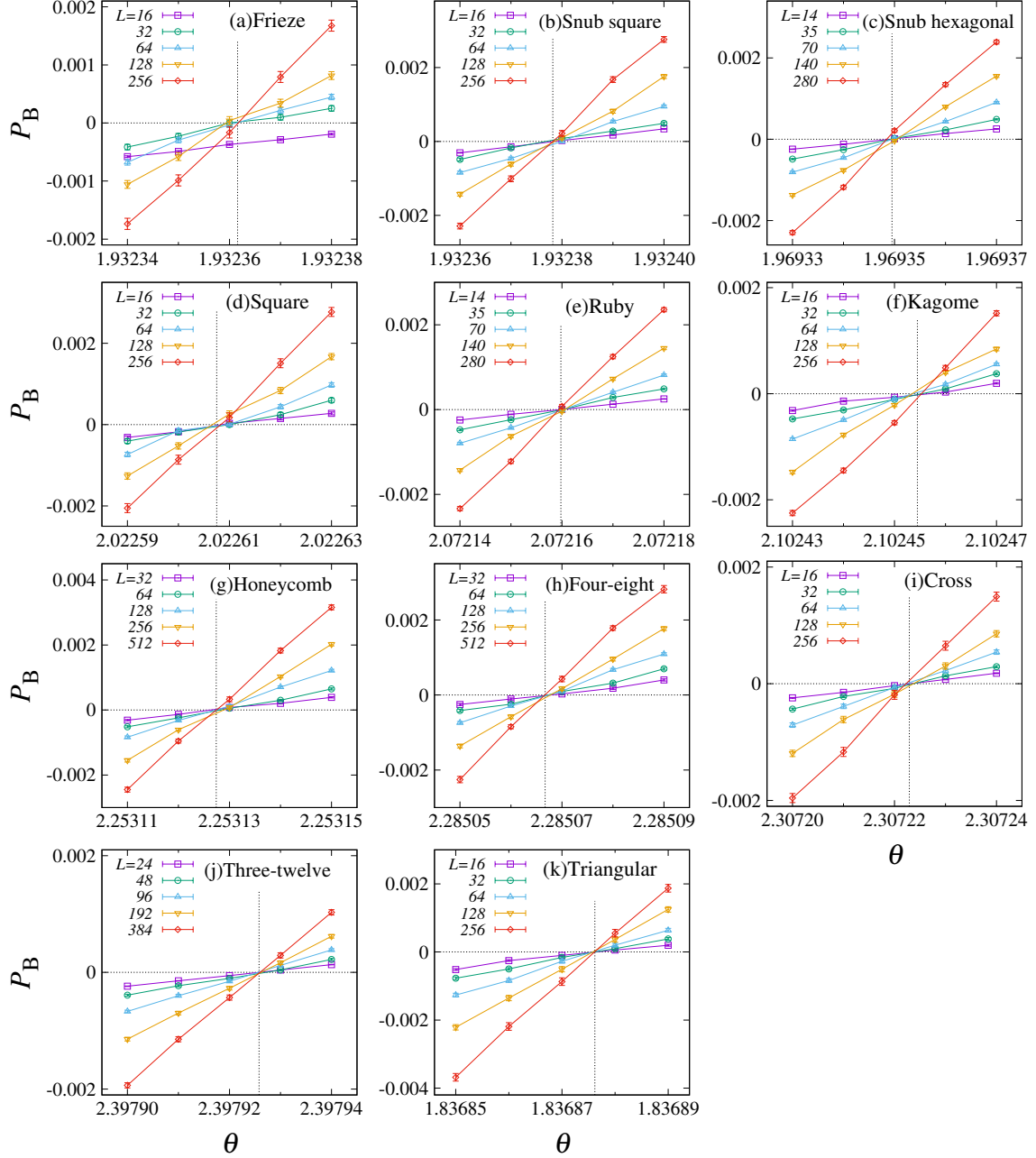


FIG. S13: Intersection plots for one-patch spheres on different lattices. The vertical dashed lines show the estimated threshold values θ_c .

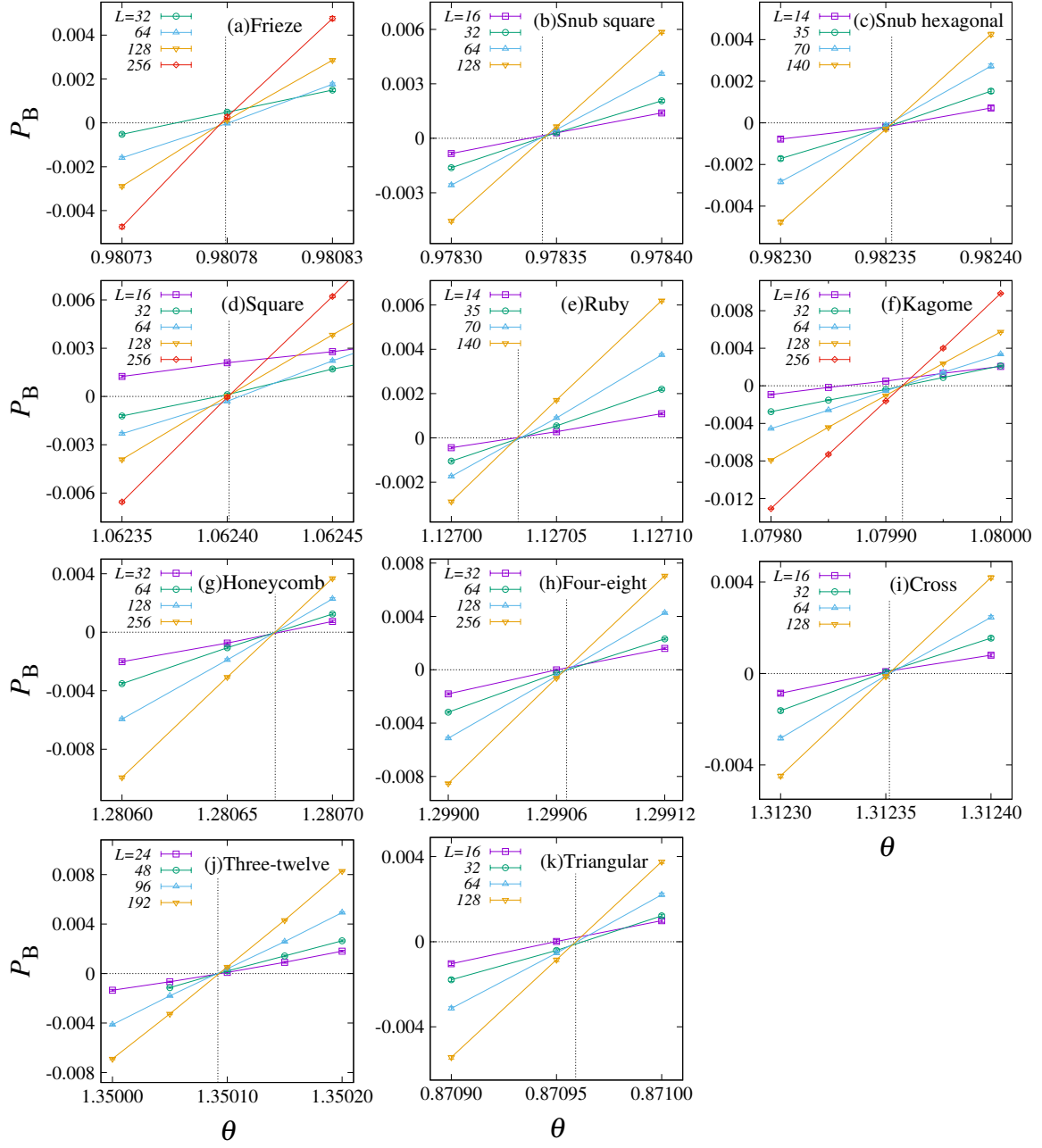


FIG. S14: Intersection plots for two-patch disks on different lattices. The vertical dashed lines show the estimated threshold values θ_c .

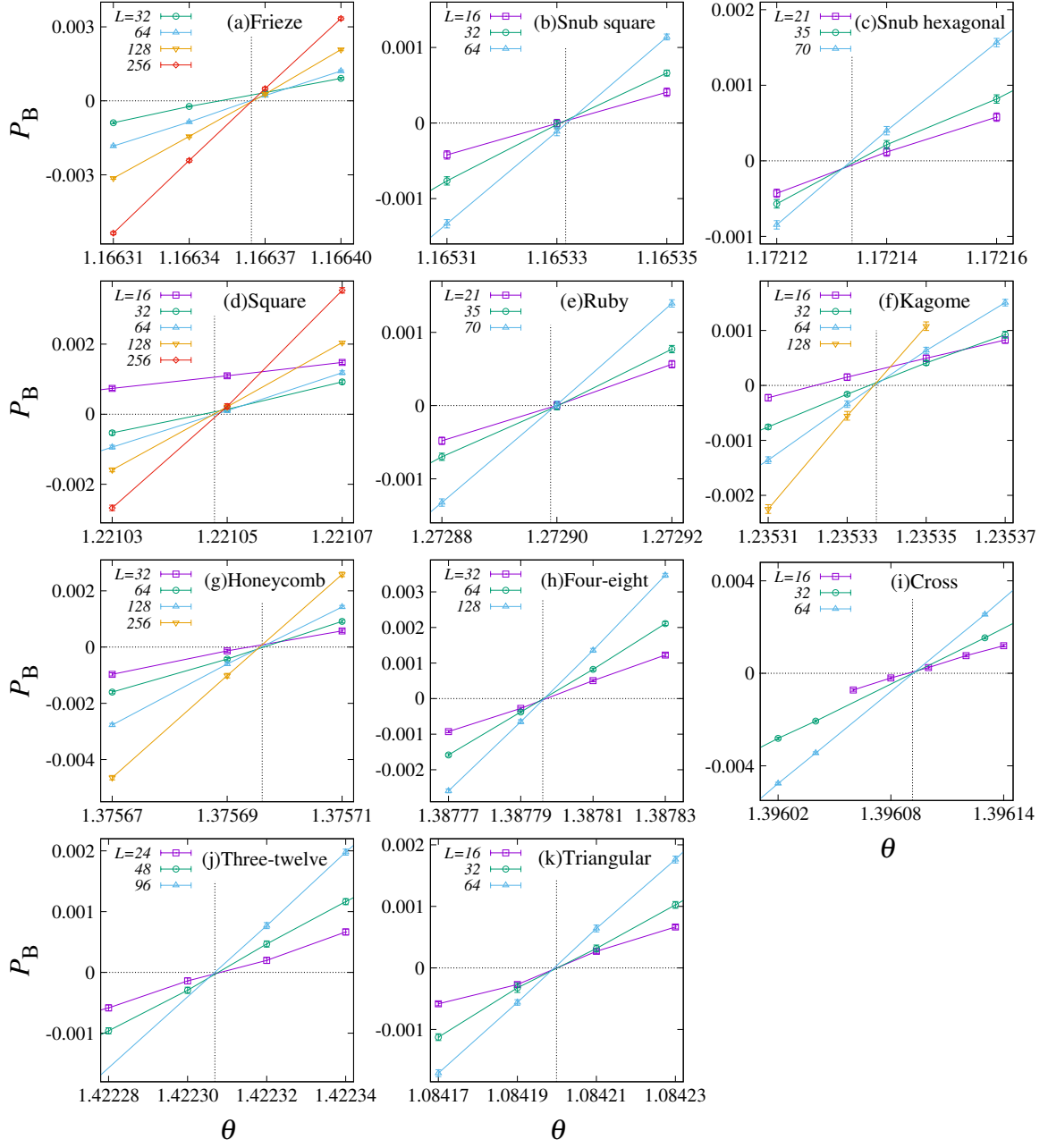


FIG. S15: Intersection plots for two-patch spheres on different lattices. The vertical dashed lines show the estimated threshold values θ_c .

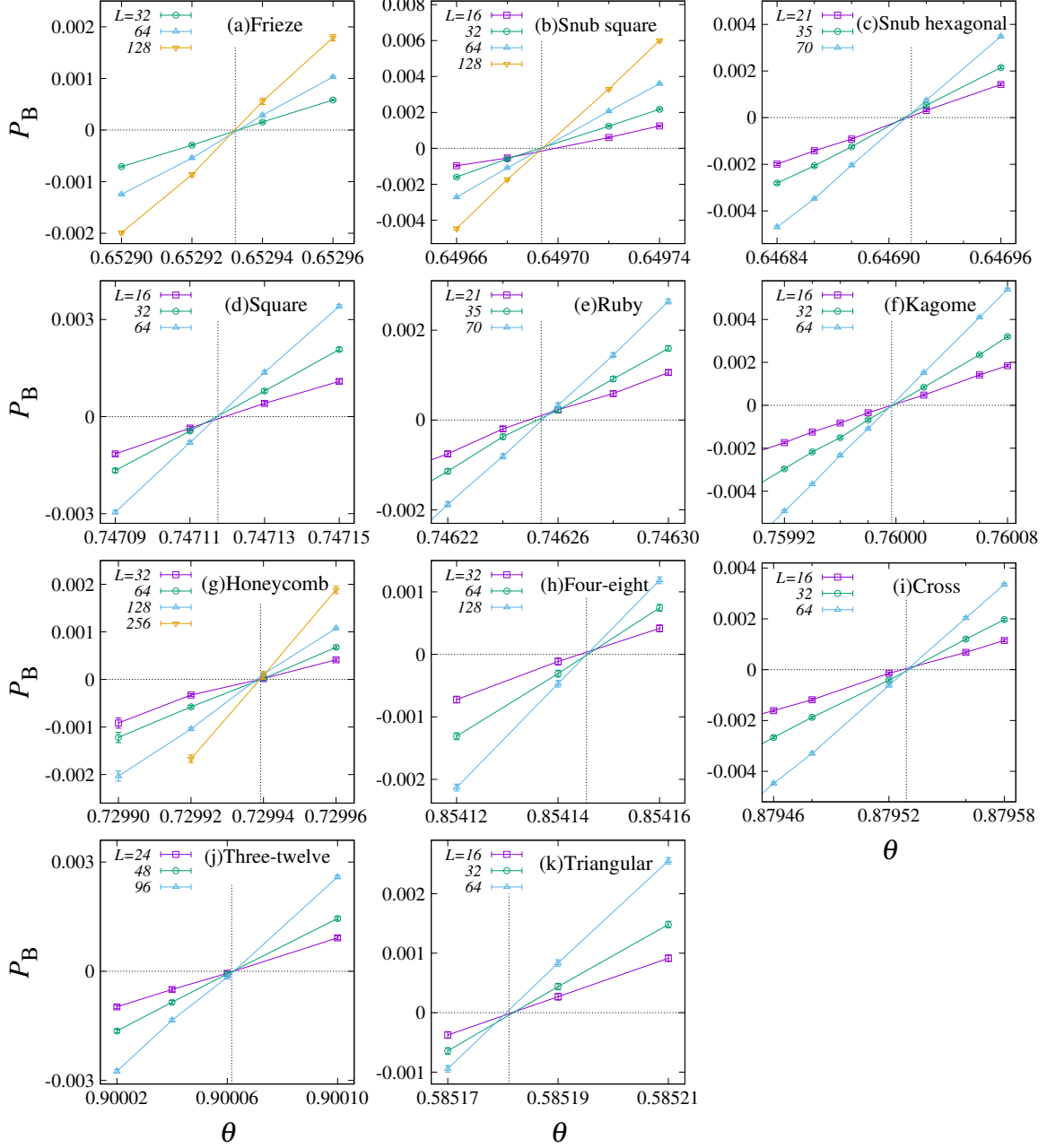


FIG. S16: Intersection plots for three-patch disks on different lattices. The vertical dashed lines show the estimated threshold values θ_c .

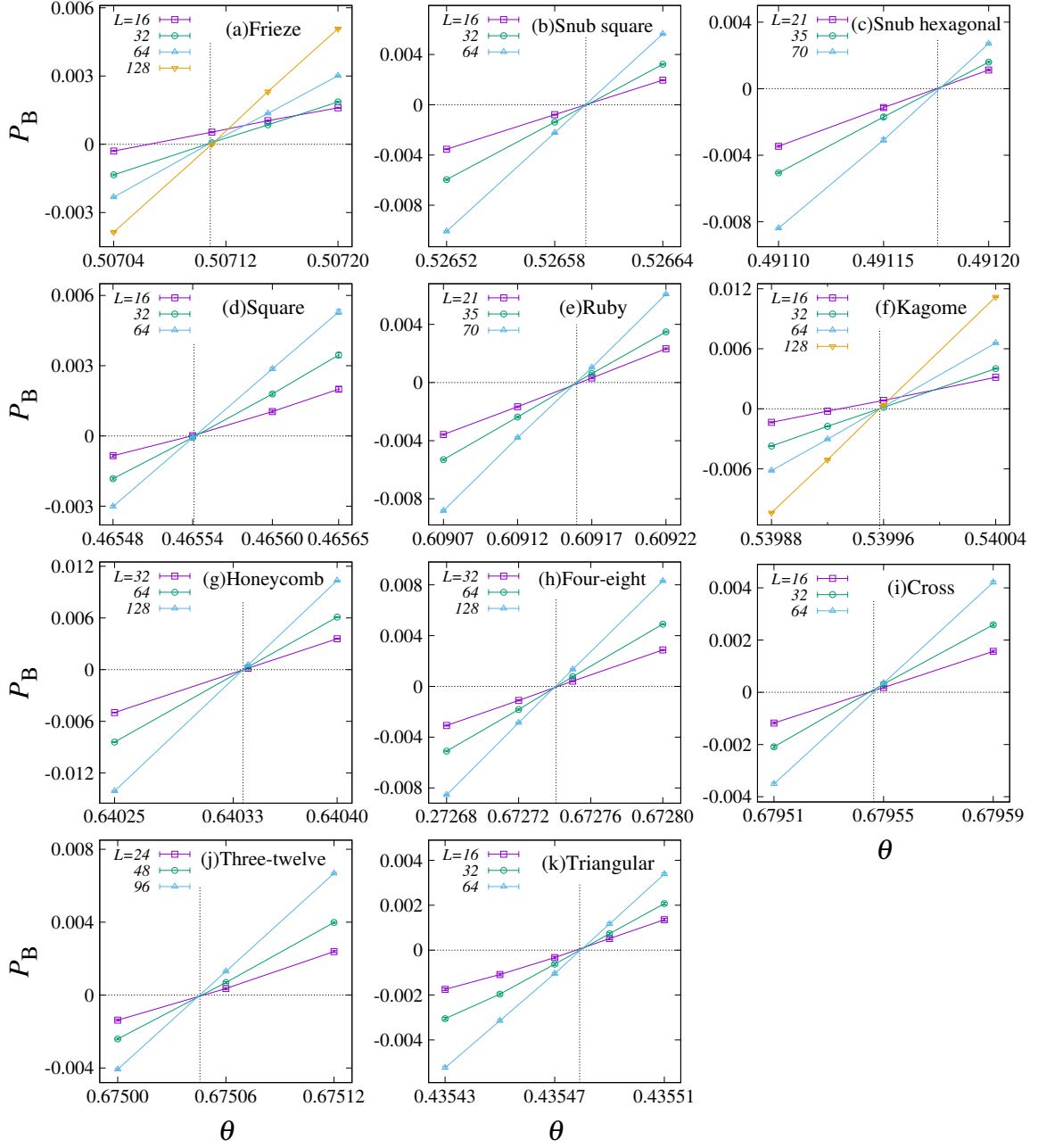


FIG. S17: Intersection plots for four-patch disks on different lattices. The vertical dashed lines show the estimated threshold values θ_c .

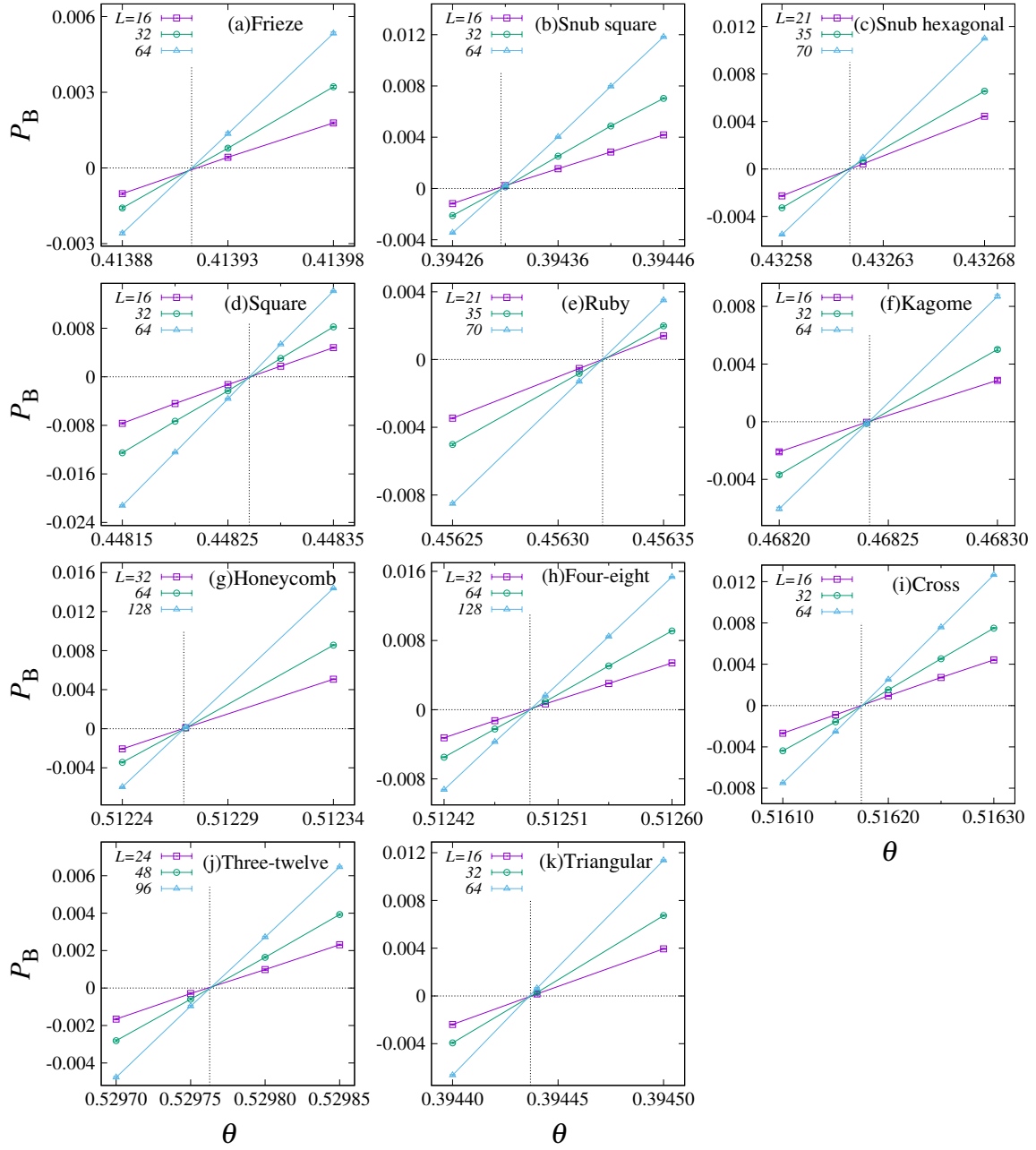


FIG. S18: Intersection plots for five-patch disks on different lattices. The vertical dashed lines show the estimated threshold values θ_c .

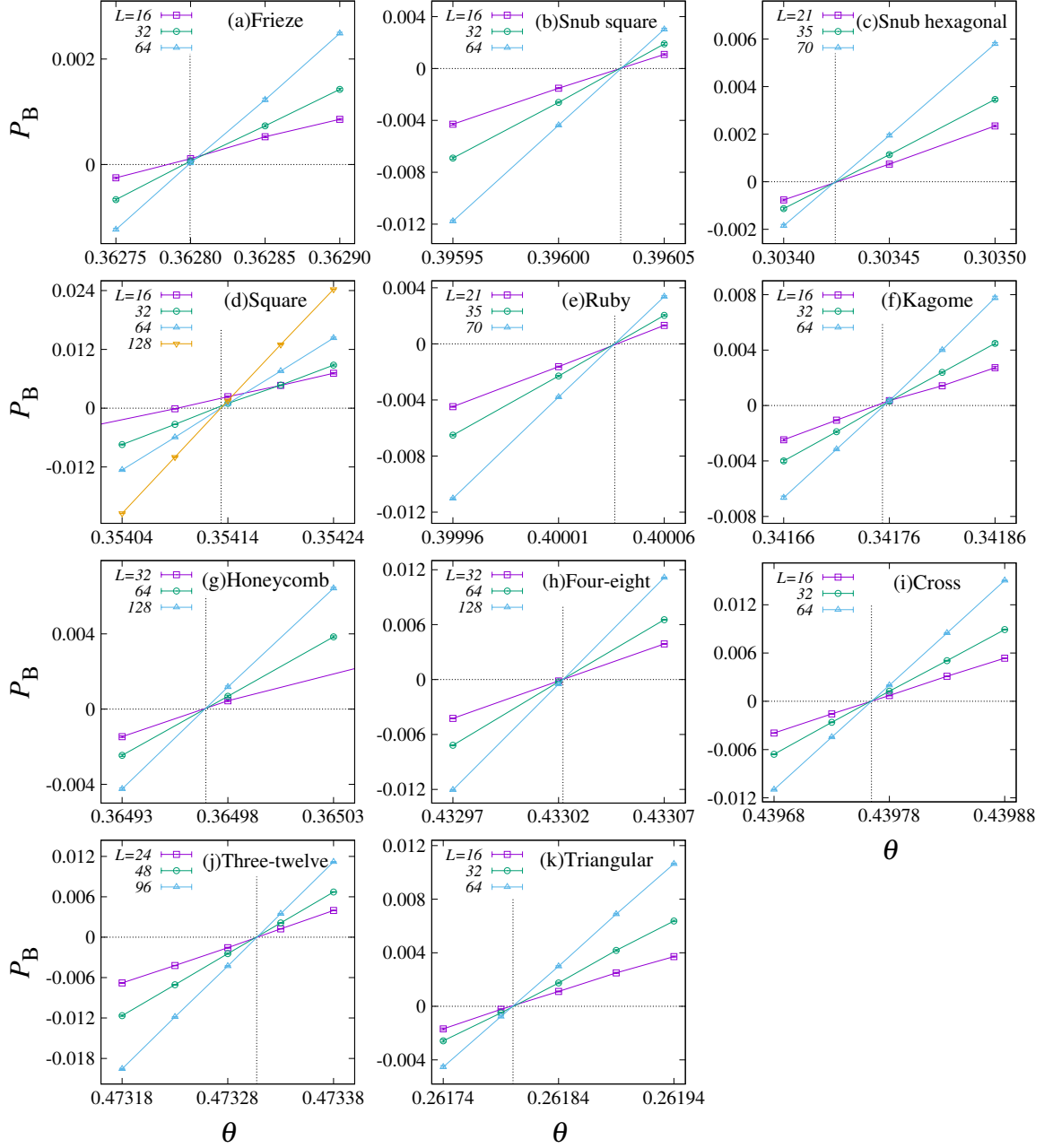


FIG. S19: Intersection plots for six-patch disks on different lattices. The vertical dashed lines show the estimated threshold values θ_c .

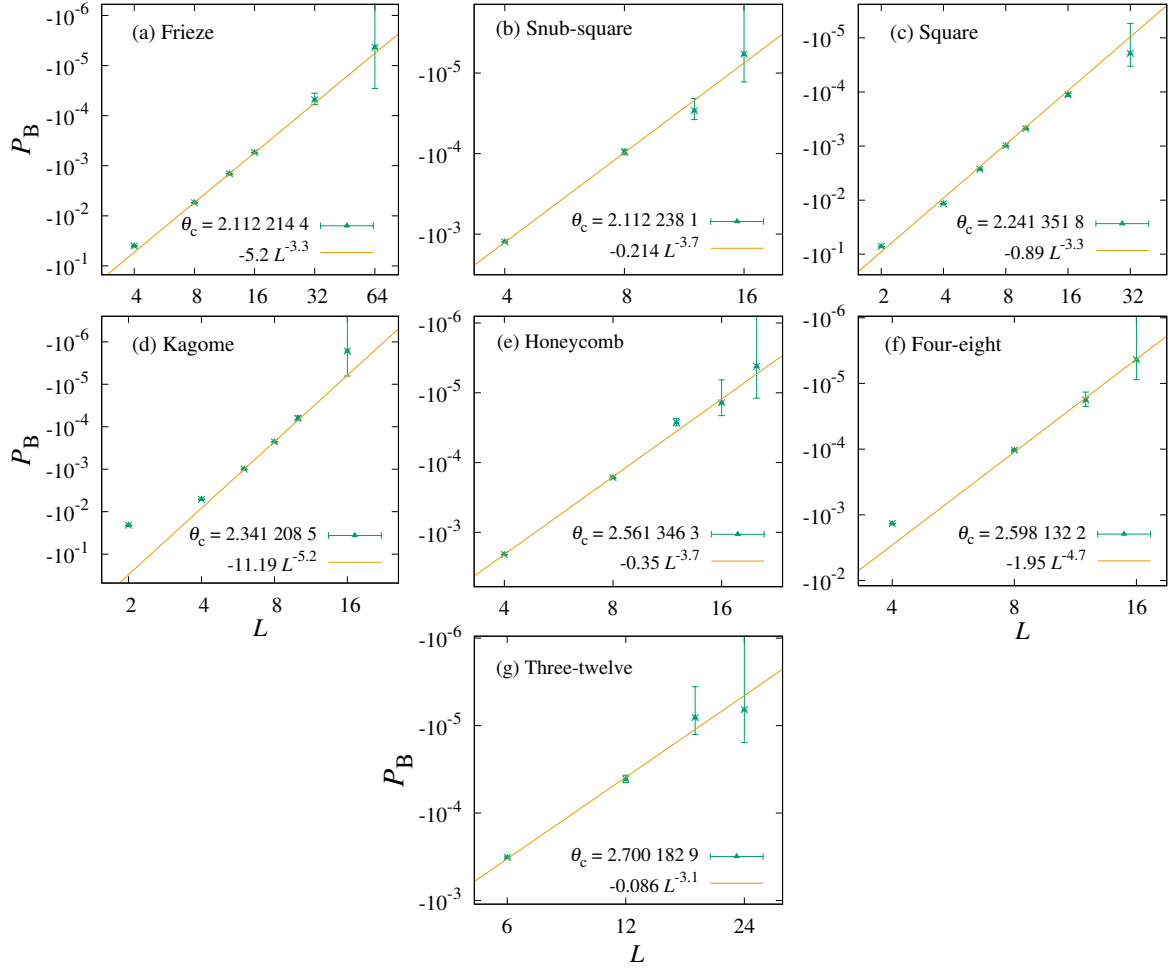


FIG. S20: Plots of P_B versus L at the percolation threshold θ_c for one-patch disks on different lattices.

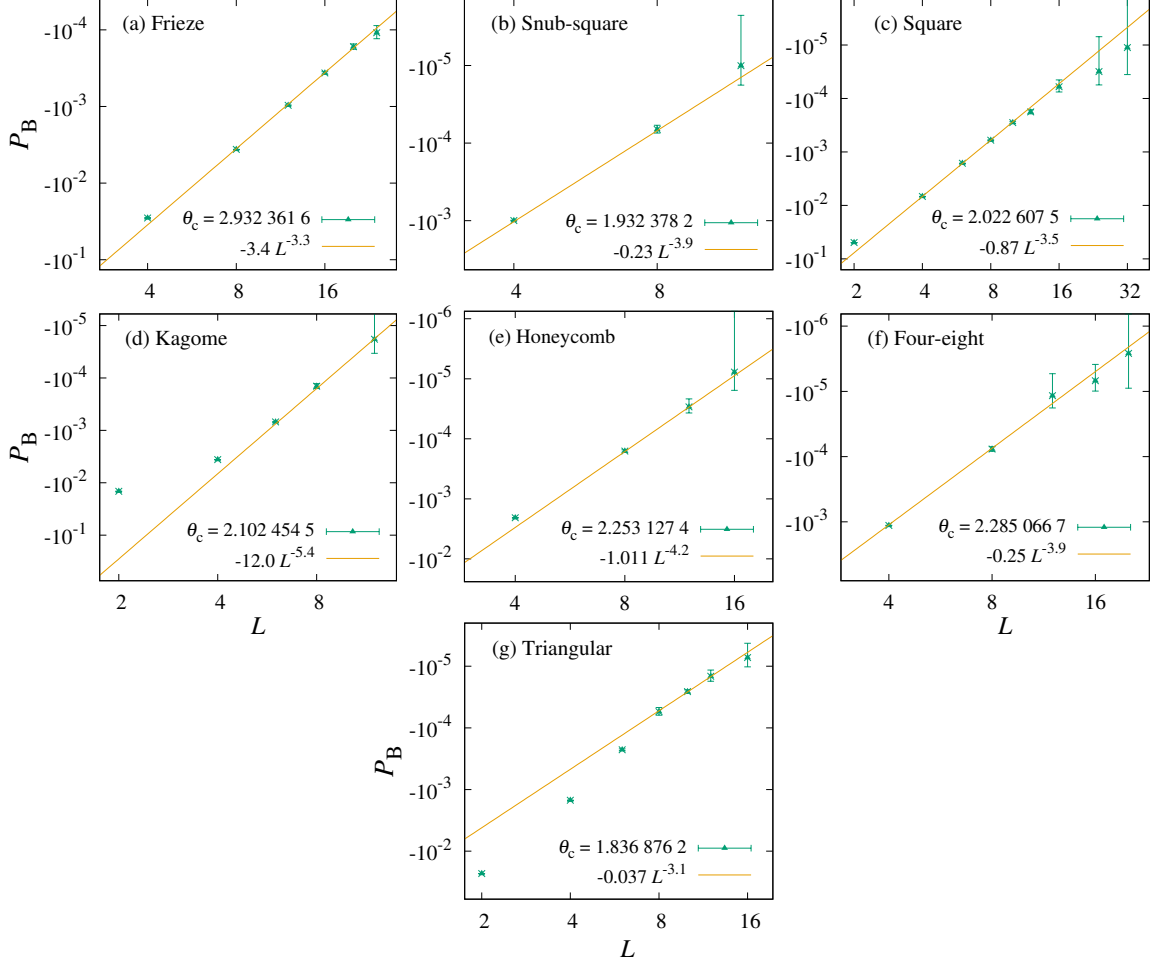


FIG. S21: Plots of P_B versus L at the percolation threshold θ_c for one-patch spheres on different lattices.

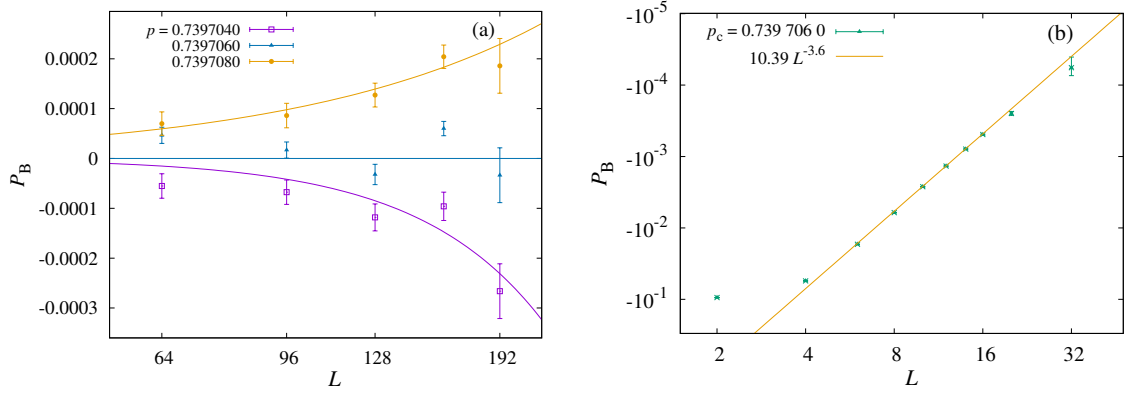


FIG. S22: The data of critical polynomial P_B for site percolation on the Lieb lattice in 2D.

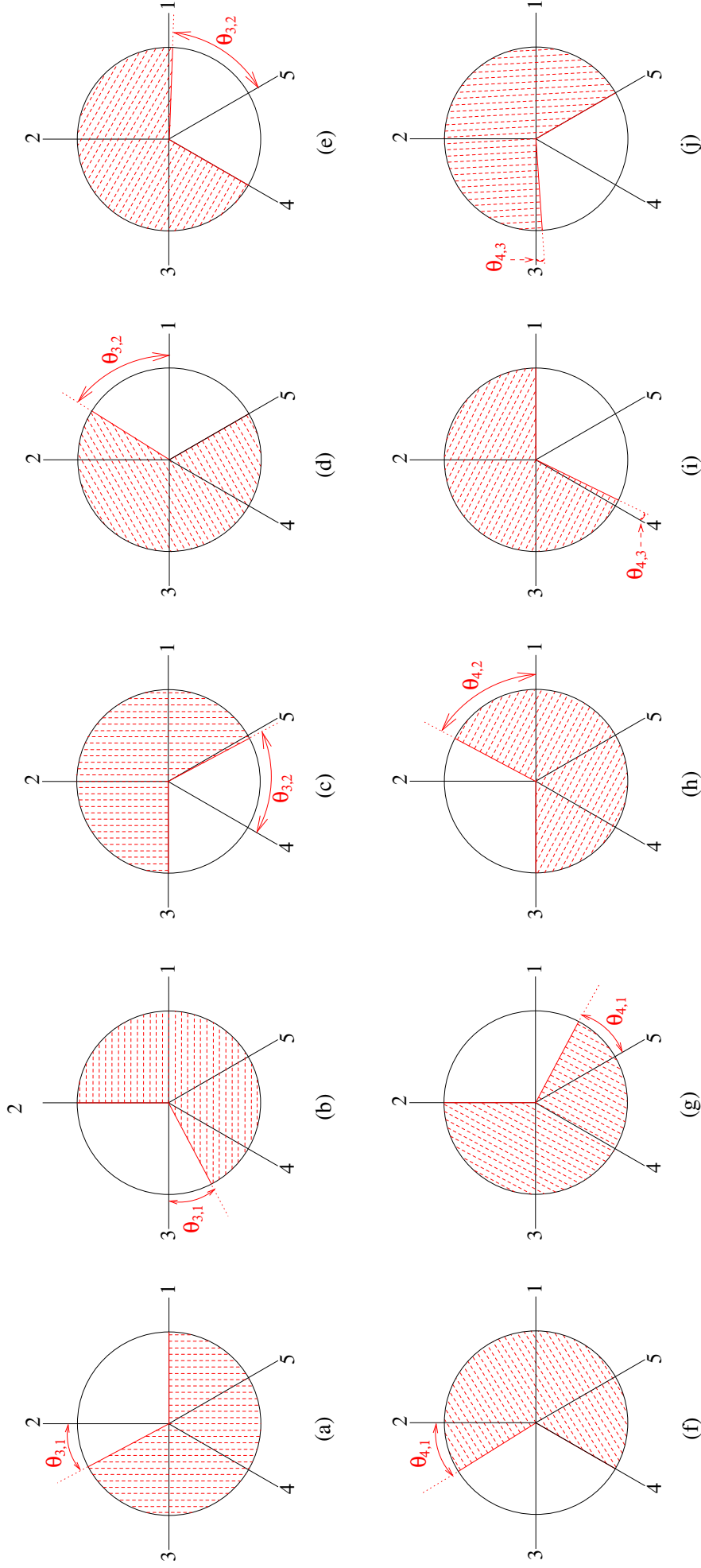


FIG. S23: The plots show different patch-covering structures for a one-patch disk on the frieze lattice. For each plot, when the disk rotates clockwise within the given angle ($\theta_{i,j} = 2\pi\chi_{i,j}$ with $\chi_{i,j}$ values given in the text), the patch-covering states of edges do not change, Plots (a-e) are 3-edge patch-covering structures, and plots (f-j) are four-edge patch-covering structures.

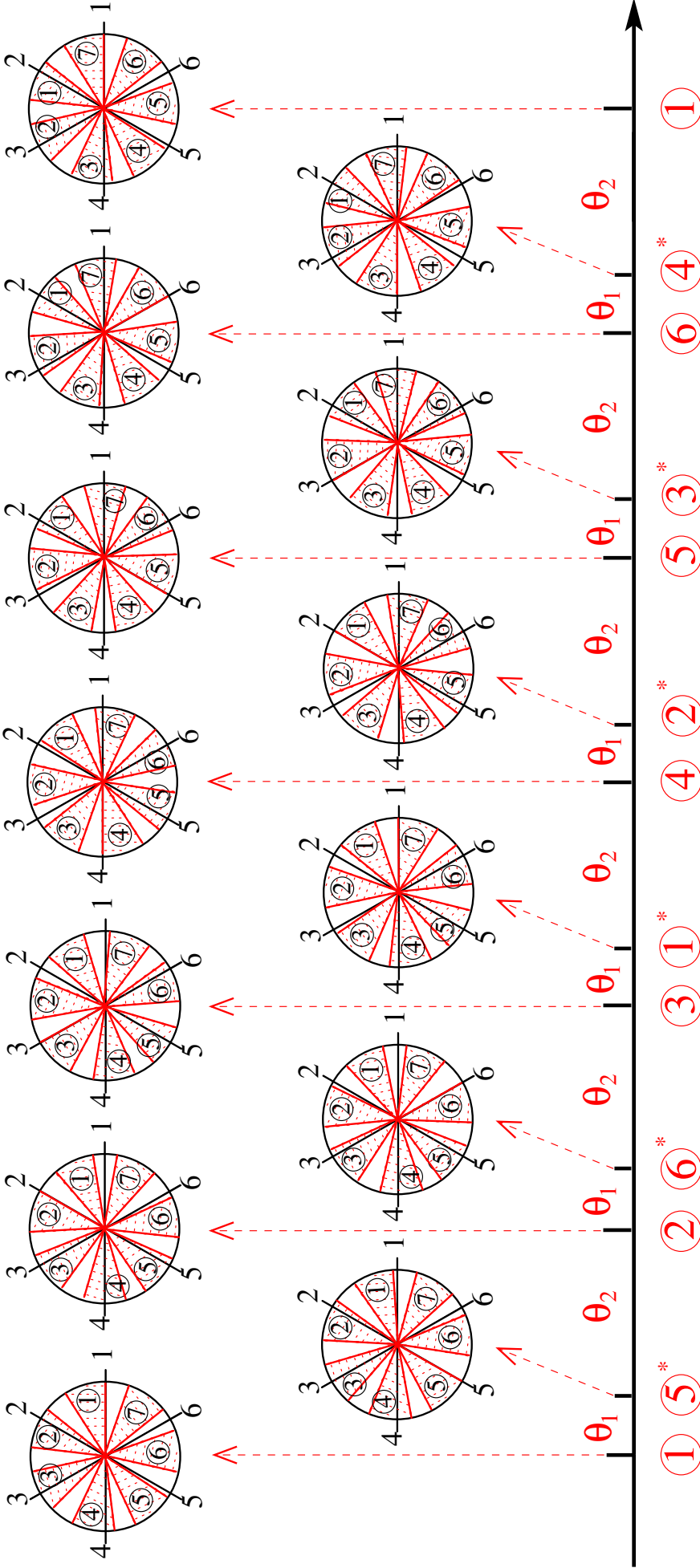


FIG. S24: A seven-patch disk rotates counterclockwise on a vertex of the triangular lattice. Initially, patch 1 is to the left of edge 1 (the direction is defined assuming that the observer stands at the disk center and faces outwards), with its right boundary touches the edge. When the disk rotates by an angle θ_1 ($\theta_1 = 2\pi\chi_1$, with χ_1 given by Eq. S10 in the text), the left boundary patch 5 (the patch is to the right side of edge 5). Within this angle θ_1 , the patches always covers three edges, i.e. edge 2, 3 and 4. And within the following angle θ_2 ($\theta_2 = 2\pi\chi_2$, with χ_2 given by Eq. S11 in the text), the patches always cover four edges, i.e. edge 2, 3, 4 and 5. As the disk rotates counterclockwise further, 3-edge patch-covering structures and 4-edge patch-covering structures appear in turn within an angle θ_1 or θ_2 , respectively. At the bottom, the symbol \textcircled{k} means that edge k is going to be uncovered by a patch to its left side, and \textcircled{k}^* means that edge k is going to be covered by a patch to its right side. The total angle between two $\textcircled{1}$ s is $2\pi/7$.

TABLE S4: Probabilities of different patch-covering structures for patch sizes χ near χ_c , for n -patch disks on the triangular, square and honeycomb lattices.

Lattice	mod (n, n_0)	Type	Probability
Triangular $n_0 = 6$	1	3-edge	$\left(\frac{1-\chi}{n} + \frac{n-1}{3} \cdot \frac{1}{n} - \frac{1}{3}\right) \cdot n \cdot 6 = 4 - 6\chi$
		4-edge	$\left(\frac{\chi}{n} + \frac{n-1}{2} \cdot \frac{1}{n} - \frac{1}{2}\right) \cdot n \cdot 6 = 6\chi - 3$
	2	2-edge	$\left(\frac{1-\chi}{n} + \frac{2n-1}{3} \cdot \frac{1}{n} - \frac{2}{3}\right) \cdot n \cdot 3 = 2 - 3\chi$
		4-edge	$\left(\frac{\chi}{n} + \frac{2n-1}{3} \cdot \frac{1}{n} - \frac{2}{3}\right) \cdot n \cdot 3 = 3\chi - 1$
	3	3-edge	$\frac{1-\chi}{n} \cdot n \cdot 2 = 2 - 2\chi$
		6-edge	$\left(\frac{1}{6} - \frac{n-3}{6} \cdot \frac{1}{n} - \frac{1-\chi}{n}\right) \cdot n \cdot 2 = 2\chi - 1$
	4	2-edge	$\left(\frac{1-\chi}{n} + \frac{n-1}{3} \cdot \frac{1}{n} - \frac{1}{3}\right) \cdot n \cdot 3 = 2 - 3\chi$
		4-edge	$\left(\frac{\chi}{n} + \frac{n-1}{3} \cdot \frac{1}{n} - \frac{1}{3}\right) \cdot n \cdot 3 = 3\chi - 1$
	5	3-edge	$\left(\frac{1-\chi}{n} + \frac{2n-1}{3} \cdot \frac{1}{n} - \frac{2}{3}\right) \cdot n \cdot 6 = 4 - 6\chi$
		4-edge	$\left(\frac{\chi}{n} + \frac{n-1}{2} \cdot \frac{1}{n} - \frac{1}{2}\right) \cdot n \cdot 6 = 6\chi - 3$
Square $n_0 = 4$	1	2-edge	$\left(\frac{1-\chi}{n} + \frac{n-1}{4} \cdot \frac{1}{n} - \frac{1}{4}\right) \cdot n \cdot 4 = 3 - 4\chi$
		3-edge	$\left(\frac{\chi}{n} + \frac{n-1}{2} \cdot \frac{1}{n} - \frac{1}{2}\right) \cdot n \cdot 4 = 4\chi - 2$
	2	2-edge	$\frac{1-\chi}{n} \cdot n \cdot 2 = 2 - 2\chi$
		4-edge	$\left(\frac{1}{4} - \frac{n-2}{4} \cdot \frac{1}{n} - \frac{1-\chi}{n}\right) \cdot n \cdot 2 = 2\chi - 1$
	3	2-edge	$\left(\frac{1-\chi}{n} + \frac{3n-1}{4} \cdot \frac{1}{n} - \frac{3}{4}\right) \cdot n \cdot 4 = 3 - 4\chi$
		3-edge	$\left(\frac{\chi}{n} + \frac{n-1}{2} \cdot \frac{1}{n} - \frac{1}{2}\right) \cdot n \cdot 4 = 4\chi - 2$
Honeycomb $n_0 = 3$	1	2-edge	$\frac{1-\chi}{n} \cdot n \cdot 3 = 3 - 3\chi$
		3-edge	$\left(\frac{\chi}{n} + \frac{2n-2}{3} \cdot \frac{1}{n} - \frac{2}{3}\right) \cdot n \cdot 3 = 3\chi - 2$
	2	2-edge	$\frac{1-\chi}{n} \cdot n \cdot 3 = 3 - 3\chi$
		3-edge	$\left(\frac{\chi}{n} + \frac{n-2}{3} \cdot \frac{1}{n} - \frac{1}{3}\right) \cdot n \cdot 3 = 3\chi - 2$

TABLE S5: Probabilities of different patch-covering structures for patch sizes χ near χ_c , for n -patch disks on the snub hexagonal lattice. The period is $n_0 = 6$.

mod (n, n_0)	Type	On the triangular lattice	On the snub hexagonal lattice
1	3-edge		$(5 - 6\chi) \cdot \frac{4}{6} = \frac{10}{3} - 4\chi$
	4-edge	$\left(\frac{1-\chi}{n} + \frac{n-1}{6} \cdot \frac{1}{n} - \frac{1}{6}\right) \cdot n \cdot 6 = 5 - 6\chi$	$(5 - 6\chi) \cdot \frac{2}{6} + (6\chi - 4) \cdot \frac{5}{6} = 3\chi - \frac{5}{3}$
	5-edge	$\left(\frac{1}{3} - \frac{n-1}{3} \cdot \frac{1}{n} - \frac{1-\chi}{n}\right) \cdot n \cdot 6 = 6\chi - 4$	$(6\chi - 4) \cdot \frac{1}{6} = \chi - \frac{2}{3}$
2	1-edge		$(2 - 3\chi) \cdot \frac{2}{6} = \frac{2}{3} - \chi$
	2-edge	$\left(\frac{1}{3} - \frac{n-2}{3} \cdot \frac{1}{n} - \frac{\chi}{n}\right) \cdot n \cdot 3 = 2 - 3\chi$	$(2 - 3\chi) \cdot \frac{4}{6} = \frac{4}{3} - 2\chi$
	3-edge		$(3\chi - 1) \cdot \frac{4}{6} = 2\chi - \frac{2}{3}$
	4-edge	$\left(\frac{\chi}{n} + \frac{n-2}{6} \cdot \frac{1}{n} - \frac{1}{6}\right) \cdot n \cdot 3 = 3\chi - 1$	$(3\chi - 1) \cdot \frac{2}{6} = \chi - \frac{1}{3}$
3	2-edge		$(2 - 2\chi) \cdot \frac{3}{6} = 1 - \chi$
	3-edge	$\frac{1-\chi}{n} \cdot n \cdot 2 = 2 - 2\chi$	$(2 - 2\chi) \cdot \frac{3}{6} = 1 - \chi$
	5-edge		$(2\chi - 1) \cdot \frac{6}{6} = 2\chi - 1$
	6-edge	$\left(\frac{\chi}{n} + \frac{n-3}{6} \cdot \frac{1}{n} - \frac{1}{6}\right) \cdot n \cdot 2 = 2\chi - 1$	
4	1-edge		$(2 - 3\chi) \cdot \frac{2}{6} = \frac{2}{3} - \chi$
	2-edge	$\left(\frac{1}{6} - \frac{n-4}{6} \cdot \frac{1}{n} - \frac{\chi}{n}\right) \cdot n \cdot 3 = 2 - 3\chi$	$(2 - 3\chi) \cdot \frac{4}{6} = \frac{4}{3} - 2\chi$
	3-edge		$(3\chi - 1) \cdot \frac{4}{6} = 2\chi - \frac{2}{3}$
	4-edge	$\left(\frac{\chi}{n} + \frac{n-1}{3} \cdot \frac{1}{n} - \frac{1}{3}\right) \cdot n \cdot 3 = 3\chi - 1$	$(3\chi - 1) \cdot \frac{2}{6} = \chi - \frac{1}{3}$
5	3-edge		$(5 - 6\chi) \cdot \frac{4}{6} = \frac{10}{3} - 4\chi$
	4-edge	$\left(\frac{1}{6} - \frac{n-5}{6} \cdot \frac{1}{n} - \frac{\chi}{n}\right) \cdot n \cdot 6 = 5 - 6\chi$	$(5 - 6\chi) \cdot \frac{2}{6} + (6\chi - 4) \cdot \frac{5}{6} = 3\chi - \frac{5}{3}$
	5-edge	$\left(\frac{\chi}{n} + \frac{n-2}{3} \cdot \frac{1}{n} - \frac{1}{3}\right) \cdot n \cdot 6 = 6\chi - 4$	$(6\chi - 4) \cdot \frac{1}{6} = \chi - \frac{2}{3}$

TABLE S6: Probabilities of different patch-covering structures for patch sizes χ near χ_c , for n -patch disks on the kagome lattice. The period is $n_0 = 6$. The 2-edge structure for $\text{mod}(n, 6) = 3$ has the two edges at an angle of $2\pi/3$, while that for $\text{mod}(n, 6) = 2$ or 4 has the two edges in a straight line.

$\text{mod}(n, n_0)$	Type	On the triangular lattice	On the kagome lattice
1	2-edge		$(5 - 6\chi) \cdot \frac{2}{6} = \frac{5}{3} - 2\chi$
	3-edge		$(5 - 6\chi) \cdot \frac{4}{6} + (6\chi - 4) \cdot \frac{4}{6} = \frac{2}{3}$
	4-edge	$\left(\frac{1-\chi}{n} + \frac{n-1}{6} \cdot \frac{1}{n} - \frac{1}{6}\right) \cdot n \cdot 6 = 5 - 6\chi$	$(6\chi - 4) \cdot \frac{2}{6} = 2\chi - \frac{4}{3}$
	5-edge	$\left(\frac{1}{3} - \frac{n-1}{3} \cdot \frac{1}{n} - \frac{1-\chi}{n}\right) \cdot n \cdot 6 = 6\chi - 4$	
2	2-edge		$(3 - 3\chi) \cdot \frac{4}{6} = 2 - 2\chi$
	4-edge	$\left(\frac{1-\chi}{n}\right) \cdot n \cdot 3 = 3 - 3\chi$	$(3 - 3\chi) \cdot \frac{2}{6} + (3\chi - 2) \cdot \frac{6}{6} = 2\chi - 1$
	6-edge	$\left(\frac{1}{6} - \frac{n-2}{6} \cdot \frac{1}{n} - \frac{1-\chi}{n}\right) \cdot n \cdot 3 = 3\chi - 2$	
3	2-edge		$(2 - 2\chi) \cdot \frac{6}{6} = 2 - 2\chi$
	3-edge	$\left(\frac{1-\chi}{n}\right) \cdot n \cdot 2 = 2 - 2\chi$	
	4-edge		$(2\chi - 1) \cdot \frac{6}{6} = 2\chi - 1$
	6-edge	$\left(\frac{\chi}{n} + \frac{n-3}{6} \cdot \frac{1}{n} - \frac{1}{6}\right) \cdot n \cdot 2 = 2\chi - 1$	
4	2-edge		$(3 - 3\chi) \cdot \frac{4}{6} = 2 - 2\chi$
	4-edge	$\frac{1-\chi}{n} \cdot n \cdot 3 = 3 - 3\chi$	$(3 - 3\chi) \cdot \frac{2}{6} + (3\chi - 2) \cdot \frac{6}{6} = 2\chi - 1$
	6-edge	$\left(\frac{\chi}{n} + \frac{n-4}{6} \cdot \frac{1}{n} - \frac{1}{6}\right) \cdot n \cdot 3 = 3\chi - 2$	
5	2-edge		$(5 - 6\chi) \cdot \frac{2}{6} = \frac{5}{3} - 2\chi$
	3-edge		$(5 - 6\chi) \cdot \frac{4}{6} + (6\chi - 4) \cdot \frac{4}{6} = \frac{2}{3}$
	4-edge	$\left(\frac{1}{6} - \frac{n-5}{6} \cdot \frac{1}{n} - \frac{\chi}{n}\right) \cdot 6 = 5 - 6\chi$	$(6\chi - 4) \cdot \frac{2}{6} = 2\chi - \frac{4}{3}$
	5-edge	$\left(\frac{\chi}{n} + \frac{n-2}{3} \cdot \frac{1}{n} - \frac{1}{3}\right) \cdot 6 = 6\chi - 4$	

TABLE S7: Probabilities of different patch-covering structures for patch sizes χ near χ_c , for n -patch disks on the four-eight lattice. The period is $n_0 = 8$. For intermediate results on the regular octagon, the patch disk is placed at the center of the octagon and its patches cover edges connecting the center and vertices of the octagon. This table should be read together with Table S8.

mod (n, n_0)	Type	On the regular octagon	On the four-eight lattice
1	2-edge		$(7 - 8\chi) \cdot \frac{6}{8} + (8\chi - 6) \cdot \frac{3}{8} = 3 - 3\chi$
	3-edge		$(7 - 8\chi) \cdot \frac{2}{8} + (8\chi - 6) \cdot \frac{5}{8} = 3\chi - 2$
	6-edge	$\left(\frac{1 - \chi}{n} + \frac{n - 1}{8} \cdot \frac{1}{n} - \frac{1}{8}\right) \cdot n \cdot 8 = 7 - 8\chi$	
	7-edge	$\left(\frac{1}{4} - \frac{n - 1}{4} \cdot \frac{1}{n} - \frac{1 - \chi}{n}\right) \cdot n \cdot 8 = 8\chi - 6$	
2	2-edge		$(4 - 4\chi) \cdot \frac{6}{8} = 3 - 3\chi$
	3-edge		$(4 - 4\chi) \cdot \frac{2}{8} + (4\chi - 3) \cdot \frac{8}{8} = 3\chi - 2$
	6-edge	$\left(\frac{1 - \chi}{n}\right) \cdot n \cdot 4 = 4 - 4\chi$	
	8-edge	$\left(\frac{1}{8} - \frac{n - 2}{8} \cdot \frac{1}{n} - \frac{1 - \chi}{n}\right) \cdot n \cdot 4 = 4\chi - 3$	
3	1-edge		$(7 - 8\chi) \cdot \frac{2}{8} = \frac{7}{4} - 2\chi$
	2-edge		$(7 - 8\chi) \cdot \frac{2}{8} + (8\chi - 6) \cdot \frac{3}{8} = \chi - \frac{1}{2}$
	3-edge		$(7 - 8\chi) \cdot \frac{4}{8} + (8\chi - 6) \cdot \frac{5}{8} = \chi - \frac{1}{4}$
	6-edge	$\left(\frac{1 - \chi}{n} + \frac{3n - 1}{8} \cdot \frac{1}{n} - \frac{3}{8}\right) \cdot n \cdot 8 = 7 - 8\chi$	
	7-edge	$\left(\frac{\chi}{n} + \frac{n - 3}{4} \cdot \frac{1}{n} - \frac{1}{4}\right) \cdot n \cdot 8 = 8\chi - 6$	
4	1-edge		$(2 - 2\chi) \cdot \frac{4}{8} = 1 - \chi$
	2-edge		$(2 - 2\chi) \cdot \frac{4}{8} = 1 - \chi$
	3-edge		$(2\chi - 1) \cdot \frac{8}{8} = 2\chi - 1$
	4-edge	$\frac{1 - \chi}{n} \cdot n \cdot 2 = 2 - 2\chi$	
	8-edge	$\left(\frac{\chi}{n} + \frac{n - 4}{8} \cdot \frac{1}{n} - \frac{1}{8}\right) \cdot n \cdot 2 = 2\chi - 1$	

TABLE S8: Probabilities of different patch-covering structures for patch sizes χ near χ_c , for n -patch disks on the four-eight lattice. The period is $n_0 = 8$. For intermediate results on the regular octagon, the patch disk is placed at the center of the octagon and its patches cover edges connecting the center and vertices of the octagon. This table should be read together with Table S7.

mod (n, n_0)	Type	On the regular octagon	On the four-eight lattice
5	1-edge		$(7 - 8\chi) \cdot \frac{2}{8} = \frac{7}{4} - 2\chi$
	2-edge		$(7 - 8\chi) \cdot \frac{2}{8} + (8\chi - 6) \cdot \frac{3}{8} = \chi - \frac{1}{2}$
	3-edge		$(7 - 8\chi) \cdot \frac{4}{8} + (8\chi - 6) \cdot \frac{5}{8} = \chi - \frac{1}{4}$
	6-edge	$\left(\frac{3}{8} - \frac{3n-7}{8} \cdot \frac{1}{n} - \frac{\chi}{n}\right) \cdot n \cdot 8 = 7 - 8\chi$	
	7-edge	$\left(\frac{1}{4} - \frac{n-1}{4} \cdot \frac{1}{n} - \frac{1-\chi}{n}\right) \cdot n \cdot 8 = 8\chi - 6$	
6	2-edge		$(4 - 4\chi) \cdot \frac{6}{8} = 3 - 3\chi$
	3-edge		$(4 - 4\chi) \cdot \frac{2}{8} + (4\chi - 3) \cdot \frac{8}{8} = 3\chi - 2$
	6-edge	$\left(\frac{1-\chi}{n}\right) \cdot n \cdot 4 = 4 - 4\chi$	
	8-edge	$\left(\frac{\chi}{n} + \frac{n-6}{8} \cdot \frac{1}{n} - \frac{1}{8}\right) \cdot n \cdot 4 = 4\chi - 3$	
7	2-edge		$(7 - 8\chi) \cdot \frac{6}{8} + (8\chi - 6) \cdot \frac{3}{8} = 3 - 3\chi$
	3-edge		$(7 - 8\chi) \cdot \frac{2}{8} + (8\chi - 6) \cdot \frac{5}{8} = 3\chi - 2$
	6-edge	$\left(\frac{1}{8} - \frac{n-7}{8} \cdot \frac{1}{n} - \frac{\chi}{n}\right) \cdot n \cdot 8 = 7 - 8\chi$	
	7-edge	$\left(\frac{\chi}{n} + \frac{n-3}{4} \cdot \frac{1}{n} - \frac{1}{4}\right) \cdot n \cdot 8 = 8\chi - 6$	

TABLE S9: Probabilities of different patch-covering structures for patch sizes χ near χ_c , for n -patch disks on the frieze lattice. The period is $n_0 = 12$. For intermediate results on the regular dodecagon, the patch disk is placed at the center of the dodecagon and its patches cover edges connecting the center and vertices of the dodecagon. This table should be read together with Tables S10 and S11.

mod (n, n_0)	Type	On the regular dodecagon	On the frieze lattice
1	3-edge		$(9 - 12\chi) \cdot \frac{8}{12} + (12\chi - 8) \cdot \frac{3}{12} = 4 - 5\chi$
	4-edge		$(9 - 12\chi) \cdot \frac{4}{12} + (12\chi - 8) \cdot \frac{9}{12} = 5\chi - 3$
	8-edge	$\left(\frac{1-\chi}{n} + \frac{n-1}{4} \cdot \frac{1}{n} - \frac{1}{4}\right) \cdot n \cdot 12 = 9 - 12\chi$	
	9-edge	$\left(\frac{1}{3} - \frac{n-1}{3} \cdot \frac{1}{n} - \frac{1-\chi}{n}\right) \cdot n \cdot 12 = 12\chi - 8$	
2	2-edge		$(4 - 6\chi) \cdot \frac{6}{12} = 2 - 3\chi$
	3-edge		$(4 - 6\chi) \cdot \frac{6}{12} + (6\chi - 3) \cdot \frac{8}{12} = \chi$
	4-edge		$(6\chi - 3) \cdot \frac{4}{12} = 2\chi - 1$
	6-edge	$\left(\frac{1-\chi}{n} + \frac{n-2}{6} \cdot \frac{1}{n} - \frac{1}{6}\right) \cdot n \cdot 6 = 4 - 6\chi$	
	8-edge	$\left(\frac{1}{4} - \frac{n-2}{4} \cdot \frac{1}{n} - \frac{1-\chi}{n}\right) \cdot n \cdot 6 = 6\chi - 3$	
3	2-edge		$(3 - 4\chi) \cdot \frac{6}{12} = \frac{3}{2} - 2\chi$
	3-edge		$(3 - 4\chi) \cdot \frac{6}{12} + (4\chi - 2) \cdot \frac{6}{12} = \frac{1}{2}$
	4-edge		$(4\chi - 2) \cdot \frac{3}{12} = \chi - \frac{1}{2}$
	5-edge		$(4\chi - 2) \cdot \frac{3}{12} = \chi - \frac{1}{2}$
	6-edge	$\left(\frac{1-\chi}{n} + \frac{n-3}{12} \cdot \frac{1}{n} - \frac{1}{12}\right) \cdot n \cdot 4 = 3 - 4\chi$	
	9-edge	$\left(\frac{\chi}{n} + \frac{n-3}{6} \cdot \frac{1}{n} - \frac{1}{6}\right) \cdot n \cdot 4 = 4\chi - 2$	
4	1-edge		$(2 - 3\chi) \cdot \frac{8}{12} = \frac{4}{3} - 2\chi$
	2-edge		$(3\chi - 1) \cdot \frac{4}{12} = \chi - \frac{1}{3}$
	3-edge		$(2 - 3\chi) \cdot \frac{4}{12} = \frac{2}{3} - \chi$
	4-edge	$\left(\frac{1}{6} - \frac{n-4}{6} \cdot \frac{1}{n} - \frac{\chi}{n}\right) \cdot n \cdot 3 = 2 - 3\chi$	$(3\chi - 1) \cdot \frac{8}{12} = 2\chi - \frac{2}{3}$
	8-edge	$\left(\frac{\chi}{n} + \frac{n-4}{12} \cdot \frac{1}{n} - \frac{1}{12}\right) \cdot n \cdot 3 = 3\chi - 1$	

TABLE S10: Probabilities of different patch-covering structures for patch sizes χ near χ_c , for n -patch disks on the frieze lattice. The period is $n_0 = 12$. For intermediate results on the regular dodecagon, the patch disk is placed at the center of the dodecagon and its patches cover edges connecting the center and vertices of the dodecagon. This table should be read together with Tables S9 and S11.

mod (n, n_0)	Type	On the regular dodecagon	On the frieze lattice
5	1-edge		$(8 - 12\chi) \cdot \frac{2}{12} = \frac{4}{3} - 2\chi$
	2-edge		$(8 - 12\chi) \cdot \frac{3}{12} + (12\chi - 7) \cdot \frac{4}{12} = \chi - \frac{1}{3}$
	3-edge		$(8 - 12\chi) \cdot \frac{2}{12} + (12\chi - 7) \cdot \frac{2}{12} = \frac{1}{6}$
	4-edge		$(8 - 12\chi) \cdot \frac{4}{12} + (12\chi - 7) \cdot \frac{4}{12} = \frac{1}{3}$
	5-edge		$(8 - 12\chi) \cdot \frac{1}{12} + (12\chi - 7) \cdot \frac{2}{12} = \chi - \frac{1}{2}$
	7-edge	$\left(\frac{1}{3} - \frac{n-2}{3} \cdot \frac{1}{n} - \frac{\chi}{n}\right) \cdot n \cdot 12 = 8 - 12\chi$	
8-edge	$\left(\frac{1}{12} - \frac{n-5}{12} \cdot \frac{1}{n} - \frac{1-\chi}{n}\right) \cdot n \cdot 12 = 12\chi - 7$		
6	1-edge		$(2 - 2\chi) \cdot \frac{6}{12} = 1 - \chi$
	4-edge		$(2 - 2\chi) \cdot \frac{6}{12} = 1 - \chi$
	5-edge		$(2\chi - 1) \cdot \frac{12}{12} = 2\chi - 1$
	6-edge	$\left(\frac{1-\chi}{n}\right) \cdot n \cdot 2 = 2 - 2\chi$	
12-edge	$\left(\frac{\chi}{n} + \frac{n-6}{12} \cdot \frac{1}{n} - \frac{1}{12}\right) \cdot n \cdot 2 = 2\chi - 1$		
7	1-edge		$(8 - 12\chi) \cdot \frac{2}{12} = \frac{4}{3} - 2\chi$
	2-edge		$(8 - 12\chi) \cdot \frac{3}{12} + (12\chi - 7) \cdot \frac{4}{12} = \chi - \frac{1}{3}$
	3-edge		$(8 - 12\chi) \cdot \frac{2}{12} + (12\chi - 7) \cdot \frac{2}{12} = \frac{1}{6}$
	4-edge		$(8 - 12\chi) \cdot \frac{4}{12} + (12\chi - 7) \cdot \frac{4}{12} = \frac{1}{3}$
	5-edge		$(8 - 12\chi) \cdot \frac{1}{12} + (12\chi - 7) \cdot \frac{2}{12} = \chi - \frac{1}{2}$
	7-edge	$\left(\frac{1-\chi}{n} + \frac{n-1}{3} \cdot \frac{1}{n} - \frac{1}{3}\right) \cdot n \cdot 12 = 8 - 12\chi$	
8-edge	$\left(\frac{\chi}{n} + \frac{n-7}{12} \cdot \frac{1}{n} - \frac{1}{12}\right) \cdot n \cdot 12 = 12\chi - 7$		

TABLE S11: Probabilities of different patch-covering structures for patch sizes χ near χ_c , for n -patch disks on the frieze lattice. The period is $n_0 = 12$. For intermediate results on the regular dodecagon, the patch disk is placed at the center of the dodecagon and its patches cover edges connecting the center and vertices of the dodecagon. This table should be read together with Tables S9 and S10.

mod (n, n_0)	Type	On the regular dodecagon	On the frieze lattice
8	1-edge		$(2 - 3\chi) \cdot \frac{8}{12} = \frac{4}{3} - 2\chi$
	2-edge		$(3\chi - 1) \cdot \frac{4}{12} = \chi - \frac{1}{3}$
	3-edge		$(2 - 3\chi) \cdot \frac{4}{12} = \frac{2}{3} - \chi$
	4-edge	$\left(\frac{1}{12} - \frac{n-8}{12} \cdot \frac{1}{n} - \frac{\chi}{n}\right) \cdot n \cdot 3 = 2 - 3\chi$	$(3\chi - 1) \cdot \frac{8}{12} = 2\chi - \frac{2}{3}$
	8-edge	$\left(\frac{\chi}{n} + \frac{n-2}{6} \cdot \frac{1}{n} - \frac{1}{6}\right) \cdot n \cdot 3 = 3\chi - 1$	
9	2-edge		$(3 - 4\chi) \cdot \frac{6}{12} = \frac{3}{2} - 2\chi$
	3-edge		$(3 - 4\chi) \cdot \frac{6}{12} + (4\chi - 2) \cdot \frac{6}{12} = \frac{1}{2}$
	4-edge		$(4\chi - 2) \cdot \frac{3}{12} = \chi - \frac{1}{2}$
	5-edge		$(4\chi - 2) \cdot \frac{3}{12} = \chi - \frac{1}{2}$
	6-edge	$\left(\frac{1}{12} - \frac{n-9}{12} \cdot \frac{1}{n} - \frac{\chi}{n}\right) \cdot n \cdot 4 = 3 - 4\chi$	
	9-edge	$\left(\frac{\chi}{n} + \frac{n-3}{6} \cdot \frac{1}{n} - \frac{1}{6}\right) \cdot n \cdot 4 = 4\chi - 2$	
10	2-edge		$(4 - 6\chi) \cdot \frac{6}{12} = 2 - 3\chi$
	3-edge		$(4 - 6\chi) \cdot \frac{6}{12} + (6\chi - 3) \cdot \frac{8}{12} = \chi$
	4-edge		$(6\chi - 3) \cdot \frac{4}{12} = 2\chi - 1$
	6-edge	$\left(\frac{1}{6} - \frac{n-4}{6} \cdot \frac{1}{n} - \frac{\chi}{n}\right) \cdot n \cdot 6 = 4 - 6\chi$	
	8-edge	$\left(\frac{\chi}{n} + \frac{n-2}{4} \cdot \frac{1}{n} - \frac{1}{4}\right) \cdot n \cdot 6 = 6\chi - 3$	
11	3-edge		$(9 - 12\chi) \cdot \frac{8}{12} + (12\chi - 8) \cdot \frac{3}{12} = 4 - 5\chi$
	4-edge		$(9 - 12\chi) \cdot \frac{4}{12} + (12\chi - 8) \cdot \frac{9}{12} = 5\chi - 3$
	8-edge	$\left(\frac{1}{4} - \frac{n-3}{4} \cdot \frac{1}{n} - \frac{\chi}{n}\right) \cdot n \cdot 12 = 9 - 12\chi$	
	9-edge	$\left(\frac{\chi}{n} + \frac{n-2}{3} \cdot \frac{1}{n} - \frac{1}{3}\right) \cdot n \cdot 12 = 12\chi - 8$	

TABLE S12: Probabilities of different patch-covering structures for patch sizes χ near χ_c , for n -patch disks on the snub square lattice. The period is $n_0 = 12$. For intermediate results on the regular dodecagon, the patch disk is placed at the center of the dodecagon and its patches cover edges connecting the center and vertices of the dodecagon. This table should be read together with Tables S13 and S14.

mod (n, n_0)	Type	On the regular dodecagon	On the snub square lattice
1	3-edge		$(9 - 12\chi) \cdot \frac{8}{12} + (12\chi - 8) \cdot \frac{3}{12} = 4 - 5\chi$
	4-edge		$(9 - 12\chi) \cdot \frac{4}{12} + (12\chi - 8) \cdot \frac{9}{12} = 5\chi - 3$
	8-edge	$\left(\frac{1-\chi}{n} + \frac{n-1}{4} \cdot \frac{1}{n} - \frac{1}{4}\right) \cdot n \cdot 12 = 9 - 12\chi$	
	9-edge	$\left(\frac{1}{3} - \frac{n-1}{3} \cdot \frac{1}{n} - \frac{1-\chi}{n}\right) \cdot n \cdot 12 = 12\chi - 8$	
2	2-edge		$(4 - 6\chi) \cdot \frac{6}{12} = 2 - 3\chi$
	3-edge		$(4 - 6\chi) \cdot \frac{6}{12} + (6\chi - 3) \cdot \frac{8}{12} = \chi$
	4-edge		$(6\chi - 3) \cdot \frac{4}{12} = 2\chi - 1$
	6-edge	$\left(\frac{1}{3} - \frac{n-2}{3} \cdot \frac{1}{n} - \frac{\chi}{n}\right) \cdot n \cdot 6 = 4 - 6\chi$	
	8-edge	$\left(\frac{\chi}{n} + \frac{n-2}{4} \cdot \frac{1}{n} - \frac{1}{4}\right) \cdot n \cdot 6 = 6\chi - 3$	
3	2-edge		$(3 - 4\chi) \cdot \frac{6}{12} = \frac{3}{2} - 2\chi$
	3-edge		$(3 - 4\chi) \cdot \frac{6}{12} + (4\chi - 2) \cdot \frac{3}{12} = 1 - \chi$
	4-edge		$(4\chi - 2) \cdot \frac{9}{12} = 3\chi - \frac{3}{2}$
	6-edge	$\left(\frac{1}{4} - \frac{n-3}{4} \cdot \frac{1}{n} - \frac{\chi}{n}\right) \cdot n \cdot 4 = 3 - 4\chi$	
	9-edge	$\left(\frac{\chi}{n} + \frac{n-3}{6} \cdot \frac{1}{n} - \frac{1}{6}\right) \cdot n \cdot 4 = 4\chi - 2$	
4	3-edge		$(3 - 3\chi) \cdot \frac{8}{12} = 2 - 2\chi$
	4-edge		$(3 - 3\chi) \cdot \frac{4}{12} + (3\chi - 2) \cdot \frac{4}{12} = \frac{1}{3}$
	5-edge		$(3\chi - 2) \cdot \frac{8}{12} = 2\chi - \frac{4}{3}$
	8-edge	$\left(\frac{1-\chi}{n}\right) \cdot n \cdot 3 = 3 - 3\chi$	
	12-edge	$\left(\frac{\chi}{n} + \frac{n-4}{6} \cdot \frac{1}{n} - \frac{1}{6}\right) \cdot n \cdot 3 = 3\chi - 2$	

TABLE S13: Probabilities of different patch-covering structures for patch sizes χ near χ_c , for n -patch disks on the snub square lattice. The period is $n_0 = 12$. For intermediate results on the regular dodecagon, the patch disk is placed at the center of the dodecagon and its patches cover edges connecting the center and vertices of the dodecagon. This table should be read together with Tables S12 and S14.

mod (n, n_0)	Type	On the regular dodecagon	On the snub square lattice
5	0-edge		$(8 - 12\chi) \cdot \frac{1}{12} = \frac{2}{3} - \chi$
	1-edge		$(8 - 12\chi) \cdot \frac{2}{12} + (12\chi - 7) \cdot \frac{2}{12} = \frac{1}{6}$
	2-edge		$(8 - 12\chi) \cdot \frac{2}{12} + (12\chi - 7) \cdot \frac{2}{12} = \frac{1}{6}$
	3-edge		$(8 - 12\chi) \cdot \frac{2}{12} + (12\chi - 7) \cdot \frac{2}{12} = \frac{1}{6}$
	4-edge		$(8 - 12\chi) \cdot \frac{2}{12} + (12\chi - 7) \cdot \frac{2}{12} = \frac{1}{6}$
	5-edge		$(8 - 12\chi) \cdot \frac{3}{12} + (12\chi - 7) \cdot \frac{4}{12} = \chi - \frac{1}{3}$
	7-edge	$\left(\frac{1}{3} - \frac{n-2}{3} \cdot \frac{1}{n} - \frac{\chi}{n}\right) \cdot n \cdot 12 = 8 - 12\chi$	
	8-edge	$\left(\frac{1}{12} - \frac{n-5}{12} \cdot \frac{1}{n} - \frac{1-\chi}{n}\right) \cdot n \cdot 12 = 12\chi - 7$	
6	2-edge		$(2 - 2\chi) \cdot \frac{6}{12} = 1 - \chi$
	3-edge		$(2 - 2\chi) \cdot \frac{6}{12} = 1 - \chi$
	5-edge		$(2\chi - 1) \cdot \frac{12}{12} = 2\chi - 1$
	6-edge	$\left(\frac{1-\chi}{n}\right) \cdot n \cdot 2 = 2 - 2\chi$	
12-edge	$\left(\frac{\chi}{n} + \frac{n-6}{12} \cdot \frac{1}{n} - \frac{1}{12}\right) \cdot n \cdot 2 = 2\chi - 1$		
7	0-edge		$(8 - 12\chi) \cdot \frac{1}{12} = \frac{2}{3} - \chi$
	1-edge		$(8 - 12\chi) \cdot \frac{2}{12} + (12\chi - 7) \cdot \frac{2}{12} = \frac{1}{6}$
	2-edge		$(8 - 12\chi) \cdot \frac{2}{12} + (12\chi - 7) \cdot \frac{2}{12} = \frac{1}{6}$
	3-edge		$(8 - 12\chi) \cdot \frac{2}{12} + (12\chi - 7) \cdot \frac{2}{12} = \frac{1}{6}$
	4-edge		$(8 - 12\chi) \cdot \frac{2}{12} + (12\chi - 7) \cdot \frac{2}{12} = \frac{1}{6}$
	5-edge		$(8 - 12\chi) \cdot \frac{3}{12} + (12\chi - 7) \cdot \frac{4}{12} = \chi - \frac{1}{3}$
	7-edge	$\left(\frac{1-\chi}{n} + \frac{n-1}{3} \cdot \frac{1}{n} - \frac{1}{3}\right) \cdot n \cdot 12 = 8 - 12\chi$	
	8-edge	$\left(\frac{\chi}{n} + \frac{n-7}{12} \cdot \frac{1}{n} - \frac{1}{12}\right) \cdot n \cdot 12 = 12\chi - 7$	

TABLE S14: Probabilities of different patch-covering structures for patch sizes χ near χ_c , for n -patch disks on the snub square lattice. The period is $n_0 = 12$. For intermediate results on the regular dodecagon, the patch disk is placed at the center of the dodecagon and its patches cover edges connecting the center and vertices of the dodecagon. This table should be read together with Tables S12 and S13.

mod (n, n_0)	Type	On the regular dodecagon	On the snub square lattice
8	3-edge		$(3 - 3\chi) \cdot \frac{8}{12} = 2 - 2\chi$
	4-edge		$(3 - 3\chi) \cdot \frac{4}{12} + (3\chi - 2) \cdot \frac{4}{12} = \frac{1}{3}$
	5-edge		$(3\chi - 2) \cdot \frac{8}{12} = 2\chi - \frac{4}{3}$
	8-edge	$\left(\frac{1-\chi}{n}\right) \cdot n \cdot 3 = 3 - 3\chi$	
	12-edge	$\left(\frac{\chi}{n} + \frac{n-8}{12} \cdot \frac{1}{n} - \frac{1}{12}\right) \cdot n \cdot 3 = 3\chi - 2$	
9	2-edge		$(3 - 4\chi) \cdot \frac{6}{12} = \frac{3}{2} - 2\chi$
	3-edge		$(3 - 4\chi) \cdot \frac{6}{12} + (4\chi - 2) \cdot \frac{3}{12} = 1 - \chi$
	4-edge		$(4\chi - 2) \cdot \frac{9}{12} = 3\chi - \frac{3}{2}$
	6-edge	$\left(\frac{1}{12} - \frac{n-9}{12} \cdot \frac{1}{n} - \frac{\chi}{n}\right) \cdot n \cdot 4 = 3 - 4\chi$	
	9-edge	$\left(\frac{\chi}{n} + \frac{n-3}{6} \cdot \frac{1}{n} - \frac{1}{6}\right) \cdot n \cdot 4 = 4\chi - 2$	
10	2-edge		$(4 - 6\chi) \cdot \frac{6}{12} = 2 - 3\chi$
	3-edge		$(4 - 6\chi) \cdot \frac{6}{12} + (6\chi - 3) \cdot \frac{8}{12} = \chi$
	4-edge		$(6\chi - 3) \cdot \frac{4}{12} = 2\chi - 1$
	6-edge	$\left(\frac{1}{6} - \frac{n-4}{6} \cdot \frac{1}{n} - \frac{\chi}{n}\right) \cdot n \cdot 6 = 4 - 6\chi$	
	8-edge	$\left(\frac{\chi}{n} + \frac{n-2}{4} \cdot \frac{1}{n} - \frac{1}{4}\right) \cdot n \cdot 6 = 6\chi - 3$	
11	3-edge		$(9 - 12\chi) \cdot \frac{8}{12} + (12\chi - 8) \cdot \frac{3}{12} = 4 - 5\chi$
	4-edge		$(9 - 12\chi) \cdot \frac{4}{12} + (12\chi - 8) \cdot \frac{9}{12} = 5\chi - 3$
	8-edge	$\left(\frac{1}{4} - \frac{n-3}{4} \cdot \frac{1}{n} - \frac{\chi}{n}\right) \cdot n \cdot 12 = 9 - 12\chi$	
	9-edge	$\left(\frac{\chi}{n} + \frac{n-2}{3} \cdot \frac{1}{n} - \frac{1}{3}\right) \cdot n \cdot 12 = 12\chi - 8$	

TABLE S15: Probabilities of different patch-covering structures for patch sizes χ near χ_c , for n -patch disks on the ruby lattice. The period is $n_0 = 12$. For intermediate results on the regular dodecagon, the patch disk is placed at the center of the dodecagon and its patches cover edges connecting the center and vertices of the dodecagon. This table should be read together with Tables S16 and S17.

mod (n, n_0)	Type	On the regular dodecagon	On the ruby lattice
1	2-edge		$(9 - 12\chi) \cdot \frac{4}{12} + (12\chi - 8) \cdot \frac{1}{12} = \frac{7}{3} - 3\chi$
	3-edge		$(9 - 12\chi) \cdot \frac{8}{12} + (12\chi - 8) \cdot \frac{10}{12} = 2\chi - \frac{2}{3}$
	4-edge		$(12\chi - 8) \cdot \frac{1}{12} = \chi - \frac{2}{3}$
	8-edge	$\left(\frac{1-\chi}{n} + \frac{n-1}{4} \cdot \frac{1}{n} - \frac{1}{4}\right) \cdot n \cdot 12 = 9 - 12\chi$	
	9-edge	$\left(\frac{1}{3} - \frac{n-1}{3} \cdot \frac{1}{n} - \frac{1-\chi}{n}\right) \cdot n \cdot 12 = 12\chi - 8$	
2	2-edge		$(5 - 6\chi) \cdot \frac{4}{12} = \frac{5}{3} - 2\chi$
	3-edge		$(5 - 6\chi) \cdot \frac{8}{12} + (6\chi - 4) \cdot \frac{4}{12} = \frac{2}{3}$
	4-edge		$(6\chi - 4) \cdot \frac{8}{12} = 2\chi - \frac{4}{3}$
	8-edge	$\left(\frac{1-\chi}{n} + \frac{n-2}{12} \cdot \frac{1}{n} - \frac{1}{12}\right) \cdot n \cdot 6 = 5 - 6\chi$	
	10-edge	$\left(\frac{\chi}{n} + \frac{n-2}{3} \cdot \frac{1}{n} - \frac{1}{3}\right) \cdot n \cdot 6 = 6\chi - 4$	
3	1-edge		$(3 - 4\chi) \cdot \frac{6}{12} = \frac{3}{2} - 2\chi$
	2-edge		$(4\chi - 2) \cdot \frac{3}{12} = \chi - \frac{1}{2}$
	3-edge		$(3 - 4\chi) \cdot \frac{6}{12} + (4\chi - 2) \cdot \frac{6}{12} = \frac{1}{2}$
	4-edge		$(4\chi - 2) \cdot \frac{3}{12} = \chi - \frac{1}{2}$
	6-edge	$\left(\frac{1}{4} - \frac{n-3}{4} \cdot \frac{1}{n} - \frac{\chi}{n}\right) \cdot n \cdot 4 = 3 - 4\chi$	
	9-edge	$\left(\frac{\chi}{n} + \frac{n-3}{6} \cdot \frac{1}{n} - \frac{1}{6}\right) \cdot n \cdot 4 = 4\chi - 2$	
4	2-edge		$(3 - 3\chi) \cdot \frac{8}{12} = 2 - 2\chi$
	4-edge		$(3 - 3\chi) \cdot \frac{4}{12} + (3\chi - 2) \cdot \frac{12}{12} = 2\chi - 1$
	8-edge	$\left(\frac{1-\chi}{n}\right) \cdot n \cdot 3 = 3 - 3\chi$	
	12-edge	$\left(\frac{\chi}{n} + \frac{n-4}{6} \cdot \frac{1}{n} - \frac{1}{6}\right) \cdot n \cdot 3 = 3\chi - 2$	

TABLE S16: Probabilities of different patch-covering structures for patch sizes χ near χ_c , for n -patch disks on the ruby lattice. The period is $n_0 = 12$. For intermediate results on the regular dodecagon, the patch disk is placed at the center of the dodecagon and its patches cover edges connecting the center and vertices of the dodecagon. This table should be read together with Tables S15 and S17.

mod (n, n_0)	Type	On the regular dodecagon	On the ruby lattice
5	1-edge		$(9 - 12\chi) \cdot \frac{2}{12} = \frac{3}{2} - 2\chi$
	2-edge		$(9 - 12\chi) \cdot \frac{4}{12} + (12\chi - 8) \cdot \frac{5}{12} = \chi - \frac{1}{3}$
	3-edge		$(9 - 12\chi) \cdot \frac{2}{12} + (12\chi - 8) \cdot \frac{2}{12} = \frac{1}{6}$
	4-edge		$(9 - 12\chi) \cdot \frac{4}{12} + (12\chi - 8) \cdot \frac{5}{12} = \chi - \frac{1}{3}$
	8-edge	$\left(\frac{1-\chi}{n} + \frac{n-1}{4} \cdot \frac{1}{n} - \frac{1}{4}\right) \cdot n \cdot 12 = 9 - 12\chi$	
	9-edge	$\left(\frac{\chi}{n} + \frac{n-2}{3} \cdot \frac{1}{n} - \frac{1}{3}\right) \cdot n \cdot 12 = 12\chi - 8$	
6	2-edge		$(2 - 2\chi) \cdot \frac{12}{12} = 2 - 2\chi$
	4-edge		$(2\chi - 1) \cdot \frac{12}{12} = 2\chi - 1$
	6-edge	$\left(\frac{1-\chi}{n}\right) \cdot n \cdot 2 = 2 - 2\chi$	
	12-edge	$\left(\frac{\chi}{n} + \frac{n-6}{12} \cdot \frac{1}{n} - \frac{1}{12}\right) \cdot n \cdot 2 = 2\chi - 1$	
7	1-edge		$(9 - 12\chi) \cdot \frac{2}{12} = \frac{3}{2} - 2\chi$
	2-edge		$(9 - 12\chi) \cdot \frac{4}{12} + (12\chi - 8) \cdot \frac{5}{12} = \chi - \frac{1}{3}$
	3-edge		$(9 - 12\chi) \cdot \frac{2}{12} + (12\chi - 8) \cdot \frac{2}{12} = \frac{1}{6}$
	4-edge		$(9 - 12\chi) \cdot \frac{4}{12} + (12\chi - 8) \cdot \frac{5}{12} = \chi - \frac{1}{3}$
	8-edge	$\left(\frac{1}{4} - \frac{n-3}{4} \cdot \frac{1}{n} - \frac{\chi}{n}\right) \cdot n \cdot 12 = 9 - 12\chi$	
	9-edge	$\left(\frac{1}{3} - \frac{n-1}{3} \cdot \frac{1}{n} - \frac{1-\chi}{n}\right) \cdot n \cdot 12 = 12\chi - 8$	
8	2-edge		$(3 - 3\chi) \cdot \frac{12}{12} = 2 - 2\chi$
	4-edge		$(3 - 3\chi) \cdot \frac{6}{12} + (3\chi - 2) \cdot \frac{12}{12} = 2\chi - 1$
	8-edge	$\left(\frac{1-\chi}{n}\right) \cdot n \cdot 3 = 3 - 3\chi$	
	12-edge	$\left(\frac{\chi}{n} + \frac{n-8}{12} \cdot \frac{1}{n} - \frac{1}{12}\right) \cdot n \cdot 3 = 3\chi - 2$	

TABLE S17: Probabilities of different patch-covering structures for patch sizes χ near χ_c , for n -patch disks on the ruby lattice. The period is $n_0 = 12$. For intermediate results on the regular dodecagon, the patch disk is placed at the center of the dodecagon and its patches cover edges connecting the center and vertices of the dodecagon. This table should be read together with Tables S15 and S16.

mod (n, n_0)	Type	On the regular dodecagon	On the ruby lattice
9	1-edge		$(3 - 4\chi) \cdot \frac{6}{12} = \frac{3}{2} - 2\chi$
	2-edge		$(4\chi - 2) \cdot \frac{3}{12} = \chi - \frac{1}{2}$
	3-edge		$(3 - 4\chi) \cdot \frac{6}{12} + (4\chi - 2) \cdot \frac{6}{12} = \frac{1}{2}$
	4-edge		$(4\chi - 2) \cdot \frac{3}{12} = \chi - \frac{1}{2}$
	6-edge	$\left(\frac{1}{12} - \frac{n-9}{12} \cdot \frac{1}{n} - \frac{\chi}{n}\right) \cdot n \cdot 4 = 3 - 4\chi$	
	9-edge	$\left(\frac{\chi}{n} + \frac{n-3}{6} \cdot \frac{1}{n} - \frac{1}{6}\right) \cdot n \cdot 4 = 4\chi - 2$	
10	2-edge		$(5 - 6\chi) \cdot \frac{4}{12} = \frac{5}{3} - 2\chi$
	3-edge		$(5 - 6\chi) \cdot \frac{8}{12} + (6\chi - 4) \cdot \frac{4}{12} = \frac{2}{3}$
	4-edge		$(6\chi - 4) \cdot \frac{8}{12} = 2\chi - \frac{4}{3}$
	8-edge	$\left(\frac{1}{12} - \frac{n-10}{12} \cdot \frac{1}{n} - \frac{\chi}{n}\right) \cdot n \cdot 6 = 5 - 6\chi$	
	10-edge	$\left(\frac{\chi}{n} + \frac{n-4}{6} \cdot \frac{1}{n} - \frac{1}{6}\right) \cdot n \cdot 6 = 6\chi - 4$	
11	2-edge		$(9 - 12\chi) \cdot \frac{4}{12} + (12\chi - 8) \cdot \frac{1}{12} = \frac{7}{3} - 3\chi$
	3-edge		$(9 - 12\chi) \cdot \frac{8}{12} + (12\chi - 8) \cdot \frac{10}{12} = 2\chi - \frac{2}{3}$
	4-edge		$(12\chi - 8) \cdot \frac{1}{12} = \chi - \frac{2}{3}$
	8-edge	$\left(\frac{1}{4} - \frac{n-3}{4} \cdot \frac{1}{n} - \frac{\chi}{n}\right) \cdot n \cdot 12 = 9 - 12\chi$	
	9-edge	$\left(\frac{\chi}{n} + \frac{n-2}{3} \cdot \frac{1}{n} - \frac{1}{3}\right) \cdot n \cdot 12 = 12\chi - 8$	

TABLE S18: Probabilities of different patch-covering structures for patch sizes χ near χ_c , for n -patch disks on the cross lattice. The period is $n_0 = 12$. For intermediate results on the regular dodecagon, the patch disk is placed at the center of the dodecagon and its patches cover edges connecting the center and vertices of the dodecagon. This table should be read together with Tables S19 and S20.

mod (n, n_0)	Type	On the regular dodecagon	On the cross lattice
1	2-edge		$(11 - 12\chi) \cdot \frac{6}{12} + (12\chi - 10) \cdot \frac{3}{12} = 3 - 3\chi$
	3-edge		$(11 - 12\chi) \cdot \frac{6}{12} + (12\chi - 10) \cdot \frac{9}{12} = 3\chi - 2$
	10-edge	$\left(\frac{1-\chi}{n} + \frac{n-1}{12} \cdot \frac{1}{n} - \frac{1}{12}\right) \cdot n \cdot 12 = 11 - 12\chi$	
	11-edge	$\left(\frac{1}{6} - \frac{n-1}{6} \cdot \frac{1}{n} - \frac{1-\chi}{n}\right) \cdot n \cdot 12 = 12\chi - 10$	
2	2-edge		$(6 - 6\chi) \cdot \frac{6}{12} = 3 - 3\chi$
	3-edge		$(6 - 6\chi) \cdot \frac{6}{12} + (6\chi - 5) \cdot \frac{12}{12} = 3\chi - 2$
	10-edge	$\left(\frac{1-\chi}{n}\right) \cdot n \cdot 6 = 6 - 6\chi$	
	12-edge	$\left(\frac{1}{12} - \frac{n-2}{12} \cdot \frac{1}{n} - \frac{1-\chi}{n}\right) \cdot n \cdot 6 = 6\chi - 5$	
3	1-edge		$(4 - 4\chi) \cdot \frac{3}{12} = 1 - \chi$
	2-edge		$(4 - 4\chi) \cdot \frac{3}{12} = 1 - \chi$
	3-edge		$(4 - 4\chi) \cdot \frac{6}{12} + (4\chi - 3) \cdot \frac{12}{12} = 2\chi - 1$
	9-edge	$\left(\frac{1-\chi}{n}\right) \cdot n \cdot 4 = 4 - 4\chi$	
	12-edge	$\left(\frac{\chi}{n} + \frac{n-3}{4} \cdot \frac{1}{n} - \frac{1}{4}\right) \cdot n \cdot 4 = 4\chi - 3$	
4	1-edge		$(3 - 3\chi) \cdot \frac{4}{12} = 1 - \chi$
	2-edge		$(3 - 3\chi) \cdot \frac{4}{12} = 1 - \chi$
	3-edge		$(3 - 3\chi) \cdot \frac{4}{12} + (3\chi - 2) \cdot \frac{12}{12} = 2\chi - 1$
	8-edge	$\left(\frac{1-\chi}{n}\right) \cdot n \cdot 3 = 3 - 3\chi$	
	12-edge	$\left(\frac{\chi}{n} + \frac{n-4}{6} \cdot \frac{1}{n} - \frac{1}{6}\right) \cdot n \cdot 3 = 3\chi - 2$	

TABLE S19: Probabilities of different patch-covering structures for patch sizes χ near χ_c , for n -patch disks on the cross lattice. The period is $n_0 = 12$. For intermediate results on the regular dodecagon, the patch disk is placed at the center of the dodecagon and its patches cover edges connecting the center and vertices of the dodecagon. This table should be read together with Tables S18 and S20.

mod (n, n_0)	Type	On the regular dodecagon	On the cross lattice
5	1-edge		$(10 - 12\chi) \cdot \frac{2}{12} + (12\chi - 9) \cdot \frac{1}{12} = \frac{11}{12} - \chi$
	2-edge		$(10 - 12\chi) \cdot \frac{5}{12} + (12\chi - 9) \cdot \frac{4}{12} = \frac{7}{6} - \chi$
	3-edge		$(10 - 12\chi) \cdot \frac{5}{12} + (12\chi - 9) \cdot \frac{7}{12} = 2\chi - \frac{13}{12}$
	9-edge	$\left(\frac{1}{6} - \frac{n-5}{6} \cdot \frac{1}{n} - \frac{\chi}{n}\right) \cdot n \cdot 12 = 10 - 12\chi$	
	10-edge	$\left(\frac{1}{4} - \frac{n-1}{4} \cdot \frac{1}{n} - \frac{1-\chi}{n}\right) \cdot n \cdot 12 = 12\chi - 9$	
6	1-edge		$(2 - 2\chi) \cdot \frac{6}{12} = 1 - \chi$
	2-edge		$(2 - 2\chi) \cdot \frac{6}{12} = 1 - \chi$
	3-edge		$(2\chi - 1) \cdot \frac{12}{12} = 2\chi - 1$
	6-edge	$\left(\frac{1-\chi}{n}\right) \cdot n \cdot 2 = 2 - 2\chi$	
	12-edge	$\left(\frac{\chi}{n} + \frac{n-6}{12} \cdot \frac{1}{n} - \frac{1}{12}\right) \cdot n \cdot 2 = 2\chi - 1$	
7	1-edge		$(10 - 12\chi) \cdot \frac{2}{12} + (12\chi - 9) \cdot \frac{1}{12} = \frac{11}{12} - \chi$
	2-edge		$(10 - 12\chi) \cdot \frac{5}{12} + (12\chi - 9) \cdot \frac{4}{12} = \frac{7}{6} - \chi$
	3-edge		$(10 - 12\chi) \cdot \frac{5}{12} + (12\chi - 9) \cdot \frac{7}{12} = 2\chi - \frac{13}{12}$
	9-edge	$\left(\frac{1-\chi}{n} + \frac{n-1}{6} \cdot \frac{1}{n} - \frac{1}{6}\right) \cdot n \cdot 12 = 10 - 12\chi$	
	10-edge	$\left(\frac{\chi}{n} + \frac{n-3}{4} \cdot \frac{1}{n} - \frac{1}{4}\right) \cdot n \cdot 12 = 12\chi - 9$	
8	1-edge		$(3 - 3\chi) \cdot \frac{4}{12} = 1 - \chi$
	2-edge		$(3 - 3\chi) \cdot \frac{4}{12} = 1 - \chi$
	3-edge		$(3 - 3\chi) \cdot \frac{4}{12} + (3\chi - 2) \cdot \frac{12}{12} = 2\chi - 1$
	8-edge	$\left(\frac{1-\chi}{n}\right) \cdot n \cdot 3 = 3 - 3\chi$	
	12-edge	$\left(\frac{\chi}{n} + \frac{n-8}{12} \cdot \frac{1}{n} - \frac{1}{12}\right) \cdot n \cdot 3 = 3\chi - 2$	

TABLE S20: Probabilities of different patch-covering structures for patch sizes χ near χ_c , for n -patch disks on the cross lattice. The period is $n_0 = 12$. For intermediate results on the regular dodecagon, the patch disk is placed at the center of the dodecagon and its patches cover edges connecting the center and vertices of the dodecagon. This table should be read together with Tables S18 and S19.

mod (n, n_0)	Type	On the regular dodecagon	On the cross lattice
9	1-edge		$(4 - 4\chi) \cdot \frac{3}{12} = 1 - \chi$
	2-edge		$(4 - 4\chi) \cdot \frac{3}{12} = 1 - \chi$
	3-edge		$(4 - 4\chi) \cdot \frac{6}{12} + (4\chi - 3) \cdot \frac{12}{12} = 2\chi - 1$
	9-edge	$\left(\frac{1 - \chi}{n}\right) \cdot n \cdot 4 = 4 - 4\chi$	
	12-edge	$\left(\frac{\chi}{n} + \frac{n - 9}{12} \cdot \frac{1}{n} - \frac{1}{12}\right) \cdot n \cdot 4 = 4\chi - 3$	
10	2-edge		$(6 - 6\chi) \cdot \frac{6}{12} = 3 - 3\chi$
	3-edge		$(6 - 6\chi) \cdot \frac{6}{12} + (6\chi - 5) \cdot \frac{12}{12} = 3\chi - 2$
	10-edge	$\left(\frac{1 - \chi}{n}\right) \cdot n \cdot 6 = 6 - 6\chi$	
	12-edge	$\left(\frac{\chi}{n} + \frac{n - 10}{12} \cdot \frac{1}{n} - \frac{1}{12}\right) \cdot n \cdot 6 = 6\chi - 5$	
11	2-edge		$(11 - 12\chi) \cdot \frac{6}{12} + (12\chi - 10) \cdot \frac{3}{12} = 3 - 3\chi$
	3-edge		$(11 - 12\chi) \cdot \frac{6}{12} + (12\chi - 10) \cdot \frac{9}{12} = 3\chi - 2$
	9-edge	$\left(\frac{1}{12} - \frac{n - 11}{12} \cdot \frac{1}{n} - \frac{\chi}{n}\right) \cdot n \cdot 12 = 11 - 12\chi$	
	10-edge	$\left(\frac{\chi}{n} + \frac{n - 5}{6} \cdot \frac{1}{n} - \frac{1}{6}\right) \cdot n \cdot 12 = 12\chi - 10$	

TABLE S21: Probabilities of different patch-covering structures for patch sizes χ near χ_c , for n -patch disks on the three-twelve lattice. The period is $n_0 = 12$. For intermediate results on the regular dodecagon, the patch disk is placed at the center of the dodecagon and its patches cover edges connecting the center and vertices of the dodecagon. This table should be read together with Tables S22 and S23.

mod (n, n_0)	Type	On the regular dodecagon	On the three-twelve lattice
1	2-edge		$(11 - 12\chi) \cdot \frac{6}{12} + (12\chi - 10) \cdot \frac{3}{12} = 3 - 3\chi$
	3-edge		$(11 - 12\chi) \cdot \frac{6}{12} + (12\chi - 10) \cdot \frac{9}{12} = 3\chi - 2$
	10-edge	$\left(\frac{1-\chi}{n} + \frac{n-1}{12} \cdot \frac{1}{n} - \frac{1}{12}\right) \cdot n \cdot 12 = 11 - 12\chi$	
	11-edge	$\left(\frac{1}{6} - \frac{n-1}{6} \cdot \frac{1}{n} - \frac{1-\chi}{n}\right) \cdot n \cdot 12 = 12\chi - 10$	
2	2-edge		$(6 - 6\chi) \cdot \frac{6}{12} = 3 - 3\chi$
	3-edge		$(6 - 6\chi) \cdot \frac{6}{12} + (6\chi - 5) \cdot \frac{12}{12} = 3\chi - 2$
	10-edge	$\left(\frac{1-\chi}{n}\right) \cdot n \cdot 6 = 6 - 6\chi$	
	12-edge	$\left(\frac{1}{12} - \frac{n-2}{12} \cdot \frac{1}{n} - \frac{1-\chi}{n}\right) \cdot n \cdot 6 = 6\chi - 5$	
3	2-edge		$(4 - 4\chi) \cdot \frac{9}{12} = 3 - 3\chi$
	3-edge		$(4 - 4\chi) \cdot \frac{3}{12} + (4\chi - 3) \cdot \frac{12}{12} = 3\chi - 2$
	9-edge	$\left(\frac{1-\chi}{n}\right) \cdot n \cdot 4 = 4 - 4\chi$	
	12-edge	$\left(\frac{\chi}{n} + \frac{n-3}{4} \cdot \frac{1}{n} - \frac{1}{4}\right) \cdot n \cdot 4 = 4\chi - 3$	
4	2-edge		$(3 - 3\chi) \cdot \frac{12}{12} = 3 - 3\chi$
	3-edge		$(3\chi - 2) \cdot \frac{12}{12} = 3\chi - 2$
	8-edge	$\left(\frac{1-\chi}{n}\right) \cdot n \cdot 3 = 3 - 3\chi$	
	12-edge	$\left(\frac{\chi}{n} + \frac{n-4}{6} \cdot \frac{1}{n} - \frac{1}{6}\right) \cdot n \cdot 3 = 3\chi - 2$	
5	1-edge		$(11 - 12\chi) \cdot \frac{2}{12} = \frac{11}{6} - 2\chi$
	2-edge		$(11 - 12\chi) \cdot \frac{2}{12} + (12\chi - 10) \cdot \frac{2}{12} = \frac{1}{6}$
	3-edge		$(11 - 12\chi) \cdot \frac{8}{12} + (12\chi - 10) \cdot \frac{10}{12} = 2\chi - 1$
	10-edge	$\left(\frac{1-\chi}{n} + \frac{5n-1}{12} \cdot \frac{1}{n} - \frac{5}{12}\right) \cdot n \cdot 12 = 11 - 12\chi$	
	11-edge	$\left(\frac{\chi}{n} + \frac{n-5}{6} \cdot \frac{1}{n} - \frac{1}{6}\right) \cdot n \cdot 12 = 12\chi - 10$	

TABLE S22: Probabilities of different patch-covering structures for patch sizes χ near χ_c , for n -patch disks on the three-twelve lattice. The period is $n_0 = 12$. For intermediate results on the regular dodecagon, the patch disk is placed at the center of the dodecagon and its patches cover edges connecting the center and vertices of the dodecagon. This table should be read together with Tables S21 and S23.

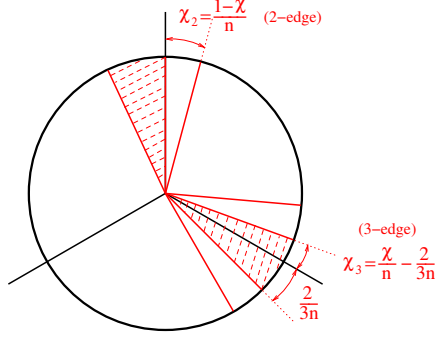
mod (n, n_0)	Type	On the regular dodecagon	On the three-twelve lattice
6	1-edge		$(2 - 2\chi) \cdot \frac{6}{12} = 1 - \chi$
	2-edge		$(2 - 2\chi) \cdot \frac{6}{12} = 1 - \chi$
	3-edge		$(2\chi - 1) \cdot \frac{12}{12} = 2\chi - 1$
	6-edge	$\left(\frac{1 - \chi}{n}\right) \cdot n \cdot 2 = 2 - 2\chi$	
	12-edge	$\left(\frac{\chi}{n} + \frac{n - 6}{12} \cdot \frac{1}{n} - \frac{1}{12}\right) \cdot n \cdot 2 = 2\chi - 1$	
7	1-edge		$(11 - 12\chi) \cdot \frac{2}{12} = \frac{11}{6} - 2\chi$
	2-edge		$(11 - 12\chi) \cdot \frac{2}{12} + (12\chi - 10) \cdot \frac{2}{12} = \frac{1}{6}$
	3-edge		$(11 - 12\chi) \cdot \frac{8}{12} + (12\chi - 10) \cdot \frac{10}{12} = 2\chi - 1$
	10-edge	$\left(\frac{5}{12} - \frac{5n - 11}{12} \cdot \frac{1}{n} - \frac{\chi}{n}\right) \cdot n \cdot 12 = 11 - 12\chi$	
	11-edge	$\left(\frac{1}{6} - \frac{n - 1}{6} \cdot \frac{1}{n} - \frac{1 - \chi}{n}\right) \cdot n \cdot 12 = 12\chi - 10$	
8	2-edge		$(3 - 3\chi) \cdot \frac{12}{12} = 3 - 3\chi$
	4-edge		$(3\chi - 2) \cdot \frac{12}{12} = 3\chi - 2$
	8-edge	$\left(\frac{1 - \chi}{n}\right) \cdot n \cdot 3 = 3 - 3\chi$	
	12-edge	$\left(\frac{\chi}{n} + \frac{n - 8}{12} \cdot \frac{1}{n} - \frac{1}{12}\right) \cdot n \cdot 3 = 3\chi - 2$	
9	2-edge		$(4 - 4\chi) \cdot \frac{9}{12} = 3 - 3\chi$
	3-edge		$(4 - 4\chi) \cdot \frac{3}{12} + (4\chi - 3) \cdot \frac{12}{12} = 3\chi - 2$
	9-edge	$\left(\frac{1 - \chi}{n}\right) \cdot n \cdot 4 = 4 - 4\chi$	
	12-edge	$\left(\frac{\chi}{n} + \frac{n - 9}{12} \cdot \frac{1}{n} - \frac{1}{12}\right) \cdot n \cdot 4 = 4\chi - 3$	

TABLE S23: Probabilities of different patch-covering structures for patch sizes χ near χ_c , for n -patch disks on the three-twelve lattice. The period is $n_0 = 12$. For intermediate results on the regular dodecagon, the patch disk is placed at the center of the dodecagon and its patches cover edges connecting the center and vertices of the dodecagon. This table should be read together with Tables S21 and S22.

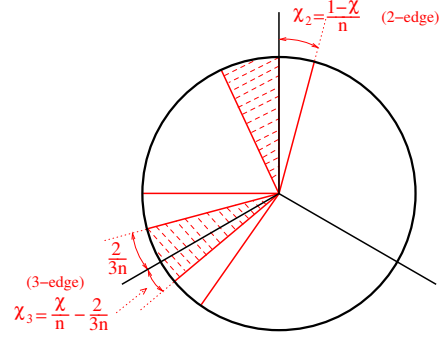
mod (n, n_0)	Type	On the regular dodecagon	On the three-twelve lattice
10	2-edge		$(6 - 6\chi) \cdot \frac{6}{12} = 3 - 3\chi$
	3-edge		$(6 - 6\chi) \cdot \frac{6}{12} + (6\chi - 5) \cdot \frac{12}{12} = 3\chi - 2$
	10-edge	$\left(\frac{1 - \chi}{n}\right) \cdot n \cdot 6 = 6 - 6\chi$	
	12-edge	$\left(\frac{\chi}{n} + \frac{n - 10}{12} \cdot \frac{1}{n} - \frac{1}{12}\right) \cdot n \cdot 6 = 6\chi - 5$	
11	2-edge		$(11 - 12\chi) \cdot \frac{6}{12} + (12\chi - 10) \cdot \frac{3}{12} = 3 - 3\chi$
	3-edge		$(11 - 12\chi) \cdot \frac{6}{12} + (12\chi - 10) \cdot \frac{9}{12} = 3\chi - 2$
	9-edge	$\left(\frac{1}{12} - \frac{n - 11}{12} \cdot \frac{1}{n} - \frac{\chi}{n}\right) \cdot n \cdot 12 = 11 - 12\chi$	
	10-edge	$\left(\frac{\chi}{n} + \frac{n - 5}{6} \cdot \frac{1}{n} - \frac{1}{6}\right) \cdot n \cdot 12 = 12\chi - 10$	

(a) Honeycomb

mod(n,3)=1

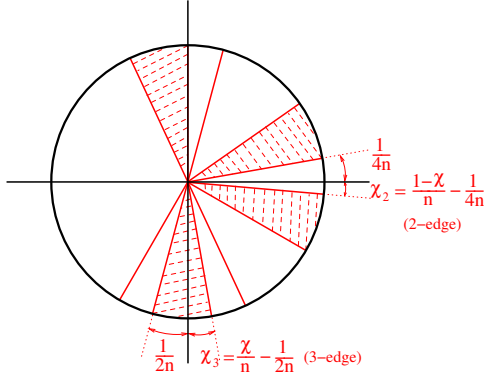


mod(n,3)=2

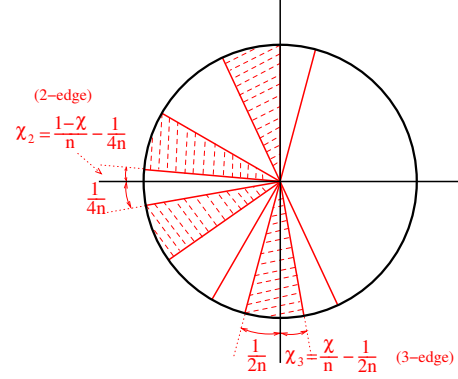


(b) Square

mod(n,4)=1

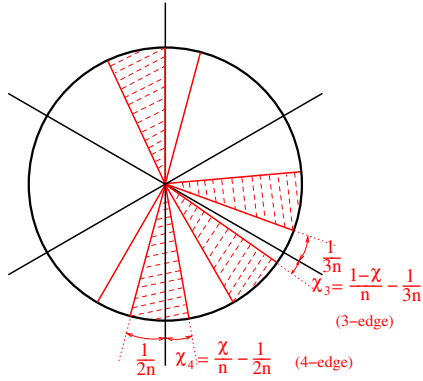


mod(n,4)=3

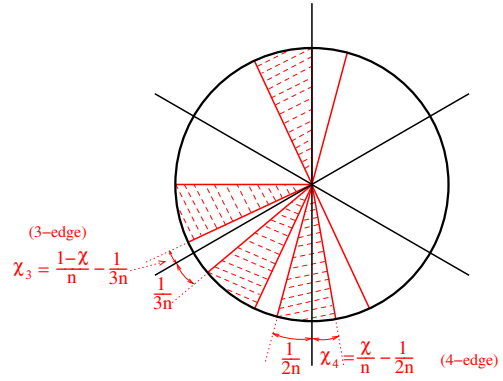


(c) Triangular

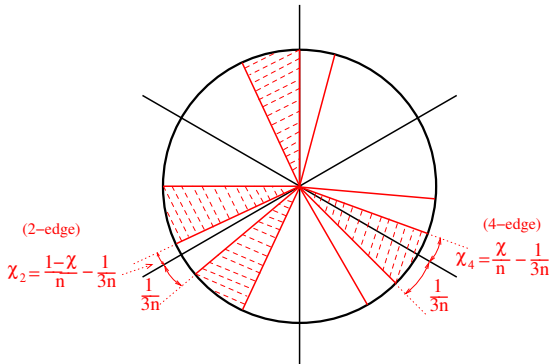
mod(n,6)=1



mod(n,6)=5



mod(n,6)=2



mod(n,6)=4

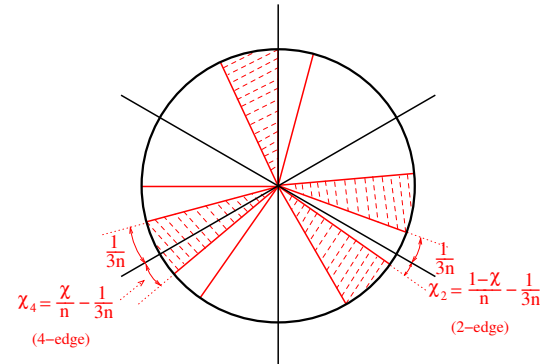


FIG. S25: Plots demonstrating symmetries between n -patch disks with $\text{mod}(n, n_0) = m$ and $n_0 - m$. The angles χ_i for i -edge patch-covering structures are from expressions in Table S4.